STRUCTURE AND REACTIVITY OF SELECTED BINAPHTHYL DERIVATIVES

by

Rodriguez Yav Kabwit

(B.Tech Chemistry, Cape Peninsula University of Technology)

Thesis presented to the

CAPE PENINSULA UNIVERSITY OF TECHNOLOGY

for the degree of

MASTER OF TECHNOLOGY

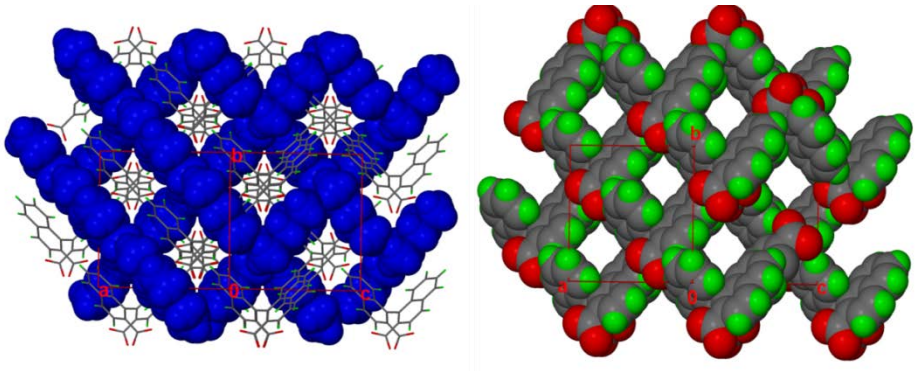

Department of Chemistry, Cape Peninsula University of Technology,

Cape Town Campus, Zonnebloem,

October 2013

DEDICACE

TO THE ONE WHO HAS MY LIFE IN HIS HAND, DECIDING UPON MY LIFE AND MY FUTURE,

TO THE ONE I CHOSE MYSELF AND HAVE DECIDED TO SQUEEZE HER LIFE INTO MINE SO THAT WE MAY FORM A SUPERMOLECULE,

TO THOSE ONES WHO ARE MY SEED AND CALLED TO PURSUE WITH THIS FIELD,

I DEDICATE THIS THESIS

ACKNOWLEDGEMENTS

I would like to thank,

Prof Ayesha Jacobs, for her support, and especially during this year, without which, maybe this thesis could not been done. Her guidance, her encouragement and especially her help, sign of the expertise in the domain.

Prof Luigi R. Nassimbeni, for his willingness to help. His knowledge was for us like the consultant library.

Dr Nicky Bathori, for being there sometimes for us.

Prof Weber, for supplying the 1,1'-binaphthyl-2,2'-dicarboxylic acid used in this project.

Dr Hong Su, for the single crystal X-ray diffraction data collection.

All my colleagues and friends, past or present, in the crystal engineering lab for their friendship, support and encouragement.

My Family and brotherhood for their love, prayers and support.

ABSTRACT

Title : Structure and reactivity of selected binaphthyl derivatives

Author: Rodriguez Yav Kabwit

Date: October 2013

In this thesis, the complexation behaviour of the host compounds, 1,1'-binaphthyl-2,2'-dicarboxylic acid (**BNDA**) and 1,1'-binaphthyl-2,2'-diol (**BINOL**) were investigated. These hosts are large, bulky and scissor shaped; they contain functionalities to selectively interact with other molecules. A series of small organic compounds, particularly amines, were used in the preparation of the complexes. **BNDA** formed three complexes with acyclic amines, two complexes with the cyclic amines and two complexes with a racemic amine in different solvents.

All the complexes formed were salts. The amines used were diethylamine, di-*n*-butylamine, cyclohexylamine, dicyclohexylamine, and *sec*-butylamine. For the studies with the acyclic amines and cyclic amines, crystals were grown in methanol as a co-solvent.

Similar experiments were conducted with **BINOL**. Successful complexation only occurred with cyclohexylamine and dicyclohexylamine respectively. An amine host, 1,1'-binaphthyl-2,2'- diamine (**BINDIA**) was also considered with acidic and amide guests to extend the study of the binaphthyl derivatives, but from the array of guests used, the host only formed an inclusion compound with dimethylacetamide (DMA).

The structures of all the complexes were elucidated using single crystal X-ray diffraction. Thermal analysis was performed in order to determine the thermal stability of the complexes, including techniques such as thermogravimetry, differential scanning calorimetry and hot stage microscopy. The kinetics of desolvation was investigated for some of the complexes.

ABBREVIATIONS AND SYMBOLS USED IN THIS THESIS

α	Angle between b and c unit cell axes or extent of reaction
β	Angle between a and c unit cell axes or extent of reaction
γ	Angle between a and b unit cell axes or extent of reaction
t	torsion angle
A	Arrhenius pre-exponential factor
bp	Boiling point
BNDA	1,1'-binaphthyl-2,2'-dicarboxylic acid
$BNDA^{2-}$	Anion 1,1'-binaphthyl-2,2'-dicarboxylate
BINDIA	1,1'-binaphthyl-2,2'-diamine
BINOL	1,1'-binaphthyl-2,2'-diol
$BINOL^{-}$	Anion1,1'-binaphthyl-2-hydroxylate
CHA	Cyclohexylamine
CHA^{+}	Cation cyclohexylammonium
CSD	Cambridge Structural Database
DEA	Diethylamine
DEA^{+}	Cation diethylammonium
DBA	Dibutylamine
DBA^{+}	Cation dibutylammonium
DCHA	Dicyclohexylamine
$DCHA^{+}$	Cation dicyclohexylammonium
DMSO	Dimethylacetamide
DSC	Differential Scanning Calorimeter
Ea	Activation energy
Endo	Endothermic
F(α)	Kinetic expression

G	Guest
H	Host
H:G	Host to guest ratio
HSM	Hot stage microscopy
K	Rate constant
Mp	Melting point
Mr	Molecular mass
PXRD	Powder X-ray diffraction
R	Gas constant = 8.314 J K^{-1} mol^{-1}
Secbuam	Sec-butylamine
$Secbuam^{+}$	Cation sec-butylammonium
T_{on}	Onset temperature
Tpeak	Peak temperature
Tb	Boiling temperature
TG	Thermogravimetry
U	Isotropic atomic displacement
V	Unit cell volume
XRD	X-ray diffraction
PXRD	Powder X-ray diffraction
Z	Number of formula units per cell

CONTENT

CHAPTER I. INTRODUCTION

The history of chemistry as a modern science, spanning the last two centuries, was based on the understanding of covalent bonds. It's only in the last thirty years that the study of non-bonded interactions, the so-called secondary bonds, has attracted serious attention. This has allowed scientists to understand the forces that control the properties of large assemblies of molecules, both in biological systems and synthetic materials such as polymers: Hence, the birth of supramolecular chemistry.

INTRODUCTION

What is supramolecular chemistry?

- "Chemistry beyond the molecule.[1,2]"
- "Chemistry of molecular assemblies and of intermolecular bonds.[1,3]"
- "Chemistry of non-covalent bonds.[1]"

Supramolecular Chemistry has also been defined as a kind of "lego block chemistry[2]" in which molecules as building blocks are held together and organised by means of intermolecular forces, and not by covalent bonds, to form a periodic supermolecule **(Figure1.1)**.

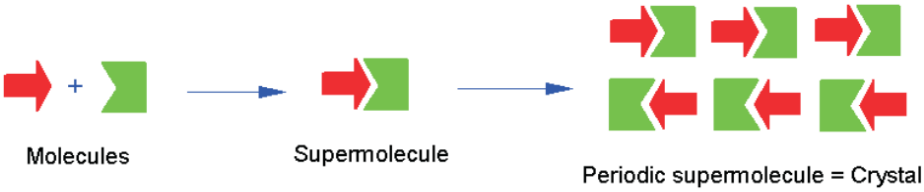

Figure 1.1 Formation of a supermolecular crystal

The molecules that comprise the supermolecule form new entities with novel properties and functions, which cannot be deduced by a simple compilation of the properties of the individual molecules.

The comparison between molecular chemistry and supramolecular chemistry is summarised in **Table 1.1**

Molecular Chemistry	Supramolecular Chemistry
Atom	Molecule
Covalent bond	Intermolecular bond
Molecule	Crystal
Synthesis	Crystal engineering
Synthon	Supramolecular synthon
Isomer	Polymorph
Transition state	Nucleus
Reaction	Crystallisation

Table 1.1[4] Analogies between molecular chemistry and supramolecular chemistry.

Charles J. Pedersen, Jean-Marie Lehn and Donald J. Cram, by their research,[5-8] have established the foundation for the development of supramolecular chemistry to be recognised as a discipline. Thus, in 1987, they were awarded the Nobel Prize in chemistry[9].

D.J. CRAM J.M. LEHN C.J.PEDERSEN

Figure 1.2 Pioneers of supramolecular chemistry.

Supramolecular chemistry can be split into two broad categories:[10]

(i) molecular recognition or host-guest chemistry,

(ii) the chemistry of molecular assemblies.

The difference between these areas is a question of size and shape. Molecular recognition chemistry deals generally with the smallest supramolecular systems, and involves interactions between just a few molecules. It is associated with a molecule recognizing another one as a partner, thus the notion of host and guest chemistry.

Host chemistry and molecular recognition

Molecular recognition describes a particular interaction between two or several molecules which are complementary in their geometry and electronic features, forming supramolecular systems. One molecule, called, a host, can recognize and bind another molecule (guest). Therefore, molecular recognition chemistry is sometimes called host–guest chemistry.[10,11] Two principles are very important in the study of molecular recognition:

- Complementarity[1]

A host must have binding sites of the correct electronic character to complement those of the guest in order to bind to the guest. It is possible for a host to possess multiple binding sites for a more stable interaction with the guest.

- The lock and key principle[1]

The ideal specific recognition depends on the size, the shape and the position of the binding sites within the active site of the host. Hosts are generally larger than guests so that they wrap around them.

Supramolecular chemistry is the chemistry of weak interactions. Those weak bonds or intermolecular forces are classified as hydrogen bonds, electrostatic interactions, π-π interactions, van der Waals interactions or hydrophobic interactions (weakest). [1-3]

The study of host-guest chemistry is of great importance to chemists. Its purpose concerns designing better host systems which could lead to a better understanding of a wide range of host-guest interactions in nature. In host-guest chemistry, the recognition of a guest by the host via molecular interactions is selective. Since intermolecular interactions are the ”concrete” that holds supermolecules together, gaining an understanding of these non-bonding forces, is one of the primary goals of host-guest chemistry.

Molecular interactions in host-guest chemistry

In the chemical systems that appear in the following sections molecular recognition is achieved through various combinations of the abovementioned molecular interactions. When several types of molecular interactions work together, a cooperative enhancement in molecular association is often observed. Finding an appropriate combination of molecular interactions is the key to designing efficient molecular recognition systems. **Table 1.2** illustrates typical intermolecular interactions.

Interaction	Strength (kJ mol^{-1})	Example
Ion-Ion	200-300	Tetrabutylammonium chloride
Ion-dipole	50-200	Sodium (15)crown-5
Dipole-dipole	5-50	acetone
Hydrogen bonding	4-120	See table 1.3
Cation-π	5-80	K^+ in benzene
π-π	0-50	Benzene and graphite
Van der Waals	<5kJ mol^{-1} but variable depending on surface area	Argon; packing in molecule crystals
Hydophobic	Related to solvent-solvent interaction energy	Cyclodextrin inclusion compounds

Table 1.2 Typical intermolecular interactions.

1. Ionic and dipolar interactions[1-3]

These interactions have three main categories which are based on Coulombic forces between opposite charges.

➢ Ion-ion interactions

The strongest of the three, ion-ion interactions, are non-directional and can be comparable in energy to covalent interactions (Figure 1.3).

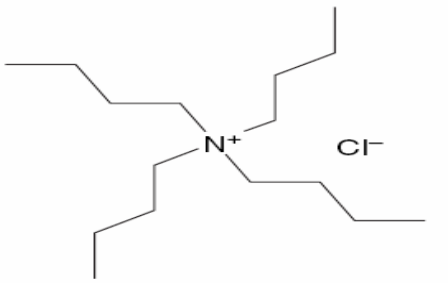

Figure 1.3 Example of ion-ion interactions in a tetrabutylammonium chloride

- **Dipole–dipole and dipole–ion interactions**

These are also electrostatic in nature but generally weaker than fully ionic interactions. Dipole-dipole interactions are the weakest of the three groups. However ion-dipole interactions (Figure 1.4a) and dipole-dipole interactions (Figure 1.4b) are directional.

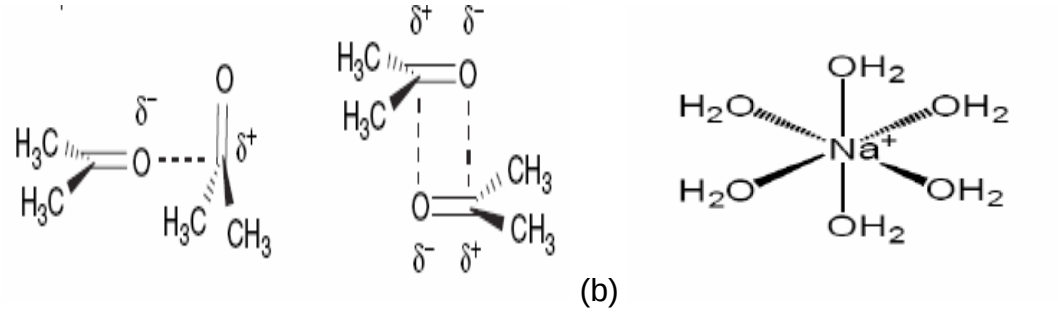

Figure 1.4 Examples of (a) dipole-dipole interactions in acetone and (b) ion-dipole interactions in a solvation.[12]

2. van der Waals interactions[1]

These weak interactions are important as they participate in the formation of inclusion compounds. They are also non-directional. The typical example is found in cyclodextrin inclusion complexes.

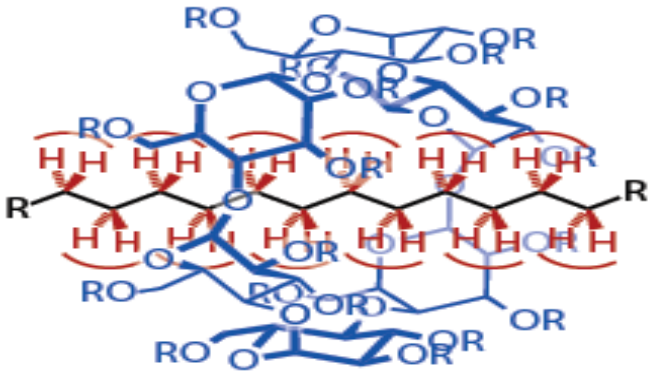

Figure 1.5 Cyclodextrin inclusion complexes.

3. ***Π*- interactions[1]**

Π- Interactions can be split into two categories namely (i) cation-*π* interactions and (ii) *π* –*π* interactions. Cation—*π* interactions are well known in the field of organometallic chemistry with the example of ferrocene seen in Figure 1.6. On the

other hand *π –π interactions* occur between aromatic rings, and exist as parallel displaced, dipolar interactions. Face-to-face and edge-to-face stacking is shown in Figure 1. 7.

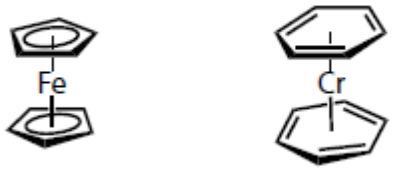

Figure 1.6 Ferrocene and *bis* (η^6-benzene) chromium.[12]

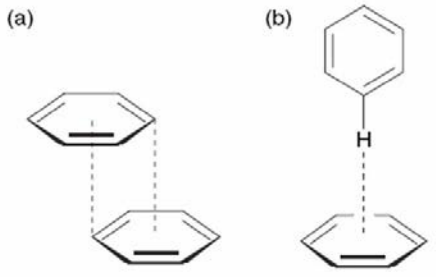

Figure 1.7 Examples of *π-π* interactions showing face-to-face(a) and edge-to-face stacking (b)

4. **Hydrogen bonding[1-3]**

Among these interactions, the hydrogen bond is the most important and well-understood of all the directional forces.

The hydrogen bond can be described by the arrangement D–H•••A, where D is the donor atom, H is the hydrogen atom and A is the acceptor atom. Hydrogen bonding plays a vital role in chemistry, nature and in all biological systems.[13] They are essential as they help in the stabilization of protein structures within the skin, muscles and other animal tissues.[14] Hydrogen bond properties differ relative to the groups of atoms surrounding them, and these can be characterised into three types; namely strong, moderate and weak interactions, as illustrated in **Table 1.3** and in **Figure 1.8**.

Hydrogen bonds	Strong	Moderate	Weak
D—H---A	Mostly covalent	Most electrostatic	Electrostatic
Bond lengths	D—H ≈ H—A	D—H < H---A	D—H << H ---A
H---A(Å)	~1.2-1.5	~1.5-2.2	2.2-3.2
D---A(Å)	2.2-2.5	2.5-3.2	3.2-4.0
Bond angles(^{0})	175-180	130-180	90-150
Bond energy(kcal mol^{-1})[a]	14-40	4-15	<4
Relative IR vibration shift (cm^{-1})[b]	25%	10-25%	<10%
H^{1} chemical shift downfield (ppm)	14-22	<14	—
Examples	Gas-phase dimers with strong acids or strong bases salts Proton sponges Pseudohydrates HF complexes	Acids-Bases Alcohols Phenols Hydrates All biological molecules	Gas phase dimers with weak acids or weaks bases Minor components of 3-centre bonds C—H—O/N bonds O/N—H---π

Table 1.3 Characteristics of strong, moderate and weak hydrogen bonds.[15]

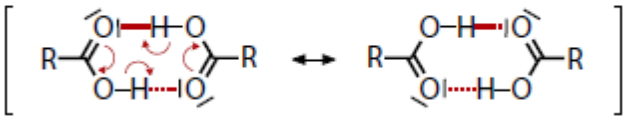

Figure 1.8 Carboxylic acid dimers

Why is the study of supermolecules important if the different species involved often interact via weak forces of attractions and therefore have low association constants?

One of the answers is the many important applications of host-guest chemistry which include the separation of mixtures of closely related compounds and enantiomers, storage of gases and toxic substances, stabilisation of reactive compounds, slow release of drugs under physiological conditions, and control of reaction pathways by inclusion within reaction vessels or channels (topochemistry).[1,16,17]Many of these

applications impact on industrially and scientifically topical fields such as nanotechnology.[10]

The ultimate goal of crystal engineering is to gain a comprehensive understanding of intermolecular interactions and exploit this knowledge to routinely construct designer materials.

Host Design and the molecular recognition

For a host-guest interaction to occur the host molecule must possess the appropriate binding sites. For example if the host has many hydrogen bond donor functionalities then the guest must ideally contain an equal number of hydrogen bond acceptor sites, which are positioned in such a way that is feasible for multiple interactions between host and guest to occur. Alternatively, if the host has Lewis acid centres then the guest must possess Lewis base functionalities. Shape control of these supermolecules is very important for function design: hence, host molecules can be classified according to their shape and functionality. For a host to be designed and be good for host-guest chemistry, it should have some of the following qualities:

• Molecular bulkiness, for a low density packing with the possibility of cavities.[17]

• Rigidity, to maintain and sustain cavities.[19]

• Functional groups, to provide suitable host-guest interactions.[20]

Many organic host compounds have been synthesized based on these principles including those containing hydroxyl, carboxyl and amine functional groups for hydrogen bonding.

Host-guest chemistry, for several years, focused on macrocyclic hosts such as crown ethers,[21] cryptands[22] and cavitands (calixarenes,[1,23,24] cyclophanes,[10,25] cyclodextrins[10,26]). Some of them are endoreceptors (bind to the guest at the interior of the host) and others are exoreceptors (the guest is bound to the exterior of the host). In this research, the focus is on the systems which make extensive use of functional group interactions between the host and guest for planned inclusion properties. The hosts have a particular geometry viz. Scissor shaped molecules classified as 1,1'-binaphthyl-2,2'-derivatives.

Scissor Type Hosts [27,28]

There is a direct structural relation between a pair of scissors and the binaphthyl compounds, due to scissor-like geometries (two fold symmetry (C_2)).

The crystalline supramolecular systems formed with scissor hosts are of the new type of ”coordinatoclathrates”,[29] which usually are more stable than the conventional clathrates. A classic example of this type of host is 1,1’-binaphthyl-2,2’-dicarboxylic acid which is the main host in this study (Figure 1.9).

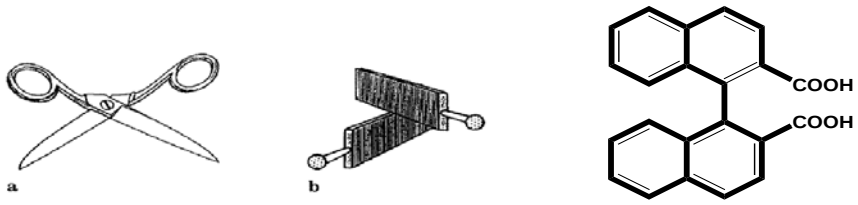

Figure 1.9 Scissor type host: *(R,S)1,1’-binaphthyl-2,2’-dicarboxylic acid.*

C2-symmetric 2,2’-derived-1,1’-binaphthyl compounds have gained much attention in recent years due to their application as novel clathrate host systems.

The 1,1’-binaphthyl-2,2’-derivatives are versatile host compounds giving crystalline inclusion complexes with almost every tested guest species.

The introduction of hydroxyl, amine and carboxylic acid functionalities are of particular importance in host–guest chemistry due to the efficiency of supramolecular synthon formation which is useful in self-assembling, crystal-engineering and solid state materials design.

The 1,1'- binaphthyl derivatives

1,1'-Binaphthyl compounds comprise a special class of biaryl molecules and they are very effective for many chemical applications, particularly enantioselective transformations.[28]

The 1,1'-bond between the two naphthyls is restricted, thus they exist as non-planar rotamers, which are not superimposable. Therefore these two naphthyl systems behave as mirror images of each other. This particular form of stereoisomerism depends on the substituents. It is called atropoisomerism and brings forth axial chirality. [30]

The configuration of a racemic 1,1'-binaphthyl molecule is designated as *R* or *S* according to the dihedral angle. When the dihedral angle between the two naphthyl rings is less than 90^o, the crystal structure of *rac*-1,1-binaphthyl exists in the *(R)-cisoid* conformation, whereas, in the *(S)-transoid* conformation, the dihedral angle is greater than 90^o. [31-33]

For the study of various 2,2'-substituted 1,1'-binaphthyl molecules, the *cisoid* conformation is preferred, when the 2,2'-substituents X are either small or capable of intramolecular hydrogen bonding (*e.g.* when X = OH, NH_2, COOH, CH_2OH, OCH_3), but when the same 2,2'-substituents are large (*e.g.* when X = CH_2Br or $CHBr_2$), the *transoid* conformation will be preferred. [34,35]

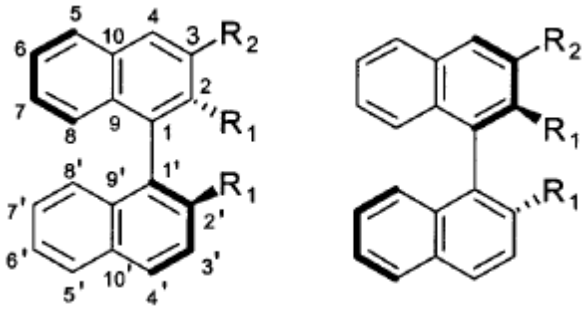

Figure 1.10 Models of the *S-enantiomer* showing the numbering (on the left) and of the *R-enantiomer* (on the right) in binaphthyls.

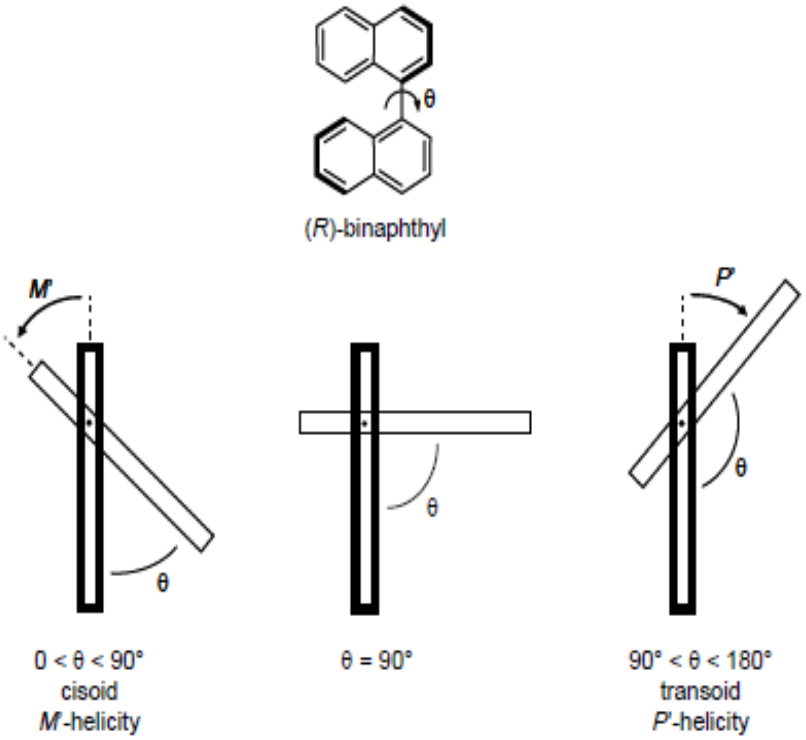

Figure 1.11 *Transoid* and *cisoid* conformers in binaphthyls.

1,1'-Binaphthyls may racemize according to two possible pathways which happen by rotation around the 1,1'-bond : the *syn* interaction state racemization where the 2,2'-H's and 8,8'-H's are in close contact, and an *anti* interaction state racemization where the close contact is observed for the 2,8-H's and 2',8'-H's.[36] Theoretically, the *anti* pathway has lower steric hindrance than the *syn* route, and calculations show that 1,1'-binaphthyl favours the *anti* inversion racemization mechanism. The aromatic rings in these transition states are significantly distorted (Figure1.12)

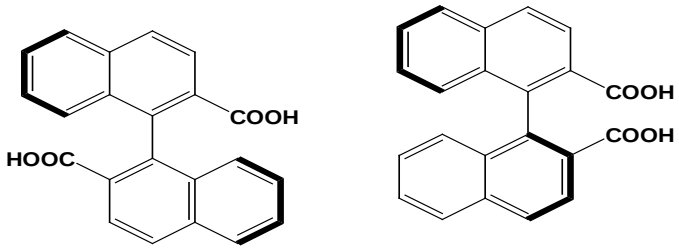

Figure 1.12 Anti interaction state of racemization (left) and syn interaction state (right) of racemization in 1,1'-binaphthyl-2,2'-dicarboxylic.

Unsubstituted 1,1'-binaphthyl has a rotational barrier of *ca 94 kJ/mol*, corresponding to a half life of about 30 min at room temperature and of 14.5 min at 50 ^{o}C.[37] The addition of bulky substituents at the 2,2' positions increase the rotational barrier. while substituents in the 8,8' positions decreases the rotational barrier considerably. Substituents in other positions do not show significant influence on this rotation. Thus in the chiral configuration, the 2,2'-positions of the 1,1'-binaphthyl compounds are more stable than others[34,38,39] For example, (*S*)-1,1*'*-binaphthyl-2,2'-dicarboxylic acid did not racemize at 175 ^{o}C in *N,N*-dimethyl formamide[40], and 2,2'-dimethyl-1,1'-binaphthyl did not racemize after 40 h at 240 ^{o}C.[41] However 1,1'-binaphthyl-8,8'-dicarboxylic acid underwent racemization at a rate similar to that of the unsubstituted 1,1'-binaphthyl and the half-life for its racemization was 51.5 min at 50 ^{o}C.[42] This can be attributed to the steric repulsion of the 1,8-substituents on the naphthalene rings of 1,1'-binaphthyl-8,8'-dicarboxylic acid, which increase the ground-state energy and cause deformation of this molecule.[31]

Because of the highly stable chiral configuration of the 2,2'-substituted 1,1'-binaphthyls, these molecules have been extensively used to control many asymmetric processes and they have demonstrated outstanding chiral discrimination properties.[43] These macrocycles are also used as host molecules in supramolecular chemistry.

They interact with the functional groups of guest molecules through weak forces such as hydrogen bonding, π–π stacking, and van der Waals forces and the common substrates used are 1,1'-binaphthyl-2,2'-diol (BINOL),[45] 1,1'-binaphthyl-2,2'-dicarboxylic acid (BNDA)[45] and 2,2'-diamino-1,1'-binaphthyl (BINDIA).[46] The chirality of the binaphthyl units in these hosts leads to their enantioselective complexation with chiral guest molecules.

Chiral resolution is a widely used method. It offers facile access to both enantiomers, which is advantageous for catalytic applications.

This chiral recognition has been applied to the resolution of racemic molecules including amino acids, amino esters, amines, sugars and other chiral alkyl or aryl compounds.

The inclusion chemistry of 1,1'-binaphthyl-2,2'-diol (BINOL) is well known and 162 structures are recorded in the Cambridge Structural Database (CSD).[47] Kawashima and Hirayama reported a convenient method for the direct resolution of BINOL using chiral 1,2-diaminocyclohexane.[48]

Toda *et al* observed that commercially available *N-alkylcinchonidium* halides are very effective for the resolution of BINOL.[49] The optical purity was enhanced to 100% by simple recrystallisation from methanol. Hu *et al* reported a modified procedure using *N-benzylcinchonidium chloride*.[50] They demonstrated that both enantiomers of BINOL could be obtained in optically pure form in this way**.** Cai *et al* developed a similar procedure using *N-benzylcinchonidium* chloride.[51] When the resolution experiments were carried out in acetonitrile, both the enantiomers were obtained in > *99% ee***.**

Although BINOL has been used extensively in complexation and asymmetric reductions, BNDA has also been recognised as a chiral catalyst for epoxidation and in particular as a versatile host due to its carboxylic acid substituents which act as strong hydrogen bond donors. 41 structures involving BNDA have been reported in the CSD,[47] and among them is the resolution of BNDA using quinine and the toxin brucine.[52] Previously, it had been shown that BNDA forms two different clathrate species with many solvents such as ethanol,[53] DMSO,[54] acetylacetone,[55] acetic acid,[56] and others.[57] For clathrates of BNDA with *N,N-dimethylformamide*, however, four different modifications have been prepared and their structures solved. An example of solvatotetramorphism and unique clathrate forming ability has been reported with different host-guest complexes between BNDA and 1,4-dioxane.[58] Recently*, Imai et al* have reported a two-component chiral supramolecular host system of achiral biphenic acid or chiral *(R)-1,1'-binaphthyl-2,2'-dicarboxylic* acid combined with *(1R,2R)-1,2-diphenylethylenediamine* or *(1S,2S)-1,2-cyclohexanediamine*.[59]

However, 1,1'-binaphthyl-2,2'-diamine (BINDIA) has not yet been studied extensively. From the 10 structures found on the CSD[47] containing BINDIA, two demonstrated the synthesis of racemic BINDIA and the remaining 8 structures

showed the use of this compound in asymmetric chemistry. Koichi Mikami *et al*[60] demonstrated the effect of an aqua palladium catalyst on biphenylphosphine ligands by BINDIA as an activator.

SALT VERSUS CO-CRYSTAL

Crystal engineering of organic molecular compounds study crystalline materials subdivided into different crystal forms. The synthesis of all these crystals offer a route to new functionalities in pharmaceutical, other chemical industries and as well as for intellectual property reasons.[61]

As there is a large landscape of crystal forms, different opinions exist on the terms[62] used for describing each form, even how to write the term. *eg.* co-crystal and salt.

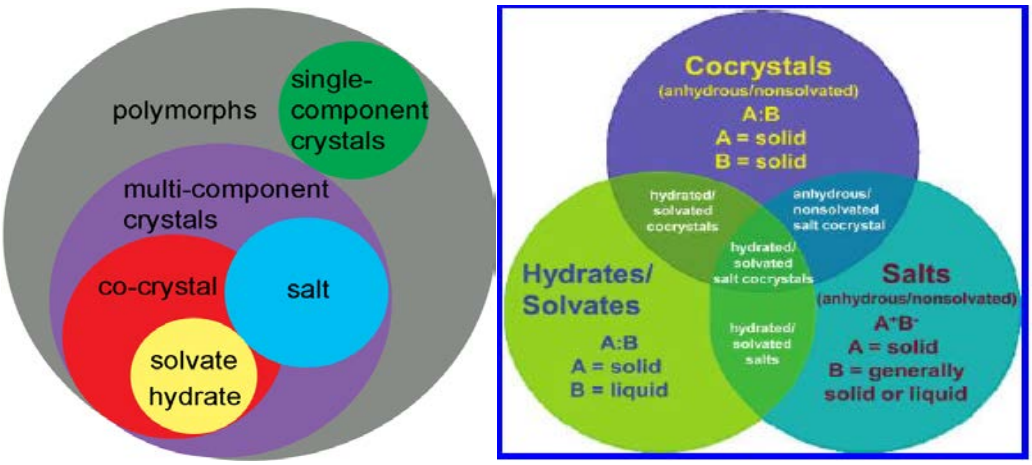

Figure 1.13 Different crystal forms of molecular crystals .

A host as a single-component crystal can have polymorphs.[63] It can crystallize with a solvent guests to form a solvate[64,65] or it can also form other multi-component molecular crystals, *i.e.* co-crystals or salts, with compounds other than solvents. The co-crystals and salts can have hydrate or solvate forms and, in addition to this, all multi-component forms themselves can have polymorphs.

For co-crystal strategies based on strong hydrogen bonds, there is a possibility that the proton involved in the hydrogen bonding interaction could be transferred from the

donor (acid) to the acceptor (base). This new compound formed, which comprises an assembly of cations and anions, is no longer a co-crystal but a salt.[65] Thus, a pharmaceutical salt comprises an active pharmaceutical ingredient (API) that is molecular and either cationic or anionic and a counterion that might be molecular or monoatomic (e.g. a halide anion) .

Salt formation is the result of three components system having an acid (A), a base (B) and one or more solvents. A salt is formed by transfer of a proton (H^+) from an acid (A) to base (B).

$$A\text{-}H + B \rightarrow (A^-)\ (B^+\text{-}\ H)$$

The formation of a salt or co-crystal can be predicted from pK_a values of the acid (A) and a base (B). In general, when the ΔpK_a between the acid and the base is more than 3, the transfer of the proton is complete resulting in complete ionization and formation of a salt .[66] IUPAC rules indicate that the salt formation generally requires a difference of about 2.7 pK_a units between the conjugate base and the conjugate acid, i.e. [pK_a (base) - pK_a (acid) ≥ 2.7].[67]

For $0 < \Delta pK_a < 3$, it is difficult to predict whether the resulting complex will be neutral or charged and base pK_a values are not sometimes sufficiently high to allow proton transfer when a co-crystal is formed.[34] The crystal structure is also useful in distinguishing between a salt and a co-crystal by measuring the difference in the C-O distances in the carboxylic moieties of the resultant compound. If the difference Δd(C-O) gives a value between 0.08 and 0.12 Å, this indicates the presence of a co-crystal while smaller differences of less than 0.04 Å is typical of the salt formation.[68,69]

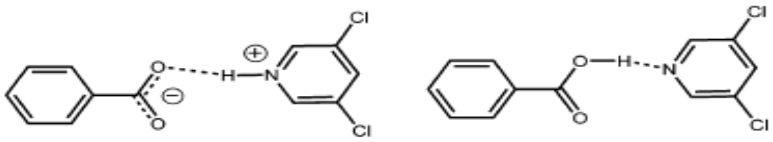

Figure 1.14 Classification as a salt (left) or co-crystal (right)

Delimitation of this thesis

For this project, we selected three of the racemic 1,1'-binaphthyl derivatives which are, 1,1'-binaphthyl 2,2'-dicarboxylic acid (BNDA); 1,1'-binaphthyl-2,2'-diamine (BINDIA) and 1,1'-binaphthyl-2,2'-diol (BINOL). These hosts are depicted in Figure 1.15 below:

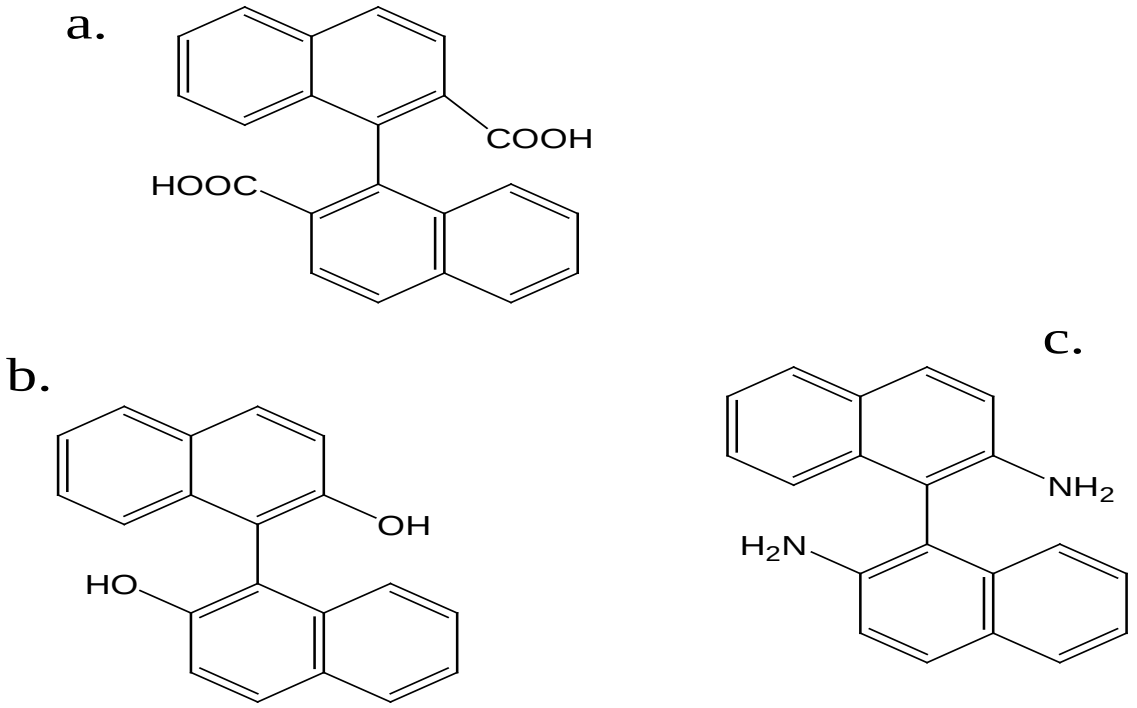

Figure 1.15 Host molecules studied a: 1,1'-binaphthyl-2,2'-dicarboxylic acid (BNDA) , b: 1,1'-binaphthyl-2,2'-diamine (BNDIA) and c: 1,1'-binaphthyl-2,2'diol (BINOL),

Selected small molecules were chosen as guests to form supramolecular complexes with the hosts. The guests used in this project were:

1. The guests which have amine functional groups.

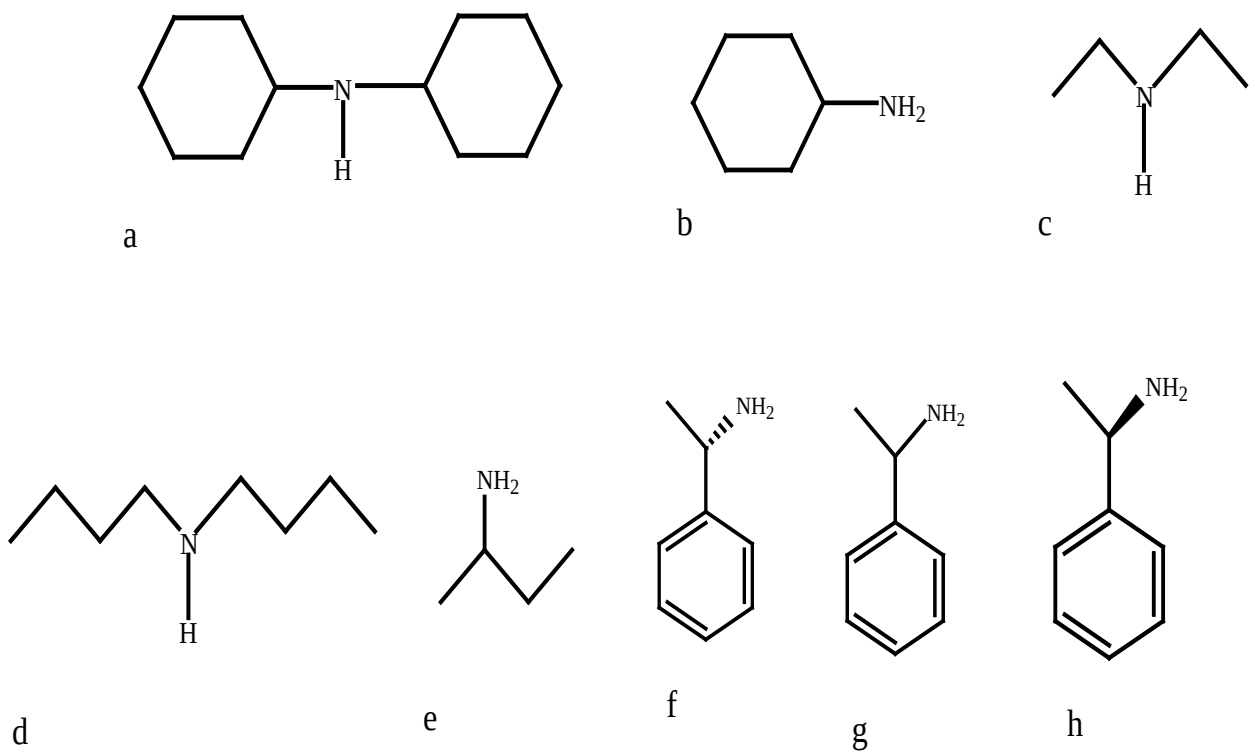

Figure 1.14 The amine guests studied a. dicylohexylamine (DCHA), b. cyclohexylamine (CHA), c. diethylamine (DEA), d. dibutylamine (DBA), e. secbutylamine (SECBUAM), f. *R*-(+)-α-methylphenylamine, g. *RS*-(+)-α-methylphenylamine, h. *S*-(-)-α-methylphenylamine,

2. The guests with an amide or acid functional group.

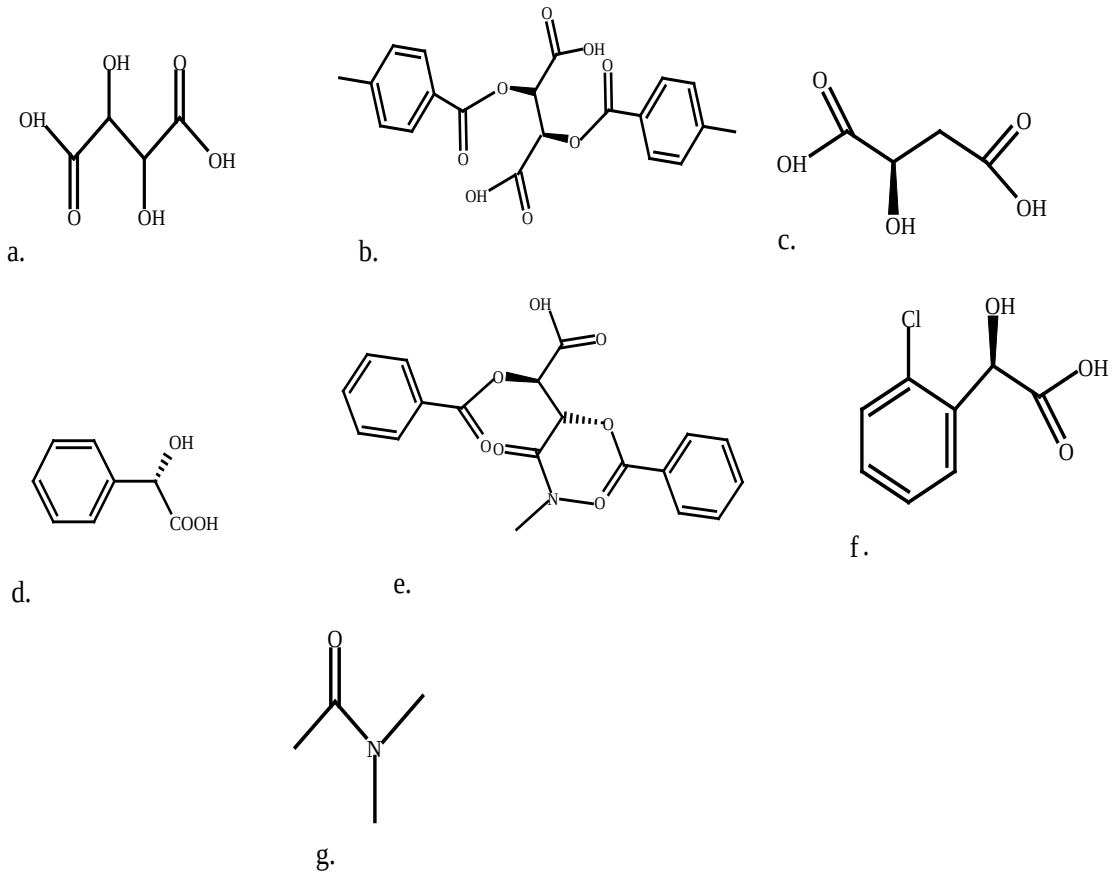

Figure 1.15 The acidic and amide guests used a. tartaric acid, b. DDTA, c. *D*-(+)-Malic acid, d. *R-(-)*-mandelic acid , e. (-)-O,O'-dibenzoyl-*L*-tartaric acid (DBTA), f. *R*-(-)-2-chloromandelic acid, g. *N,N*-dimethylacetamide (DMA)

The aims of this project were the following:

- Characterize the resultant co-crystal or salts by X-ray diffraction, thermogravimetric analysis (TGA) and differential scanning calorimetry (DSC).
- Determine the kinetics of desolvation where appropriate.
- Determine the impact of various solvents on the non-covalent interactions.

REFERENCES

1. Steed, J.W. & Atwood, J.L. (2000). *Supramolecular chemistry*, John Wiley & Sons, Ltd.
2. Steed, J.W., Turner, D.R., and Wallace*, K.J. (2007). Core Concepts in Supramolecular Chemistry and Nanochemistry*, John Wiley & Sons, Ltd.
3. Lehn*, J.M. (1978), Pure Appl. Chem*., 50, 871-875.
4. Desiraju, G.R., Vittal, J.J., Ramanan., A. (2011). *Crystal Engineering A textbook*, IISc press, World Scientific.
5. Pedersen, C.J. (1988). *Angew. Chem. Int. Ed.*, 27, 1021-1027.
6. Dietrich, B., Lehn, J.M. (1969), *Sauvage, J.P., Tetrahedron Lett.*, 34, 2885-2888
7. Cram, D.J., Dolsee, K.M. (1986)., *J.Org.Chem*, 51, 5068-5071
8. Stewart, K.D., Miesch, M., Knobler, C.B., Maverick, E.F., *Cram, D.J. (1986). Host-guest complexation 40. Synthesis and complexation of macrocyclic hosts containing cyclic ureas, and steric barriers. . J.org.chem*,51,4327-4337
9. Schmeck, H.M. (1987). "*Chemistry and Physics Nobels Hail Discoveries on Life and Superconductors*; Three Share Prize for Synthesis of Vital Enzymes". New York Times, October 15.
10. Ariga, K., *Kunitage, T. (2006) Supramolecular Chemistry-Fundamentals and Application, Advanced Textbook*. Springer Berlin Heidelberg
11. Cram, D.J., Cram*, J.M. (1974)., Science*, 183, 803-809
12. Mautner, M. (2005). *Chem. Rev*., 105, 213-284
13. Brown, T.L., LeMay, H.E., Bursten, B.E., Burdge, J.R. (2003). *Chemistry, the Central Science, 9th edition, Prentice Hall, Chapter 11*
14. Jeffrey, G. A. (1997). *An Introduction to Hydrogen Bonding;* Oxford University Press: Oxford.
15. Scheider, H.J., Jatsimirsky, A. (2000). *Principles and Methods in Supramolecular Chemistry;* Wiley: Chichester, U. K.
16. MacNicol, D. D., Toda, F., Bishop*, R. (1996). Comprehensive Supramolecular Chemistry*; Eds.; Elsevier: Oxford, U. K., Vol. 6.
17. Weber, E., Czugler, M. (1988). *In Topics in Current Chemistry: Molecular Inclusion and Molecular Recognitions Clathrates II*; Springer-Verlag: Berlin, 149, 45-135
18. Weber, E., Atwood, J.L., Davies, J.E.D., MacNicol,D.D., *In Inclusion Compounds*; Eds.; Oxford University Press: Oxford, U. K., 1991, 4, 188
19. Weber, E., MacNicol, D. D., Toda, F., Bishop, R. (1996). *In Comprehensive Supramolecular Chemistry*; Elsevier: Oxford, U. K., 6, 535.
20. Pedersen, C.J. (1988). *Organic Syntheses*, Coll. 6, 52, 395
21. Dietrich, B. (1984). *Cryptate Complexes in Inclusion Compounds***.**
22. Ramon, G., Jacobs, A., Nassimbeni, L.R., Kabwit, R.Y. (2011). *Cryst. Growth. Des*, 7, 3172-3182.

23. Ikeda, A., Shinkai*, S. (1997). Chem. Rev*. ,97, 1713-1734
24. Whitlock, B.J., Whitlock, H.W. (1997). *J. Am. Chem.Soc*, 116, 2301-2311
25. Szejtli, J. (1998). J.Chem.Rev. ,98,1743-1754
26. Weber, E., Czugler, M. (1988). *Molecular Inclusion and Molecular Recognition-Clathrate II-Topics in Current Chemistry*,139, 45-135
27. Csöregh, I., Czugler, M., Weber, .E. (1990). *J. Inclusion Phenom. Macrocyclic Chem.,* 8, 3, 309-322
28. Czugler, M., Weber, E. (1991). *J. Inclusion Phenom. Macrocyclic Chem.,* 10, 355-366.
29. IUPAC Compendium of Chemical Terminology, Electronic version, http://goldbook.iupac.org/ A00511.html (accessed July 28, 2008).
30. Setnicka, V., Urbanova, M., Bour, P., Kral, V. and Volka, K.(2001) *J. Phys. Chem. A* , 105, 8931-8938
31. Yang, X., Liu, K., Shen,Y., Fu, M. Zhang, C., Zhu and Cheng, Y. (2011). Org. Biomol. Chem., 9, 6011
32. Gottarelli, G., Spada, .G.P., Bartsch, R., Solladie, .G., Zimmermann, .R.G. (1986). *J.Org.Chem*., 51, 589
33. Pu, L. (1998). *Chem. Rev*. , 98, 2405
34. Ferrarini, A., Moro, .G.J., Nordio, P.L. (1996) *Phys.Rev. E* ,53,681
35. Mason, .S.F., Seal, .R.H., Roberts, .D.R. (1974). *Tetrahedron*, 30, 1671.
36. Kuroda, R., Mason, .S.F. (1981). *Tetrahedron*, 37, 1995.
37. Yudin, A. K., Martyn, L. J. P., Pandiaraju, S., Zheng, J., Lough, A. (2000). *Org*. *Lett*., 2, 41, 3433.
38. Kranz, M., Clark, T., Schleyer, P von R. (1993) *J Org Chem* , 58, 3317–3325.
39. Hall, D.M., Turner, E.E. (1955). *J Chem Soc,* 1242
40. Dixon, W., Harris, M.M., Mazengo, R.Z. (1971). *J Chem Soc*, 775.
41. Hall, D.M., Turner, E.E. (1955). *J Chem Soc,* 1242.
42. Dixon, W., Harris, M.M., Mazengo, R.Z. (1971). *J Chem Soc*, 775.
43. Rosini , C., Franzini, L. , Raffaelli, A., Salvadori, P. (1992). *Synthesis* , 503-517.
44. Kanoh, S., Hongoh, Y., Motoi, M. Suda, H. (1988). *Bull. Chem. Soc. Jpn*, 61, 1032-1034.
45. Miyano, S., Nawa, M., Mori, A., Hashimoto, H. (1984). *Bull. Chem. Soc. Jpn*., 57, 2171-2176.
46. ConQuest, (2001), A program for the search of the CSD, Version 1.7.
47. Kawashima, M., and Hirayama, A. (1990). *Chem. Lett.,* 2299-2300
48. Tanaka, K. T. Okada, K., and. Toda, F. (1993). *Angew. Chem*. *Int. Ed. Engl*, 32,1147-1162
49. Hu, Q. S., Vitharana, D., and Pu, L. (1995). Tetrahedron: Asymm., 6, 2123-2126
50. Cai, D., Hughes, D. L., Verhoeven, T. R. and Reider, P. J. (1995). *Tetrahedron Lett.***,** 36, 7991.

51. Kanoh, S., Hongoh, Y., Motoi, M. and Suda, H. (1988), *J. Chem. Soc. Jpn*., 61, 1032-1034.
52. Ibragimov, B. Beketov, K., Makhkamov , K. Weber, E. (1997). *J Chem Soc Perkin Trans 2*, 1349
53. Makhkamov, K. K., Ibragimov, B. T., Weber, E., Beketov, K. M. J. (1999). *Phys. Org. Chem*., 12, 157.
54. Gallardo, O., Csöregh, I., Weber, E. (1995). *J. Chem. Cryst*, 25,11 pp 769-776
55. Csoregh, I. Czugler, M. (1990). *J. Inclus. Phenom. Mol, 8, 309-322.*
56. Czugler, M. (1991). *J. Inclus. Phenom. Mol., 10, 355-366.*
57. Ibragimov, B.T., Beketov, K.M., Makhkamov, K.K., and Weber, E. (1999). *J. Incl. Phen. Macro. Chem*. 34, 31–37.
58. Imai, Y., Kawaguchi, K., Murata, K., Sato, T., Kuroda, R., and Matsubara, Y. (2008). *Org. Lett*, 10, No. 3, 469-471.
59. Koichi, M, Yusa, Y., Korenaga, T.,(2000), *Org. Lett*., 4, 1643-1645.
60. Trask, A.V. (2007). *Mol. Pharmaceutics*, 4, 301-309.
61. Desiraju, G.R. (2003), *CrystEngComm*, 5, 466-467.
62. Bernstein. (2002). *Polymorphism in Molecular Crystals, Oxford University Press, United States*, p. 352.
63. Griesser, U.J., *The Importance of Solvates. Polymorphism in the Pharmaceutical Industry, Hilfiker.,R (Ed.)*WILEY-VCH Verlag GmbH & Co. KGaA
64. Kirchener; M.T., Boese, R.,.Blaeser, D., Gehrke, A. (2004), *CrystEngComm*, 6, 60.
65. Childs, S. L., Stahly, G. P., Park, A. (2007), *Mol. Pharmaceutics*, 4, 323.
66. IUPAC Compendium of Chemical Terminology, Electronic version, http://goldbook.iupac.org/ A00511.html (accessed July 28, 2008).
67. Chandramouli, Y., Gandhimathi, R., Yasmeen, B.R., Vikram, A., Mahitha, B., Imroz, S.M. (2012), *IJMCA*, 2, 91-100
68. Jacobs, A., Nassimbeni, L. R., Ramon, G and Sebogisi., B. K.,(2010), *CrystEngComm*, 12, 3065-3070

CHAPTER II. EXPERIMENTAL

Host Compounds

The host compounds used were as 1,1'-Binaphthyl-2,2'-dicarboxylic acid, 1,1'-Binaphthyl-2,2'-diol and 1,1'-Binaphthyl-2,2'-diamine.

Guest molecules

The amine guests cyclohexylamine(CHA), dicyclohexylamine(DCHA), racemic-sec- Butylamine(Sec Buam), di-n-butylamine (DBA) and diethylamine (DEA)were used for the crystallisation. For 1,1'-Binaphthyl-2,2'-diamine , the only guest included was dimethylacetamide (DMA). Thus these six guests only will be the subject of the study in this project.

EXPERIMENTAL

EXPERIMENTAL METHODS AND MATERIALS

2.1 Materials

2.1.1 Host compounds

All the hosts used in this study were 1,1'-binaphthyl-2,2'-derivatives.

a. 1,1'-binaphthyl-2,2'-dicarboxylic acid, abbreviated as BNDA in this study, (molecular formula: $C_{22}H_{14}O_4$, Mol wt: 342.34 g mol^{-1}, mp 276-277 ^oC) was obtained from Professor Edwin Weber from the Institute for Organic Chemistry, Freiberg, Germany.
b. 1,1'-Binaphthyl-2,2'-diol, abbreviated as BINOL in this study (molecular formula: $C_{20}H_{14}O_2$, Mol wt: 286.32 g mol^{-1}, mp 215-218 ^oC), was synthesized at the University of Cape Town, and obtained from the crystallographic laboratory of the University of Cape Town headed by Professor Nassimbeni.
c. 1,1'-Binaphthyl-2,2'-diamine, abbreviated as BINDIA in this study (molecular formula: $C_{20}H_{16}N_2$, Mol wt: 284.35 g mol^{-1}, mp 176-177 ^oC); was purchased from Sigma-Aldrich.

The purity of the host compounds was confirmed by differential scanning calorimetry and thermogravimetric analyses, and these host compounds were used in this study without further recrystallization.

2.1.2 Guest compounds

The guest compounds used for the experiments were *cyclohexylamine* (CHA), *dicyclohexylamine* (DCHA), *racemic-sec-butylamine*, *di-n-butylamine* (DBA), *diethylamine* (DEA) and *dimethylacetamide* (DMA) as they complex with the host compounds (Figure 2.1). The physical properties of the guests are summarised are in Table 2.1. All the guests were chemically pure (99 %), and were used without further distillation or purification.

Cyclohexylamine (CHA) and *dicyclohexylamine (DCHA)* were supplied by Fluka Analytical while *racemic-sec- butylamine* was supplied by Sigma Aldrich Chemical Co. *Di-n-butylamine* (DBA) was obtained from Saarchem and *diethylamine* (DEA) was acquired from BDH Chemicals Ltd. Chemical Co. *Dimethylacetamide* (DMA) was also obtained from Sigma Aldrich Chemical Co.

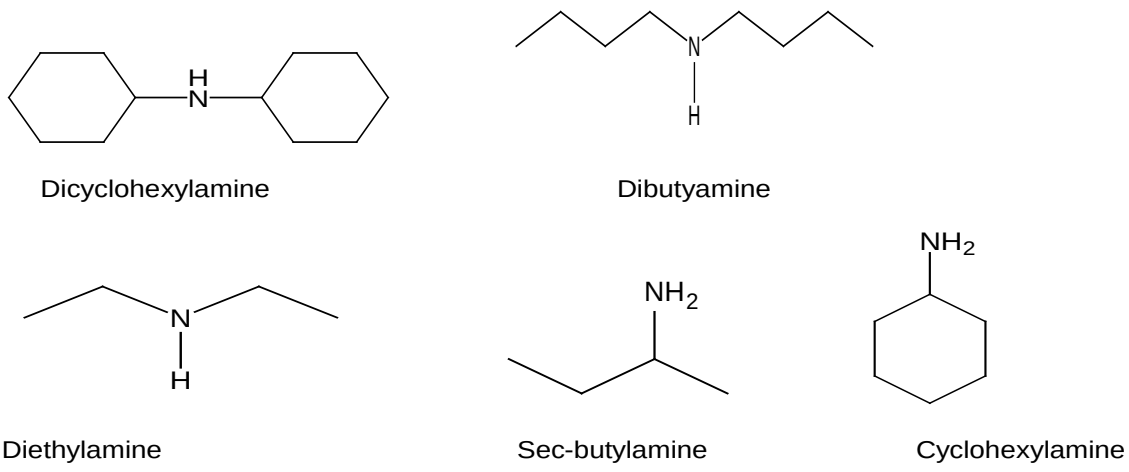

Dicyclohexylamine Dibutyamine

Diethylamine Sec-butylamine Cyclohexylamine

Figure 2.1 Schematic diagram of the selected guests.

Guest	**Formula**	**Mr (g mol^{-1})**	**Density**	**Bp (°C)**	**Mp (°C)**	**pK$_a$**
Diethylamine	$C_4H_{11}N$	73.14	0.707	55-56	-	11.25
Di-n-butylamine	$C_8H_{19}N$	129.24	0.760	137-177	-	11.39
Cyclohexylamine	$C_6H_{13}N$	99.18	0.865	134.5	-	10.64
Dicyclohexylamine	$C_{12}H_{23}N$	181.32	0.912	255-256	-	10.4
Racemic-sec- Butylamine	$C_4H_{11}N$	73.14	0.724	63	-	10.56
DMA	C_4H_9NO	87.12	0.708	165	-	

Table 2.1: Physical properties of the guest compounds studied

2.2 Methods

2.2.1 Crystal growth

The host compounds were insoluble in the liquid guests. A co-solvent was used to allow the dissolution of the host. In most cases, the co-solvent used was *methanol*, but *n-butanol* and *acetonitrile* were also used. The guest was taken in excess for all the preparations; in a separate vial the host was dissolved in the co-solvent. The two solutions were mixed, heated gently and allowed to cool at room temperature. The vials were covered with parafilm and left to crystallize.

2.2.2 Thermal analysis

The resultant precipitates were analysed using thermogravimetry (TG) and differential scanning calorimetry (DSC).

2.2.2.1 Thermogravimetry (TG)

Thermogravimetry (TG) measures the change in weight of a compound at a constant rate as a function of temperature or time. The resultant curves are referred to as mass loss curves. Thermogravimetric curves can be used to evaluate the number of decomposition stages, temperature ranges and fractional weight loss of each stage.[1]

Mass loss was determined by thermogravimetric analysis (TGA) using a Perkin-Elmer Pyris 6 system. A temperature programme of 303 K to 633 K at 10 K min^{-1} was used and the flow of nitrogen as a purge gas was set at 20 ml min^{-1}.

The crystalline samples, taken from the mother liquor, were carefully dried with filter paper, crushed and analysed at the set programme. The host: guest ratio were determined from the thermogravimetric curves.

2.2.2.2 Differential scanning calorimetry (DSC)

In differential scanning calorimetry, the sample and the reference material are exposed to a temperature programme and the heat flow is recorded as a function of time or temperature. The resultant curve is the DSC curve. The experiments were performed using a Perkin-Elmer Pyris6 system. The samples were scooped out of

the mother liquor, dried, crushed, weighed and analysed. A temperature programme similar to the one used in the TGA analysis was used to analyse the samples. A DSC curve (heat flow vs. temperature) was obtained and the onset temperatures (T_{on}) of various peaks were measured.

2.2.3 Single Crystal X-ray Diffraction

X-ray diffraction, as an analytical technique, determines crystal structures and atomic spacing. It gives unit cell dimensions, bond-lengths, bond-angles, and other information on the crystal. Crystal structures are solved by refining data obtained from X-ray analysis.[2]

X-ray crystallography is an experimental technique that exploits the fact that X-rays are diffracted by crystals. The technique relies on the fact that the atoms and their associated electron clouds in crystals form a three-dimensional grating whose spacings are comparable to the wavelength of the impinging radiation, which is approximately 1 Å, ($1x10^{-10}$ m).[3] The efficiency of X-ray crystallography has been improved due to the advances in technology. High power radiation sources that emit electromagnetic radiation by passing charged particles via magnetic fields have used as well as area detector data collection instruments. High speed computers have also contributed vividly in increasing the effectiveness of this technique.[4]

X-ray tubes or synchrotron radiation are used to generate the X-rays. A stationary or rotating solid target is bombarded with a focused electron beam that is accelerated across a high voltage field. A continuous X-ray spectrum is recorded as the electron beam collides with atoms in the target (crystalline material). The target gets ionized, the inner shell electrons are released and the free electron completes the shell causing an emission of an X-ray photon with energy that can be attributed to the target material. X-ray tubes that are frequently used are Copper (Cu) which emits 8 keV at 1.54 Å and Molybdenum (Mo) emitting 14 keV at 0.71 Å.[5]

Good quality, suitably sized crystals were selected for data collections. The crystals were coated with Paratone oil and mounted on a glass fibre. The crystal unit cell parameters were determined from intensity data measured on a Nonius Kappa CCD diffractometer or a Bruker DUO APEX 2 diffractometer. A Bruker K780 generator

was used to produce X-rays at 50 kV and 30 mA.[6] A 1.2 kW monochromated MoKα radiation of wavelength 0.7107 Å generated by a NONIUS FR590 generator was used. The operating parameters of the generator were 53 kV and 23 mA. Data were collected at room temperature (293-295 K) or at low temperature (173 K). Low temperature was achieved with a constant stream of nitrogen gas obtained from a Cryostream cooler (Oxford Cryostream, UK) at a flow rate of 20 mL min^{-1}. Intensity data were collected by the standard phi scan and omega scan techniques. The data was scaled and reduced using the Denzo-SMN[7,8] program for Nonius Kappa CCD. For the Bruker APEX 2 data, the cell refinement and data reduction was achieved by using the program SAINT.[9]

The graphical user interface X-SEED[10] which runs SHELXS-97[11] was used to solve crystal structures. The structural models were performed by the SHELXL-97[11] program which uses full-matrix least-squares minimisation of the function:

$$\left(\sum w\left(F_0^2 - kF_c^2\right)^2\right).$$

The agreement between the observed (F_0) and the calculated(F_c) structure factors are monitored by the residual R, which is the indirect measure of the accuracy of the structure. The residual index R_1 is the agreement between the observed and the calculated structure factors based on F (Eq. 1), while the residual index wR_2 is the agreement based on F^2, (Eq. 2).

Both, R_1 and wR_2 indices should be low if the model is satisfactory

$$R_1 = \frac{\sum \left\| F_0 \right| - \left| F_c \right\|}{\sum \left| F_0 \right|} \qquad \text{Eq. 1}$$

$$wR = \sqrt{\frac{\sum w\left(F_0^2 - F_c^2\right)^2}{\sum w\left(F_0^2\right)}} \qquad \text{Eq. 2}$$

w is the weighting scheme which was refined for each structure to yield a constant distribution in terms of a and b.

$$w = \frac{1}{\sigma^2 F_0^2 + (aP)^2 + bP} \qquad \text{Eq. 3}$$

$$\text{where } P = \frac{\max(0, F_0^2) + 2F_c^2}{3} \qquad \text{Eq. 4}$$

and a and b were also refined for each structure.

The goodness of fit was determined for each structure and is based on F^2. It is expressed as Eq. 5.

$$S = \left(\frac{\sum w(F_0^2 - F_c^2)^2}{n - P} \right)^{\frac{1}{2}} \qquad \text{Eq.5}$$

where n is the number of reflections and P is the total number of parameters refined.

2.2.4 Computing Components

PovRay renders graphics for structures.[12,13]

LAYER: displays intensity data as simulated precession photographs of the reciprocal lattice levels and allows for the investigation of the systematic absences which occur.[13]

LAZY PULVERIX: This software calculates the theoretical powder X-ray diffraction pattern from single crystal X-ray diffraction data.[13, 14]

POVLabel is utilized to edit the atomic labels of POV-Ray images.[16,17]

OLEX2: It is used to analyse the molecular conformations in the crystal structures and in particular calculate dihedral angles between planes .[18]

ConQuest: search engine used to explore the Cambridge Structural Database for information.[19]

CCDC Mercury: This structural software provides all-purpose and highly developed functionality for inspecting crystal structures. It can import chemical bond types from

2D connection tables and present them in 3D illustration. Most importantly it has the capability to locate, build and display networks of inter- and intramolecular non-covalent bonds. It has options for presenting numerous structures at once and performing least-squares overlay of pairs of structures.[20] It can be also used to calculate the void spaces occupied by the guests in structures.

2.2.5 Powder X-ray Diffraction

This is a quick analytical procedure principally employed for phase identification of a crystalline material. This technique can be used to acquire information on unit cell dimensions.[21] This method obtains its name from the fact that the sample is in the form of microcrystalline fine particles. About a century ago, diffraction patterns were recognized as a possible means of phase identification but a systematic means of unravelling the superimposed diffraction patterns was achieved only decades later. [22] A collection of indiscriminately oriented polycrystallites is exposed to the X-ray beam. Each of these polycrystallites causes its own diffraction pattern and individual spots on a film are spread into rings of diffracted intensity. A point or 1-D area detector is scanned across a narrow strip of the rings for measurement. A plot of total diffracted intensity against the diffracted angle, 2θ is used to represent the diffraction data.[23]

Samples were manually ground and placed in a sample holder in the path of the X-ray beam. The intensities were measured on a Hüber Imaging Plate Guinier Camera 670 using nickel-filtered CuKα_1 (1.5409 Å) radiation produced at 40 kV and 20 mA by a Philips PW1120/00 generator fitted with a Hüber long fine-focus tube PW2273/20 and a Hüber Guinier monochromator Series 611/15. The data for all experiments were determined at 298 K.

2.2.6 Kinetics

Desolvation kinetics of the solid samples was performed using thermal analytical methods[1,11] by measuring a sample property as it is heated (non-isothermal analysis) or held at a constant temperature (isothermal analysis). Thermogravimetric

techniques were used to study the kinetics of desolvation. The crystals were crushed prior to analysis to minimize the effect of the sample size distribution and particle morphology on the kinetics results. Experimental variation can't be totally eliminated. For example, sample mass may vary from one run to the next and affect a reaction (diffusion rates, thermal gradients). Sample packing could affect solid reaction kinetics and consequently a thermogram can be altered such that it falls above or below the expected thermogram for isothermal studies. This can bring about errors in the calculated kinetic parameters obtained from some isoconversional methods. When a solid sample is heated, many transformations may occur: melting, sublimation, polymorphic transformation, desolvation or degradation.[24]

Desolvation of the crystal is a solid state process of type below

$$A\ (s) \rightarrow B\ (s) + C\ (g)$$

The desolvation kinetics of such a reaction can be described by various equations and models taking the special features of their mechanism into account. The reaction rate which is the rate of the degradation of A (solid) can be calculated as follows:

$$\mathbf{d\alpha/dt = kf(\alpha)} \qquad (1)$$

with A(solid) the crystal, B and C the products formed, α is the extent of conversion of the compound at time t and k is the rate constant or reaction rate.

The constant k for a process is assumed to obey the Arrhenius equation.[25]

$$\mathbf{k = Ae^{-Ea/RT}} \ (2)$$

where A is the frequency or the pre-exponential factor , T is the absolute temperature, R is the gas constant, and E_a is the activation energy of the reaction, Substitution of Eq . (2) into Eq . (1) yields the following relationship:

$$\mathbf{d\alpha/dt = Ae^{-Ea/RT}f(\alpha)} \qquad (3)$$

When the temperature increases at a constant rate ,

$$\mathbf{dT/dt = \beta} \qquad (4)$$

Therefore

$$d\alpha/dT = A/\beta \times e^{-Ea/RT} f(\alpha) \qquad (5)$$

The kinetic conversion functions f(α) and g(α) for a solid-state reaction represent mathematical expressions of the kinetic model in the differential and integral forms respectively.

Models and mechanisms in solid-state kinetics

A model is a theoretical, mathematical expression which describes a particular reaction type which occurs experimentally. Several decomposition models for solid state reactions exist.[26-28]

-These models depend on factors such as rate of nuclei formation, interface advancement, diffusion, and/or geometrical shape of solid particles.

-There are models based on certain mechanistic underlying assumptions. Other models are more empirically based and their mathematics facilitates data analysis with less mechanistic meaning.[26]

- Nucleation
- Geometrical contraction
- Diffusion
- Reaction order

The interpretation of the mechanism in solid state kinetics usually involves identifying a reasonable reaction model because information about individual reaction steps is often difficult to obtain. The most accurate model is assumed to be the one which produces activation energy closest to that from the isoconversional analysis. This approach allows one to select models that might otherwise be indistinguishable based on the quality of regression fit alone.

Therefore, the strengths of both methods are used in the evaluation of solid-state kinetics to obtain A and E_a values as well as the best model.

Depending on the reaction mechanism, the most frequently cited kinetic models and their algebraic expressions are summarized in Table 2.2.

Designation of the model	f(α)	g (α)
Random nucleation	$1-\alpha$	$-\ln(1-\alpha)$
Generalized nth order	$(1-\alpha)^n$	$1/n\ [1-(1-\alpha)^{n-1}]$
Power law	$(2\alpha)^{1/2}$	$(\alpha)^{1/2}$
Power law	$(3\alpha)^{2/3}$	$(\alpha)^{2/3}$
Power law	$(4\alpha)^{3/4}$	$(\alpha)^{3/4}$
1D or 2D Avrami-Erofeyev	$2(1-\alpha)[-\ln(1-\alpha)]^{1/2}$	$[-\ln(1-\alpha)]^{1/2}$
2D or 3D Avrami-Erofeyev	$3(1-\alpha)[-\ln(1-\alpha)]^{2/3}$	$[-\ln(1-\alpha)]^{1/3}$
3D Avrami-Erofeyev	$4(1-\alpha)[-\ln(1-\alpha)]^{3/4}$	$[-\ln(1-\alpha)]^{1/4}$
Prout Tomkins	$\alpha\ (1-\alpha)$	$\ln [\alpha/(1-\alpha)]$
Contracting area	$2(1-\alpha)^{1/2}$	$2\ [1-(1-\alpha)^{1/2}]$
Contraction volume	$3(1-\alpha)^{1/3}$	$[1-(1-\alpha)^{1/3}]$
Generalized model of Sestak	$(1-\alpha)^n\ \alpha^m$	-
One dimensional diffusion	$1/2\alpha$	$(\alpha)^2$
Two dimensional diffusion	$[-\ln(1-\alpha)]-1$	$[(1-\alpha)\ln(1-\alpha)]+\alpha$
Three dimensional diffusion Jander	$3(1-\alpha)^{2/3}+[1-(1-\alpha)^{1/3}]$	$[1-(1-\alpha)^{1/3}]^2$
Three dimensional diffusion Ginstling-Brounshtein	$[3/2(1-\alpha)^{-1/3}-1]$	$1-(2\alpha/3)-(1-\alpha)^{2/3}$
Zero order	1	α
First order	$1-\alpha$	$-\ln\ (1-\alpha)$
Second order	$(1-\alpha)^2$	$(1-\alpha)^{-1}-1$
Third order	$(1-\alpha)^3$	$0.5(1-\alpha)^{-2}-1$

Table 2.2[26] Typical physico-geometric kinetic model functions for treating the conversion (α, fraction reacted) versus time data for solid state reactions.

Methods for studying solid-state kinetics

There are many methods used to study solid-state kinetics. These methods can be generally grouped into two categories – experimental and computational; the methods are summarized in Figure 2.2.

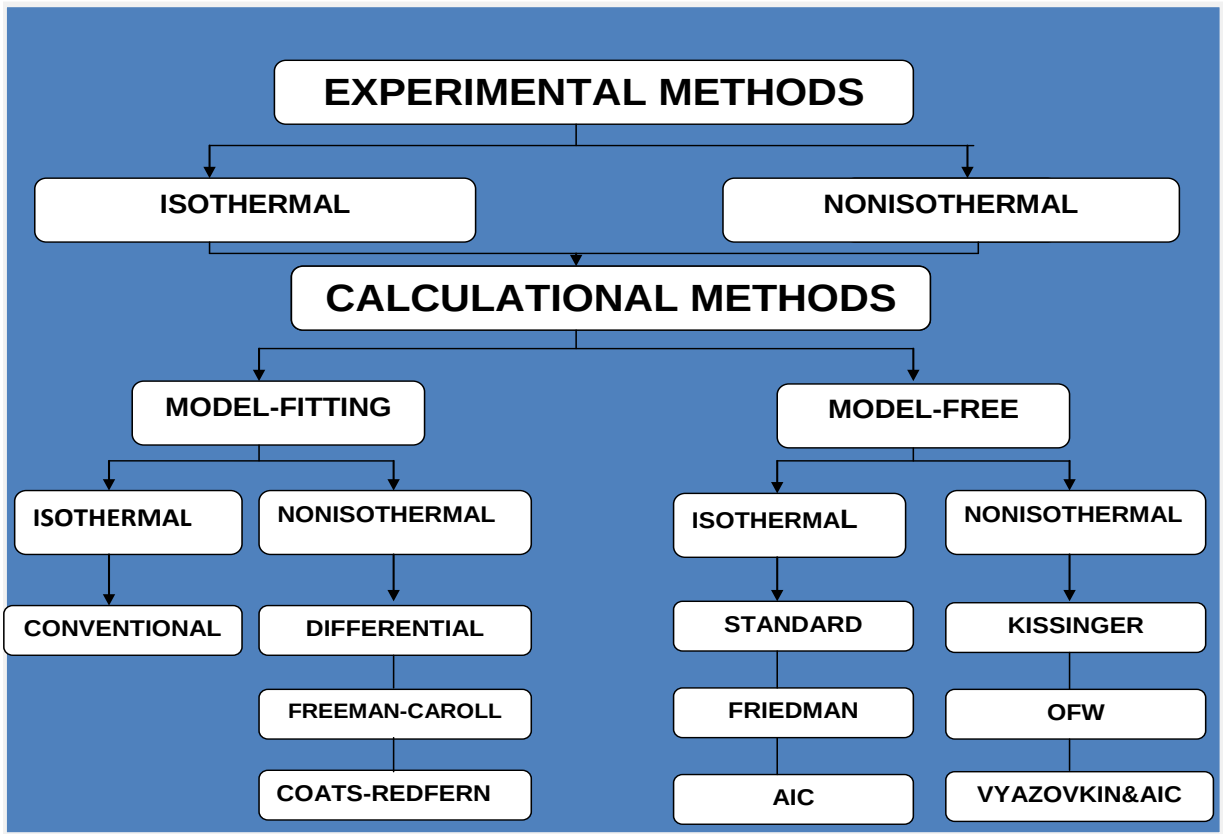

Figure2.2[26] Methods for studying solid-state kinetics

Experimental methods

Experimentally, we use two protocols to obtain solid-state kinetic data for thermal analysis: isothermal and non-isothermal methods.

For isothermal methods, reactions are carried out at several constant temperatures while in non-isothermal methods, the samples are heated at constant heating rates.

Calculation methods[29]

Two groups of methods used to analyze both isothermal and non-isothermal solid-state kinetic data are model-dependent and model-free methods.

Model-fitting methods[27]

For these methods, different models are fitted to the data and the model giving the best statistical fit is chosen as the model of choice from which the activation energy (E_a) and frequency factor (A) are calculated.

- Isothermal model-fitting methods (Conventional method)

This method is identical to that in homogenous phase kinetics. It involves two steps: the first, determines the rate constant (k) of the model that best fits the data according to Eq. (13), while the second determines specific kinetic parameters, the activation energy (Ea) and frequency factor (A) using the Arrhenius equation (Eq. (2)).

- Non-isothermal model-fitting methods

Many model fitting methods extract the three kinetic parameters known as the kinetic triplet (A, E_a and model) from non-isothermal data. These methods have been critically evaluated and it's been shown that the sole use of these methods is not recommended because:

1. They assume a constant kinetic triplet (A, E_a and model).
2. They involve fitting three parameters (A, E_a and model) which are determined from a single run (i.e. one heating rate).
3. They involve a single heating rate which is not always sufficient to determine reaction kinetics.

Direct differential method

This method uses the differential form of the non-isothermal rate law (Eq. (5)) by numerically calculating the differential $d\alpha/dT \approx \Delta\alpha/\Delta T$

Taking the logarithm of the non-isothermal rate law, Eq. (5) gives:

$$\ln (d\alpha/dT)/f(\alpha) = \ln A/\beta - E_a/RT \quad (6)$$

Plotting the left-hand side (including the model f(α)) versus 1/T gives the activation energy (E_a) and frequency factor (A) from the slope and intercept, respectively.

The model that gives the best linear fit is usually chosen as the model.

Freeman–Carroll (difference-differential) method

The Freeman and Carroll method is a differential method that was originally developed assuming a reaction-order model ($f(\alpha) = (1-\alpha)^n$). Taking the natural logarithm of the differential form of the non-isothermal rate law (Eq. (5)) gives,

$$\ln (d\alpha/dT) = \ln A/\beta - E_a/RT + \ln f(\alpha) \quad (7)$$

If incremental differences in the variables of Eq. (7) are taken, we obtain:

$$\Delta \ln (d\alpha/dT)/f(\alpha) = \Delta \ln f(\alpha) - E_a/R \Delta 1/T \quad (8)$$

Equation (8) can be rearranged to,

$$\Delta[\ln (d\alpha/dT)/f(\alpha)]/ [\Delta \ln f(\alpha)] = E_a/R \text{ X } \Delta(1/T)/\Delta f(\alpha) \quad (9)$$

The activation energy can be obtained by plotting the left-hand side of Eqs. (8) and 9) versus 1/T.

Model-free/isoconversional methods

Model-free methods calculate the reaction activation energy (E_a) without using terms such as the frequency factor (A) and model.

Isoconversional methods are model-free methods that evaluate kinetic parameters, namely the activation energy (E_a) at progressive conversion values. These methods require several kinetic curves to perform the analysis and have therefore been called, “multi-curve” analyses. Calculations from several curves at different heating rates are performed on the same value of conversion (α), thus, the name isoconversional. As a result, these methods calculate the activation energy for each conversion point (E_a, α), resulting in an isoconversional plot (E_a vs. α).

Isothermal isoconversional methods

These include the Standard and Friedman’s isoconversional method and have been used in the Ozawa and Flynn-Wall methods.

2. A non-linear approximation (more accurate) utilizing the Senum-Yang approximation has been used in the Vyazovkin method.

Ozawa, Flynn and Wall (OFW) method

This method is based on the representation of the degradation reaction by power law kinetics. It utilises the Doyle approximation to evaluate the integrated form of the rate equation and yields eq. (10) as an approximate solution. Assuming E_a/RT, it can be obtained:

$$\log(\beta) = \log AE_a/g(X)R - 2.315 - 0.4567\,E_a/RT \qquad (10)$$

where g(X) represents the weight loss function. E_a is obtained from a plot of log (β) versus 1/T for fixed degrees of conversion and the slope of the line is given by $-0.4567E_a/R$. By reducing the above equation, $d \log \beta/d(1/T) \approx (0.457/R)\,E_a$ is obtained. A plot of log β vs. 1/T yields a straight line with slope $-(0.457\,E_a)/R$.

2.2.7 Kinetics of absorption

Perfect crystals in reality are not common; most crystal lattices contain imperfections. The imperfection sites have higher free energy therefore are highly reactive.[28] Solid state kinetics occurs in different models such as nucleation, geometrical contraction, reaction order and diffusion. However the most common models are the reaction order and geometrical contraction (contracting volume and contracting area). Reaction-order models were derived using concepts applicable to gas and solution reactions. The rate of reaction is assumed to be proportional to a function of the concentration of the reactants. Order based models are from the general formula equation (Eq. 11) below.

$$\frac{d\alpha}{dt} = k(1-\alpha)^n \qquad \text{Eq. 11}$$

where $d\alpha/dt$ is the rate of reaction, k is the rate constant and n is the reaction order. For a first order reaction the integral expression below (Eq. 12) is obtained.

$$-\ln(1-\alpha) = kt \qquad \text{Eq. 12}$$

The integral expressions for contracting area and contracting volume are represented by Eq. 13 and Eq. 14 respectively.[30]

$$\left[1-(1-\alpha)^{\frac{1}{2}}\right] = kt \qquad \text{Eq. 13}$$

$$\left[1-(1-\alpha)^{\frac{1}{3}}\right] = kt \qquad \text{Eq. 14}$$

REFERENCES

1. Haines, P. J. (1995). *Thermal Methods of Analysis, Blackie Academic & Professional*, London.

2. Brown P. J. & Forsyth, J. B. (1973), *The crystal structure of solids*, Edward Arnold Limited, London.

3. Lambert, J. B., Shurvell, H. F., Verbit, L., Cooks, R. G. & Stout, G. H. (1976), *Organic Structural Analysis*, Macmillan Publishing Co., New York.

4. Rissanen, K. (2004), *X-Ray Crystallography, Encyclopedia of Supramolecular Chemistry*, Ed: Atwood, J. L. & Steed, J. W., Vol. 2:1586-1591

5. Birkholz, M. (2006) *Thin Film Analysis by X-Ray Scattering*. WILEY-VCH Verlag GmbH & Co. KGaA, Weinheim.

6. COLLECT (1998), *data collection software, Nonius*, Delft, The Netherlands.

7. APEX 2 (2005), *Version 1.0-27 Bruker AXS Inc*, Madison, Wisconsin.

8. Otwinowski, Z. & Minor, W. (1997), *Methods in Enzymology, Macromolecular Crystallography Part A*, Carter, C. W. and Sweet, R. M., (Eds), Academic Press, New York, 276:307-326.

9. Program SAINT, (2006), *Version 7,60a, Bruker AXS Inc*., Madison, WI, USA.

10. Barbour, L. J. (2003), *X-Seed, Graphical interface for SHELX program, Journal of Supramol. Chem.*, Vol. 1:189.

11. Sheldrick, G. M. (2008), *A short history of SHELX, Acta Crystallographica Section A*:112-122.

12. Heldrick, G. M. (1997*), Program for Crystal Structure Determination*, University of Göttingen, Germany.

13. Pov-Ray for windows, (1991-1999), *Version 3.1e.watcom.win32, The persistence of vision development team.*

14. Barbour, L. J. (1999), LAYER, *A computer program for the graphic display of intensity as simulated precession photographs, J. Appl. Cryst*. Vol.32:351.

15. Yvon, K., Jeitschko, W. & Parthé, E. (1977), *LAZY PULVERIX, a computer program, for calculating X-ray and neutron diffraction powder patterns, J. Appl. Cystallogr.* Vol.10: 73-74

16. Connolly, M. L. (1993), *The molecular surface package , J. Mol. Graphics*, Vol. 11: 139–141.

17. Barbour L. J. (2001), *X-Seed - A Software Tool for Supramolecular Crystallography, Journal of Supramolecular Chemistry, Vol*. 1:189-191.

18. Guzei,I.A. (2012). *Notes on olex2*.

19. ConQuest, (2001), *A program for the search of the CSD, Version 1.7*.

20. Allen, F. H. & Lipscomb, K. J. (2004), *The Cambridge Structural Database, Encyclopaedia of Supramolecular Chemistry,* Ed: Atwood, J. L. & Steed, J. W., Vol. 1:161-168.

21. Karki, S., Fábián, L., Friščić, T. and Jones, W. (2007), *Powder X-ray Diffraction as an Emerging Method to Structurally Characterize Organic Solids, Organic Letters*, Vol. 9:3133-3136

22. Jenkin, R. (2000), *X-ray Techniques: Overview, Encyclopedia of Analytical Chemistry*, pg. 13269–13288, R.A. Meyers (Ed.), John Wiley & Sons Ltd, Chichester.

23. Evans, J. S. O. (2004) *X-ray and Neutron powder diffraction, Encyclopedia of Supramolecular Chemistry,* Ed: Atwood, J. L. & Steed, J. W., Vol. 2:1592-1598.

24. Brown, M.E. (1988). *Introduction to thermal analysis: Techniques and applications*, Chapman and Hall, London, pp. 127-151.

25. Laidler, K.J.J. (1984), *Chem. Educ*. 61: 494-498.

26. Jacobs, P.W.M. and Tompkins,F.C. (1955). *Classification and theory of solid reactions*. In W. E. Garner (ed), *Chemistry of the solid state*, Academic Press, New York, pp. 184-212.

27. Brown, M.E. (1980). Dollimore D and Galwey AK. *Theory of solid state reaction kinetics.* In C. F. H. Tipper (ed), *Chemical kinetics*, Elsevier, Amsterdam, pp. 41-72.

28. Galwey A.K. and Brown M.E. (1999). *Thermal decomposition of ionic solids: Chemical properties and reactivities of ionic crystalline phases*, Elsevier, Amsterdam,pp. 75-115.

29. Khawam, A. & Flanagan D. R., (2006) *Basics and Application of Solid-State Kinetics: A Pharmaceutical Perspective, Journal of Pharmaceutical Science*, Vol. 95:472-498.

30. Khawam, A. & Flanagan D. R., (2006) *Solid-State Kinetics: Basics and Mathematical Fundamentals, Journal of Physical Chemistry B,* Vol

CHAPTER III SALTS OF 1,1'-BINAPHTHYL-2,2'-DICARBOXYLIC ACID

In this chapter the salts formed with racemic 1, 1'-binaphthyl-2,2'-dicarboxylic acid (BNDA) and selective amines were studied. Three subchapters will be discussed:

- *III.1. Salts formed between racemic 1,1'-binaphthyl-2,2'-dicarboxylic acid with acyclic secondary aliphatic amines.*
- *III.2. Salts formed between racemic 1,1'-binaphthyl-2,2'-dicarboxylic acid with cyclic aliphatic amines.*
- *III.3. Salts formed between racemic 1,1'-binaphthyl-2,2'-dicarboxylic acid with racemic amines.*

CHAPTER III SALTS OF 1,1'-BINAPHTHYL-2,2'-DICARBOXYLIC ACID

III.1 Salts of 1,1' binaphthyl-2,2'-dicarboxylic acid with acyclic secondary aliphatic amines

The salts of **(BNDA^{2-})(*DEA*$^{+}$)$_2$** and **(BNDA^{2-})(*DBA*$^{+}$)$_2$** were obtained by crystallizing BNDA with diethylamine (DEA) and dibutylamine (DBA) in methanol. The selectivity of the BNDA host for these two guests was studied by dissolution of the BNDA in an equimolar mixture of DEA and DBA. The binaphthyl host compound selected only dibutylamine. Dissolution of BNDA in a mixture of 60 % DEA and 40 % DBA resulted in a polymorph of **(BNDA^{2-})(*DBA*$^{+}$)$_2$** which will be referred to as **(BNDA^{2-})(*DBA$_2$*$^{+}$)$_2$.** The structures of **(BNDA^{2-})(*DBA*$^{+}$)$_2$** and **(BNDA^{2-})(*DBA$_2$*$^{+}$)$_2$** were solved in the triclinic space group P-1 with Z=2. **(BNDA2^{-})(*DEA*$^{+}$)$_2$** was solved successfully in the monoclinic crystal system, space group *C*2/c with Z = 4. All the three structures were obtained at room temperature. The crystal data is shown in **Table 3.1.1.**

Compound	**(BNDA^{2-})(DEA^{+})$_2$**	**(BNDA^{2-})(DBA^{+})$_2$**	**(BNDA^{2-})(DBA$_2$$^{+}$)$_2$**
Molecular Formula	$(C_{22}H_{12}O_4^{2-})(C_4H_{13}N^{+})_2$	$(C_{22}H_{12}O_4^{2-})(C_8H_{21}N^{+})_2$	$(C_{22}H_{12}O_4^{2-})(C_8H_{21}N^{+})_2$
Molecular Mass (gmol^{-1})	490.6	600.8	600.8
Data collection temp. (K)	173(2)	173(2)	173(2)
Crystal system	Monoclinic	Triclinic	Triclinic
Space group	C2/$_c$	P-1	P-1
a (Å)	17.4(4)	9.5(2)	11.8(1)
b (Å)	11.4(2)	12.4(3)	12.3(1)
c (Å)	13.7(3)	15.4(3)	13.3(2)
α (°)	90.00	81.6(3)	64.6(2)
β (°)	92.4(3)	79.5(3)	86.6(2)
γ (°)	90.00	75.4(3)	83.6(2)
Volume (Å^3)	2715.7(9)	1725.9(19)	1743.4(6)
Z	4	2	2
D_c, Calculated density (g cm^{-3})	1.1950	1.1560	1.1444
Final R indices [I>2sigma(I)]	R_1= 0.0512 wR_2=0.0982	R_1= 0.0516 wR_2=0.1339	R_1= 0.0443 wR_2=0.1007
R indices (all data)	R_1= 0.0406 wR_2=0.1052	R_1= 0.0432 wR_2=0.1216	R_1= 0.0513 wR_2=0.1610
Largest diff. peak and hole (eÅ^{-3})	0.24; -0.19	0.24; -0.20	0.42; -0.31

Table 3.1.1 Crystal data table of the salts formed between BNDA with acyclic secondary aliphatic amines.

1**. $(BNDA^{2-})(DEA^{+})_2$**

Compound name: Di-*n*-ethylammonium-1,1'-binaphthyl-2,2'-dicarboxylate

Formula: $(C_{22}H_{12}O_4^{2-})(C_4H_{12}N^{+})_2$

Asymmetric unit:

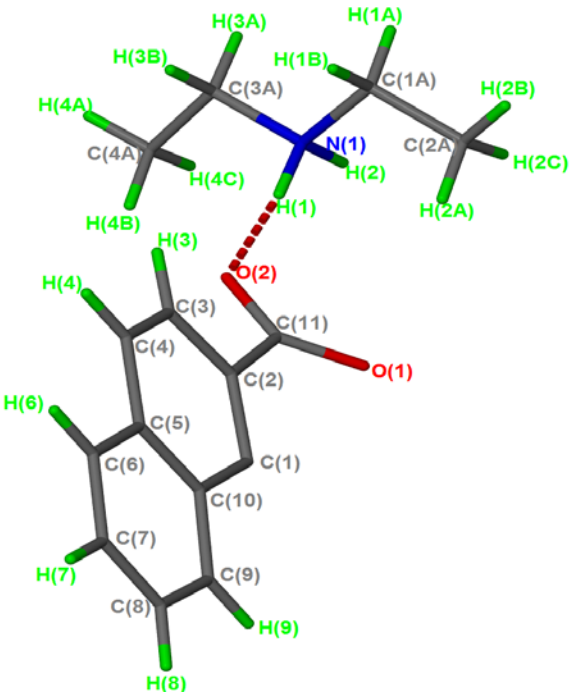

Figure 3.1.1 Asymmetric unit of **$(BNDA^{2-})(DEA^{+})_2$**

Crystal structure and refinement

The crystal structure of **$(BNDA^{2-})(DEA^{+})_2$** was solved in the monoclinic crystal system, space group C2/c. The asymmetric unit consists of half an anion of $BNDA^{2-}$ and one cation of DEA^{+}, which corresponds to a host: guest ratio of ½:1.

The crystal structure was solved by direct methods. The non-hydrogen atoms were found in the difference electron density map. All non-hydrogen atoms of the host and the guest were refined anisotropically. All hydrogen atoms not involved in hydrogen bonding were placed with geometric constraints and allowed to refine isotropically. Aromatic hydrogens were fixed at a distance of C-H = 0.95 Å and the -CH_3 and -CH_2 hydrogens were fixed with C-H = 0.98 Å. The N-H hydrogens of the cation were found in the difference electron density map and allowed to refine isotropically. By calculating the difference ΔD_{CO} of the BNDA, we found that it is equal to 0.005, value showing that the crystal yielded with BNDA and DEA is a salt.[1]

This is explained by location of two possible peaks of hydrogens for the nitrogen atom of DEA, one with the N-H distance of 0.977 Å and the other at 0.943 Å. The naphthyl fragments are nearly perpendicular to each other and the dihedral angle between the naphthyl moieties was calculated with the program Olex2[2] and gives an angle of 79.7°(2). This value doesn't falls in the narrow range (81.4−98.1) found for BNDA and its inclusion compounds studied previously.[3] The distance between the two plane-centroid is equal to 4.585 Å. The structure refined successfully to R_1= 0.0459 with wR_2 = 0.1201.

Crystal packing

The packing diagram of **$(BNDA^{2-})(DEA^{+})_2$** is shown in **Figure 3.1.2.** The unit cell contains four anions of BNDA and eight cations of DEA with each host anion situated on a centre of symmetry at Wyckoff position *e*, while the guests are in general positions. Thus, this gives a Z equals to 4.

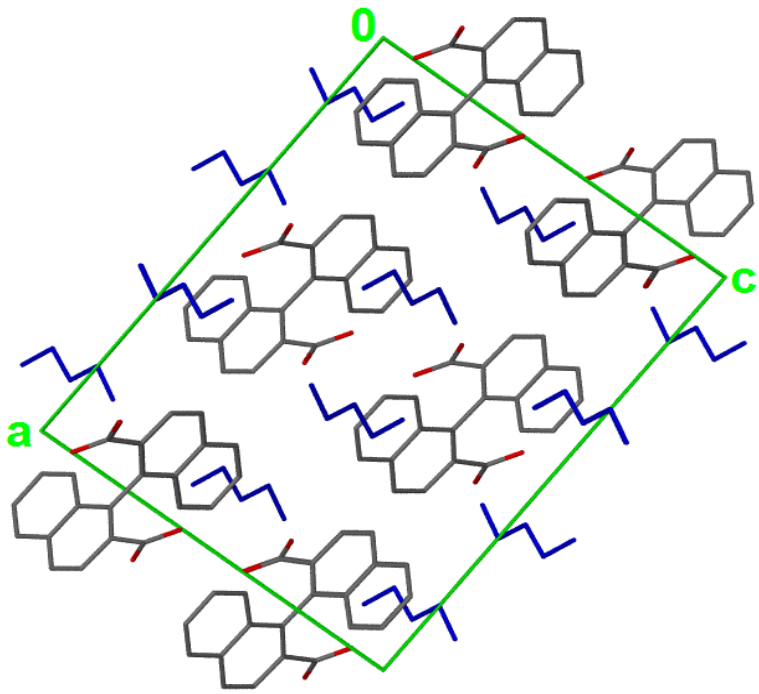

Figure 3.1.2 Packing diagram of **$(BNDA^{2-})(DEA^{+})_2$** viewed down [010] with hydrogen atoms omitted and DEA^{+} cations depicted in blue.

This structure has intersecting channels along [110] and [-110] as shown in **Figure 3.1.3**.

a b

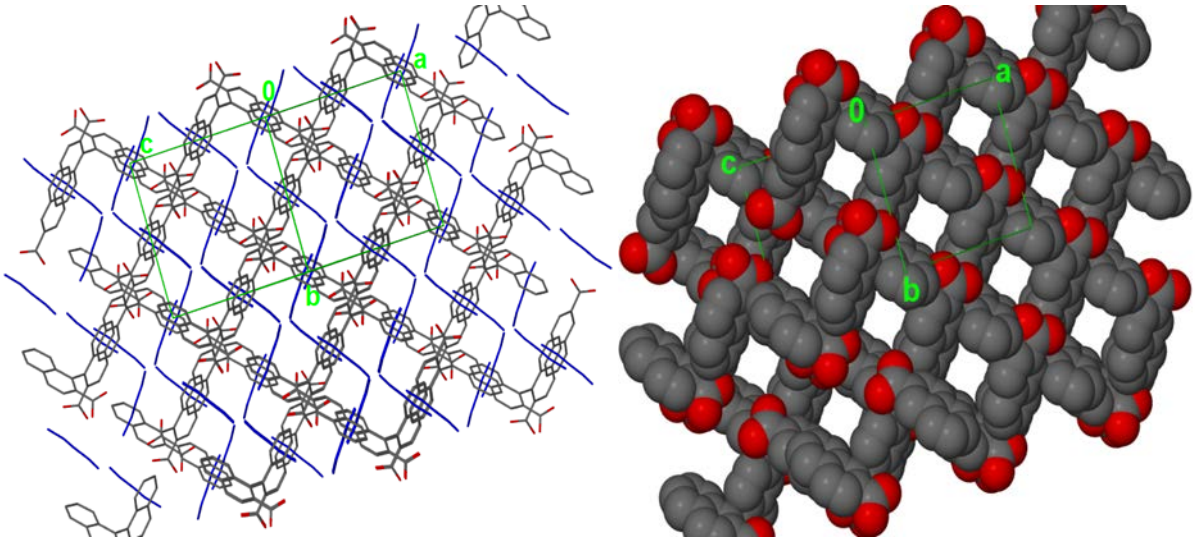

Figure 3.1.3 Packing diagrams for **$(BNDA^{2-})(DEA^{+})_2$** (a) where the guests are shown in blue and (b) with the host anions shown with van der Waals radii and the guests omitted to indicate the channels in which the guests reside. Hydrogen atoms are omitted.

The channels occupied by the guests were also visualised, using the program Mercury[4] (**Figure 3.1.4.).** This analysis was carried out with a probe radius of 1.5 Å.

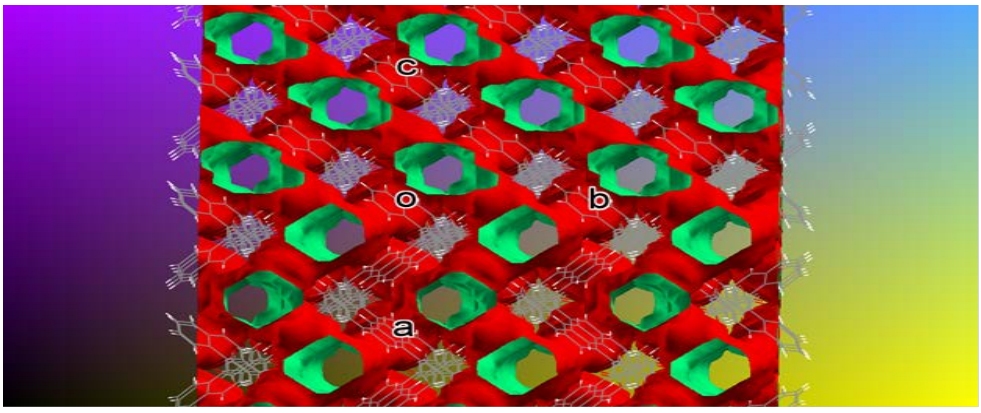

Figure 3.1.4 Channels occupied by the diethylammonium cations in **$(BNDA^{2-})(DEA^{+})_2$.**

The host anions and guest cations form hydrogen bonded rings involving the carboxylate anions and the $^{+}NH_2$ (guest) as can be seen in Figure 3.1.5. The hydrogen bonding pattern can be described as $N_2 = R_4^4(12)^5$. These host-guest rings are located in columns along the [001] direction as shown in **Figure 3.1.6.**

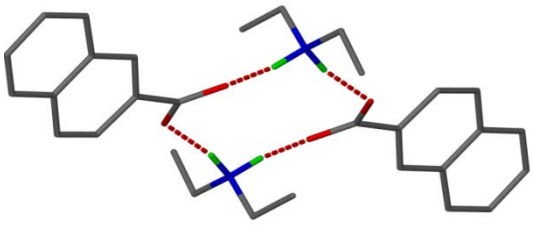

Figure 3.1.5 Hydrogen bonded rings for **(BNDA^{2-})(DEA^{+})$_2$**.

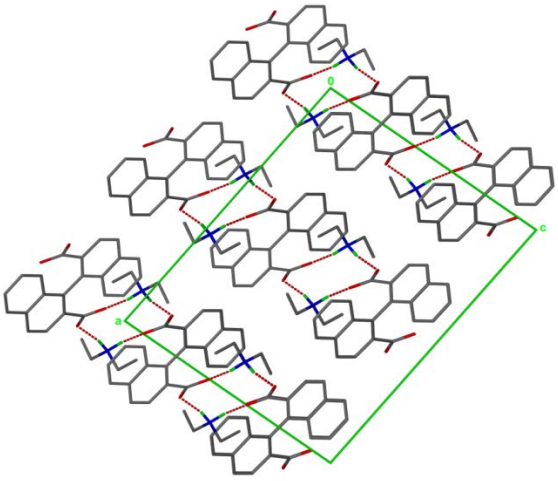

Figure 3.1.6 Hydrogen bonding interactions in **(BNDA^{2-})(DEA^{+})$_2$.**

The hydrogen bonding details appear in Table 3.1.2. The atom distances of O1•••N1 and O2•••N1 are 2.624(1) and 2.734(1) respectively. These interactions have similar strengths. The bond angles of N1—H2•••O1 and N1—H1•••O2 are 164°(1) and 170.7° (1) respectively.

These results indicated that the hydrogen bonding network in this salt complex is in such a way as to match the strongest donor and the strongest acceptor first.

D-H···A	d(D-H)(Å)	d (H···A)(Å)	<(DHA)(°)	d(D···A)(Å)	Symmetry operator
N1-H1···O2	0.955(2)	1.787(2)	170.74(1)	2.734(1)	[x,y,z]
N1-H2···O1	0.988(2)	1.661(2)	164.04(1)	2.624(1)	[-x+1, -y, -z]

Table 3.1.2 Hydrogen bonding details in **$(BNDA^{2-})(DEA^{+})_2$.**

Thermal analysis

The TGA and DSC traces of **$(BNDA^{2-})(DEA^{+})_2$** are shown in Figure 3.1.7. The DSC endotherm shows 3 peaks; the first one corresponds to the release of the first guest at T_{on} = 406.9 K and the second DEA is released at T_{on} = 511.6 K. The third peak which is broad appears at approximately 594 K and is due to the host melting.

The TG curve gave 2 mass losses: the first step of 13.8 % is due to the loss of one DEA guest. The second mass loss was difficult to determine because of the decomposition of the host which happens soon after the second guest has been released. The total mass loss expected for the two guests is 29.9%.

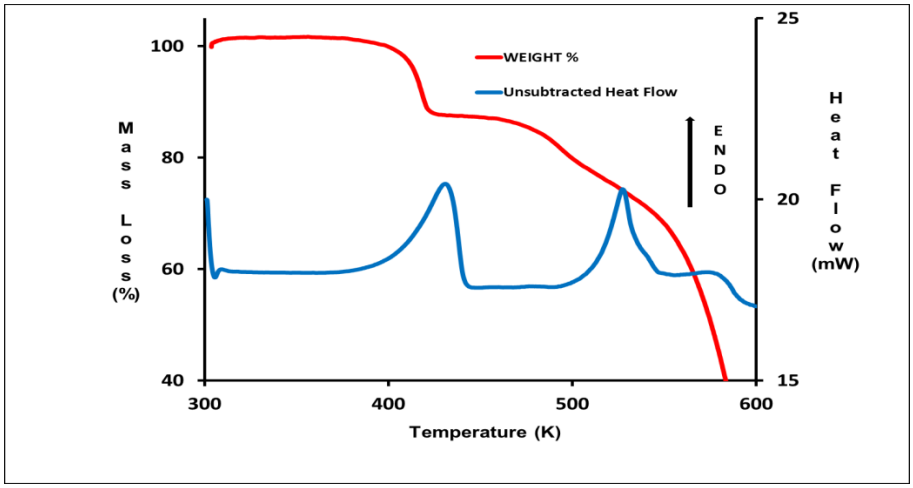

Figure 3.1.7 TG and DSC curves of **$(BNDA^{2-})(DEA^{+})_2$.**

	TG Results		
	Calc. % mass loss		**Exp. % mass loss**
mass loss 1	14.9(loss of 1 mol of DEA)		13.8
mass loss 2	14.8(loss of 1 mol of DEA)		Difficult to calculate the loss
	DSC Results		
	T_{on}(K): T_{Peak1}(K)	**T_{on}(K): T_{Peak2}(K)**	**T_{on}(K): T_{Peak3}(K)**
	406.0; 429.2	511.6; 552.2	573.1; 580.1

Table 3.1.3 Thermal analysis results of **$(BNDA^{2-})(DEA^{+})_2$.**

Hot stage analysis

A crystal of **$(BNDA^{2-})(DEA^{+})_2$** was observed using the hot stage microscope and photographs were taken at various temperatures during the heating process. The analysis is shown in **Figure 3.1.8.**

The crystal is stable up to 383 K and the guest release starts at 395 K. At 403 K the crystal becomes opaque. The crystal melts at 533 K.

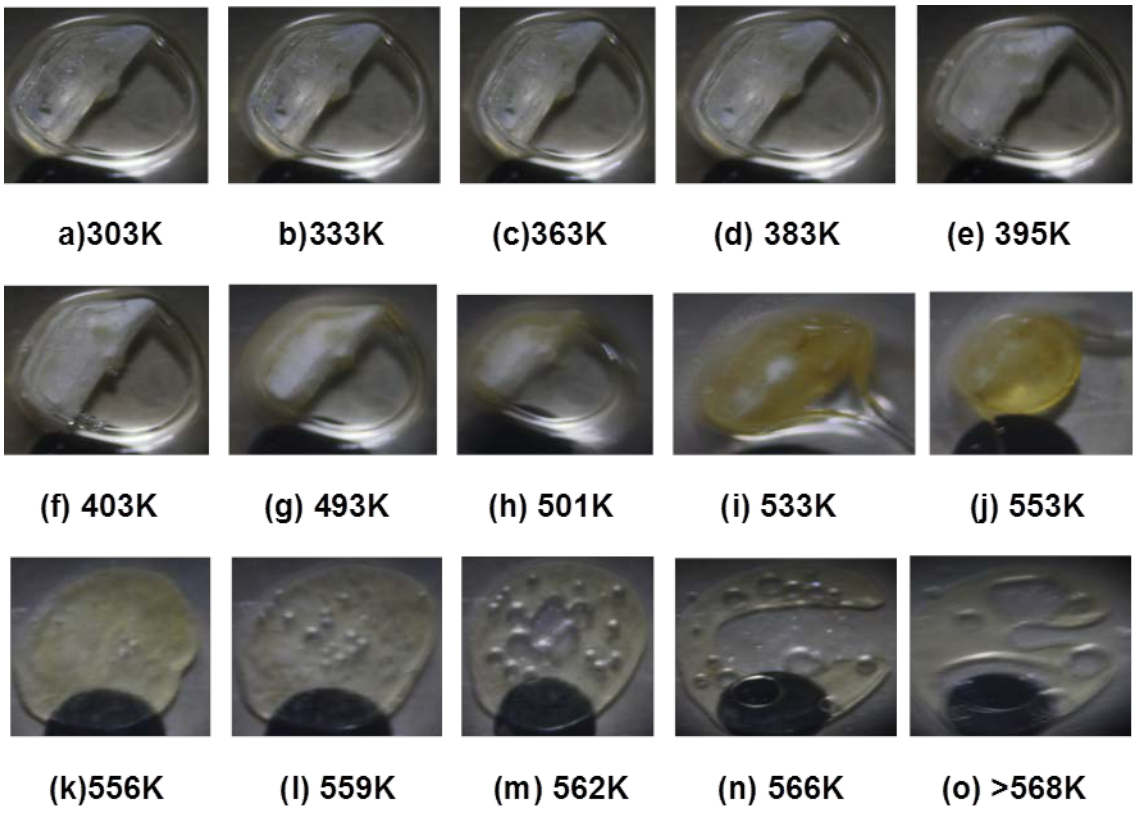

Figure 3.1.8 Thermal decomposition of the crystal of **$(BNDA^{2-})(DEA^{+})_2$.**

Kinetics of desolvation

By analysing the TGA curves a mechanism can be suggested for the desolvation reaction of **$(BNDA^{2-})(DEA^{+})_2$** as follows:

- First step: **$(BNDA^{2-})(DEA^{+})_2$** → $(BNDA^{-})(DEA^{+})$ + DEA
- Second step: $(BNDA^{-})(DEA^{+})$ → BNDA + DEA

A. Non-isothermal Kinetics

The first mass loss step was analysed using non-isothermal kinetics. The experiments were performed at heating rates of 1, 2, 10 and 16 K min^{-1}. The TG curves were converted to α - temperature plots represented in **Figure 3.1.9** and thereafter the curves were converted into plots of –log β vs 1/T as shown in **Figure 3.1.10.** Kinetic analyses were done from α equals to 10% to 60%.

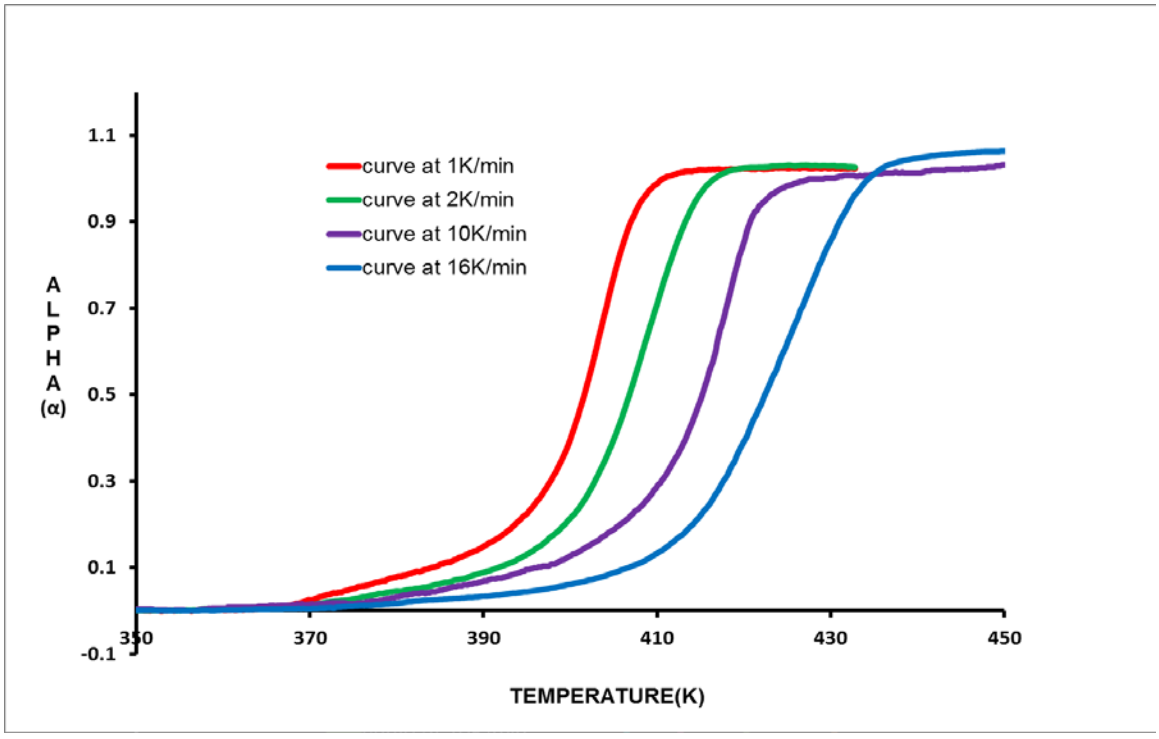

Figure 3.1.9 α versus Temperature plots for the first mass loss step **$(BNDA^{2-})(DEA^{+})_2$.**

From these non isothermal data, a model free calculation is done through the Ozawa–Flynn–Wall method[6,7] to obtain the activation energies for each α considered as reported on the **Figure 3.1.11.** The activation energy range for **$(BNDA^{2-})(DEA^{+})_2$** was 215.04 – 271.1 kJmol^{-1}.

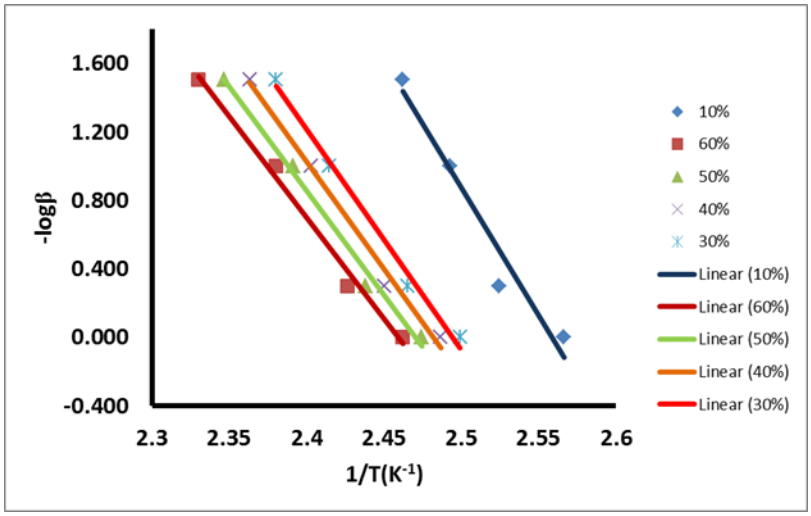

Figure 3.1.10 –log β vs 1/T plots for **$(BNDA^{2-})(DEA^{+})_2$,** first mass loss step.

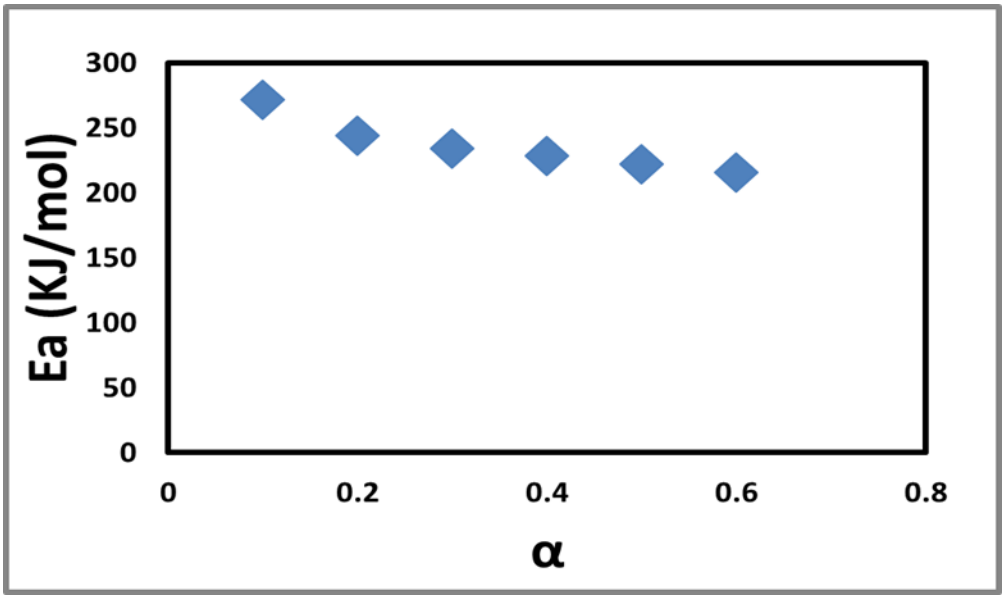

Figure 3.1.11 E_a - α plot for non-isothermal kinetics of **$(BNDA^{2-})(DEA^{+})_2$** desolvation evaluated by OWF method showing the range for non-isothermal kinetics

B. **Isothermal Kinetics**

The isothermal kinetics of desolvation for the first mass loss step of **$(BNDA^{2-})(DEA^{+})_2$** was also determined. Isoconversional methods[8] and mathematical reaction models[9] were used to determine the mechanism and the kinetic parameters (α, T, t) of the desolvation reaction.

- Isoconversional methods.

The isoconversional method used was the standard method.[10] It is also a model free method, similar to the OWF method but for isothermal data, in which activation energy is evaluated at progressive conversion values . This method was applied to the data obtained from isothermal TG curves **(Figure 3.1.12)** and the activation energies were recorded in **Figure 3.1.13.** The activation energy range is 138.8 to 223.5 kJ mol^{-1}.

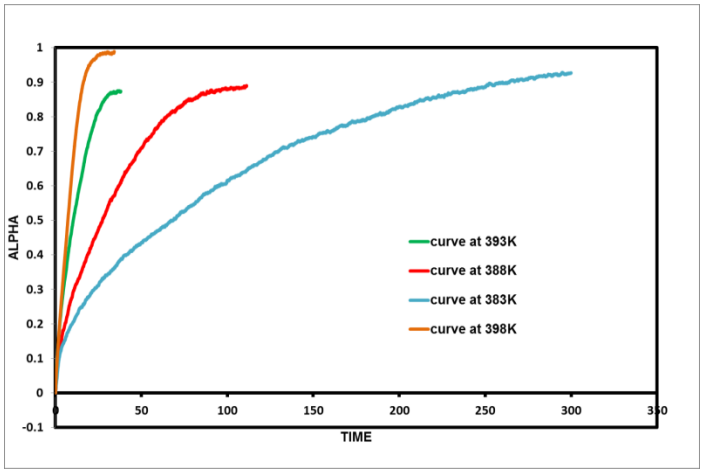

Figure 3.1.12 Isothermal TG curves of kinetic of **$(BNDA^{2-})(DEA^{+})_2$**

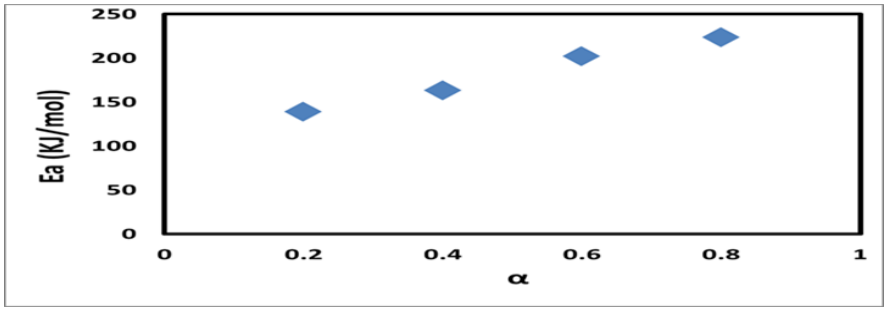

Figure 3.1.13 E_a versus α plot for isothermal kinetics of desolvation of **$(BNDA^{2-})(DEA^{+})_2$** evaluated by the standard method.

- Model-fitting method

The “model-fitting procedure” which is widely used to determine the kinetic reaction model for solid-state reactions, was used to determine the kinetic reaction model of the desolvation. [20] According to the model-fitting method, the kinetic model

of the desolvation process was determined by comparison (graphical and analytical) of the experimentally obtained function, *a*e = *f*(*t*N), to the theoretical functions for different solid state reaction models. Mathematical kinetic models fittings were performed on the isothermal data using different kinetic models to get the best fit for the experimental results. The histogram **(Figure 3.1.14)** shows the fitting of all the models in terms of percentage. These results showed that these reactions are best described by either the second order kinetics controlled reaction mecanism (F2) or by the three-dimensional diffusion function (D3).

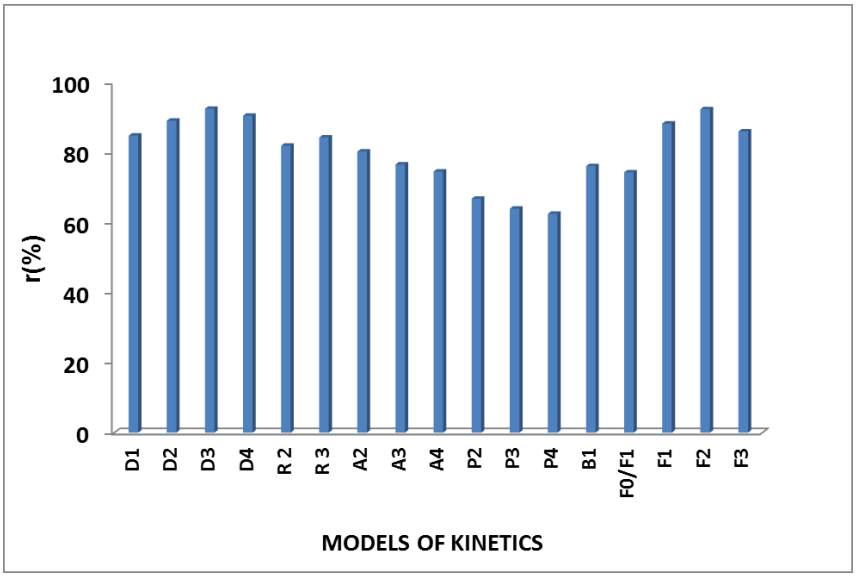

Figure 3.1.14 A histogram showing distribution of model of kinetics *vs* the standard deviation.

By analysing these two mechanisms, their activation energies were calculated .For the second order kinetics controlled reaction mecanism (F2) the activation energy

was 171.1 kJ mol^{-1}. and for the three-dimensional diffusion function (D3), the activation energy was calculated as 179.3 kJ mol^{-1} .

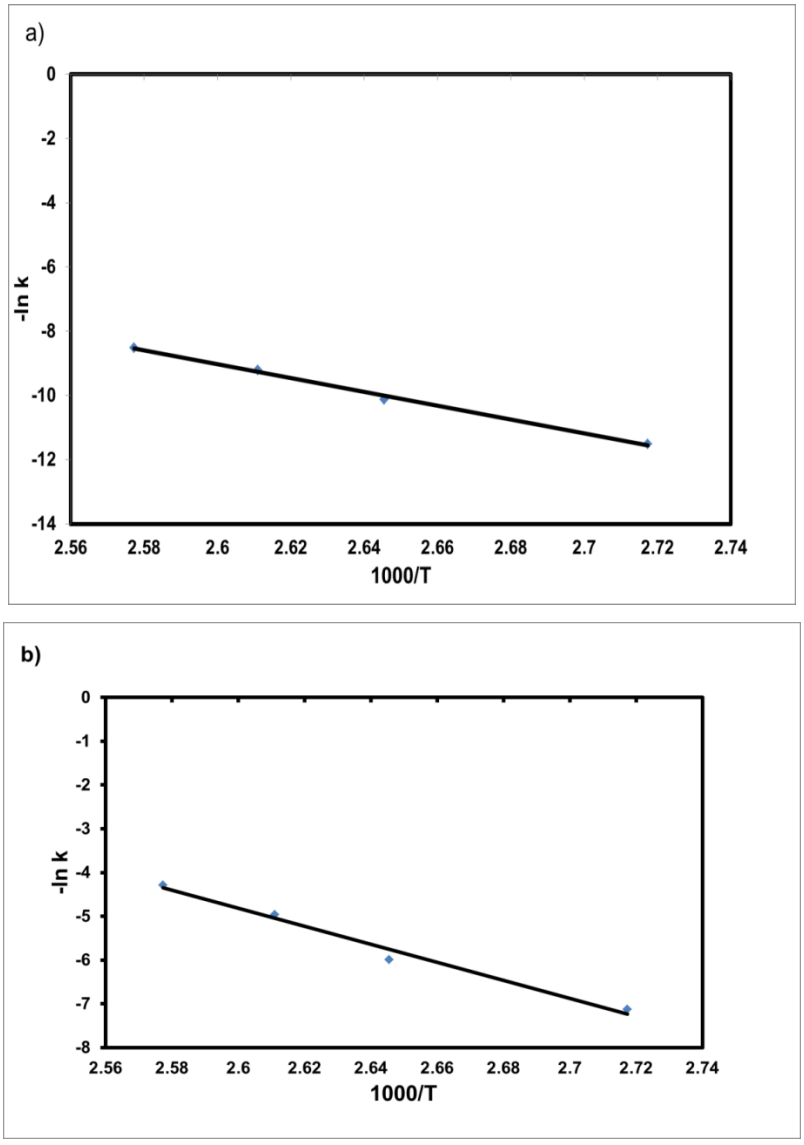

Figure 3.1.15 ln k vs 1/T graphs for(a) D3 and (b) F2

2**. $(BNDA^{2-})(DBA^{+})_2$**

Compound name: Di-*n*-butylammonium-1,1'-binaphthyl-2,2'-dicarboxylate

Formula: **$(C_{22}H_{12}O_4^{2-})(C_4H_{12}N^{+})_2$**

Asymmetric unit:

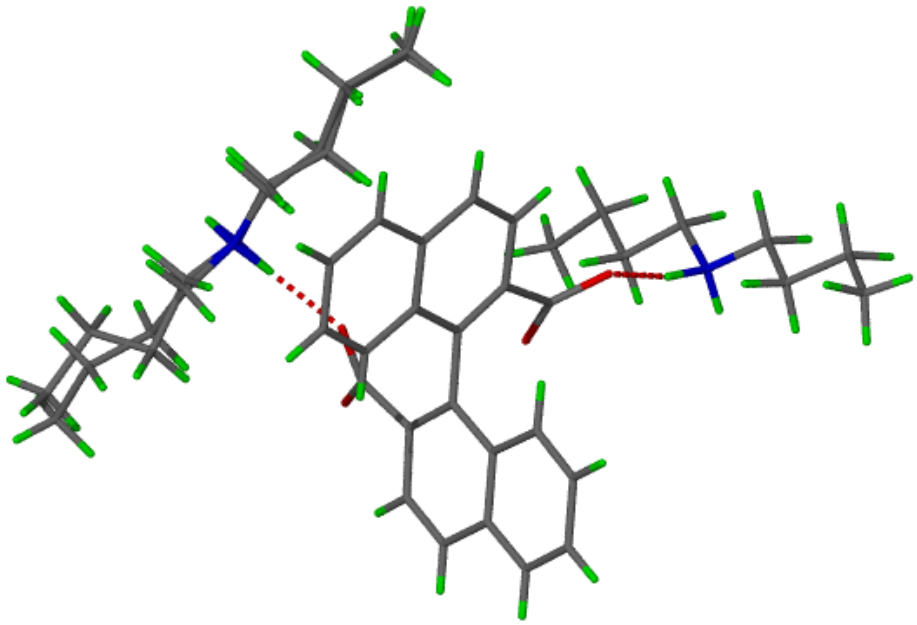

Figure 3.1.16 Asymmetric unit of **$(BNDA^{2-})(DBA^{+})_2$**

Crystal structure and refinement

The unit cell parameters of **$(BNDA^{2-})(DBA^{+})_2$** were also obtained from a Nonius Kappa CCD diffractometer. The structure crystallised in the triclinic crystal system, in space group P-1 with one host anion and two guest cations in general positions.

The crystal structure was solved by direct methods. The non-hydrogen atoms were found in the difference electron density map. All non- hydrogen atoms of the host and the guest were refined anisotropically. Aromatic hydrogens were fixed at a distance of C-H = 0.95 Å. The guest CH_2 and CH_3 hydrogens were fixed with C-H distances of 0.99 Å and 0.98 Å respectively. The N-H hydrogens were found in the

electron density map and allowed to refine anisotropically. Thus both carboxylic acid protons of the BNDA had been transferred to the nitrogens of the two DBA guests. One of the two dibutylammonium guests was disordered. The disordered guest is shown in **Figure 3.1.17** refined with site occupancies 0.624 and 0.376 respectively. The dihedral angle of two naphthalene rings of A is 94.5 °.[2] As shown in **Figure 3.1.16** , two pairs of adjacent naphthalene rings are nearly parallel to each other and partially overlapped. The centroid to centroid distance between them is 4.544 Å.[2]

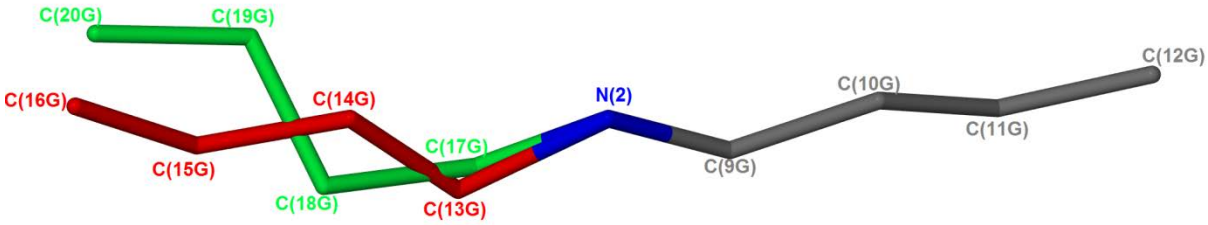

Figure 3.1.17 The disordered dibutylammonium guest with the major component shown in (red) and the minor component shown in (green). Hydrogens omitted.

Crystal packing

The packing diagram of **$(BNDA^{2-})(DBA^{+})_2$** down [100] is shown in **Figure 3.1.18.** The unit cell contains two anions of $BNDA^{2-}$ and four cations of DBA^{+} (Z = 2).

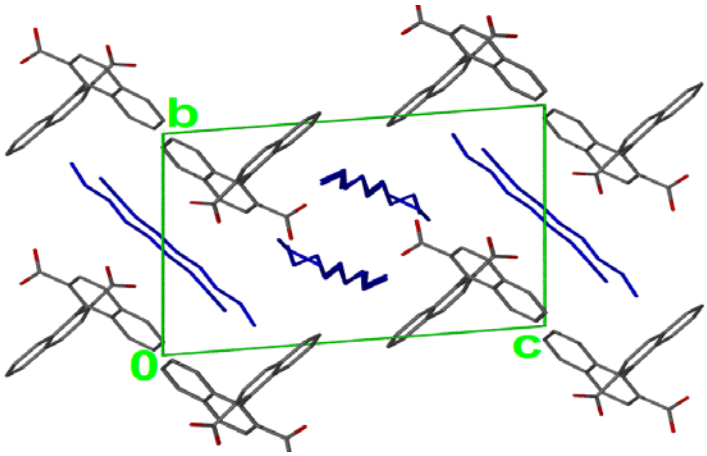

Figure 3.1.18 Packing diagram of **$(BNDA^{2-})(DBA^{+})_2$** down [100].

The space filling packing diagrams of **$(BNDA^{2-})(DBA^{+})_2$** are shown in **Figure 3.1.19** and **Figure 3.1.20.** The two dibutylammonium guests are crystallographically independent. Both guests occupy channels down [100] **(Figure 3.1.19).**

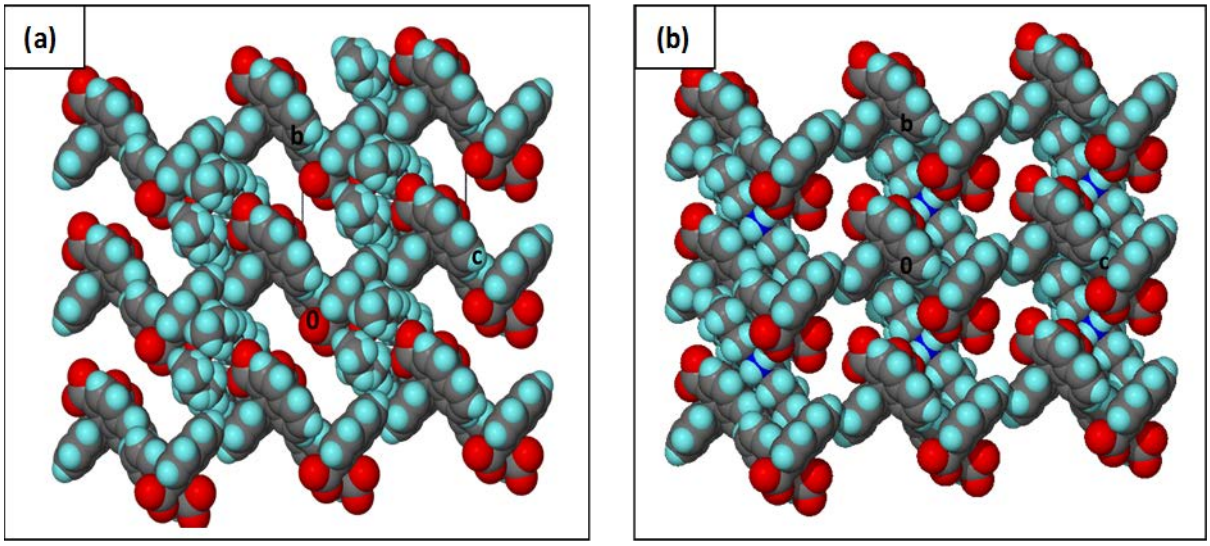

Figure 3.1.19 (a) Space filling diagram of **$(BNDA^{2-})(DBA^{+})_2$** indicating the channels down [100] with (a) the ordered guest removed and (b) the disordered guest removed.

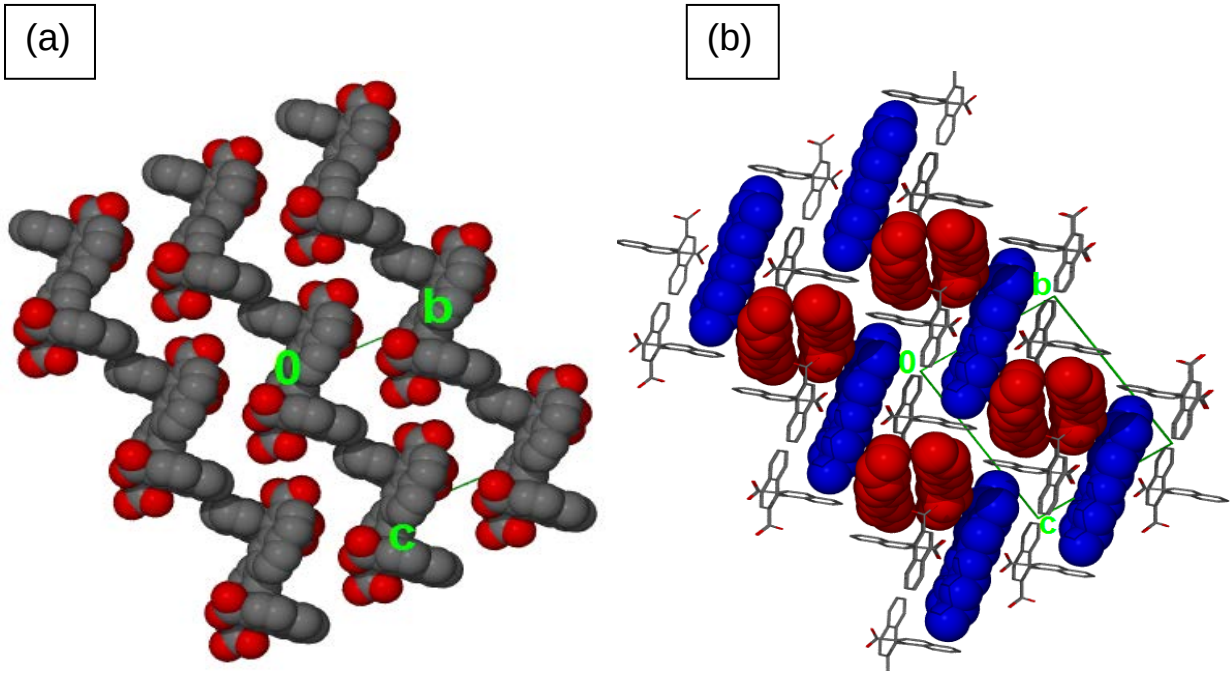

Figure 3.1.20 Space filling packing diagrams for **$(BNDA^{2-})(DBA^{+})_2$** viewed down [100] with (a) the guests omitted and (b) the ordered guests are shown in red and the

disordered guests are shown in blue. The host anions are represented as wireframes.

Analysis of these channels was carried out using MERCURY, with a probe radius of 1.5 Å. The voids form interconnected infinite channels seen in **Figure 3.1.21.**

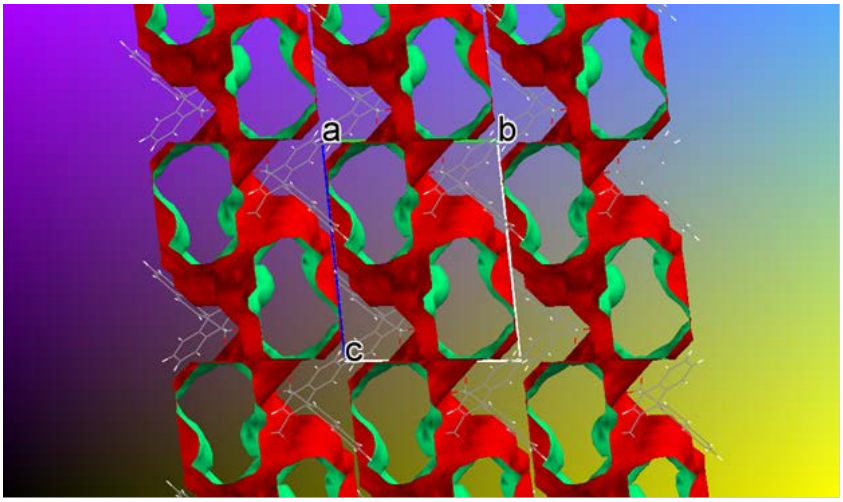

Figure 3.1.21 Channels occupied by the *n*-dibutylammonium cations in **$(BNDA^{2-})(DBA^{+})_2$** generated using a probe radius of 1.5 Å.

The structure is stabilised by ionic-hydrogen bonding. Hydrogen bonded rings involve the N-H moieties of the dibutylammonium cations acting as donor groups to the carboxylate anions **(Figure 3.1.22).** These rings can be described in graph set notation as $R_4^4(12)$.[5]

The atom distances of O1'•••N1, O2'•••N1, O1•••N2 and O2•••N2 are 2.695(2), 2.664(2), 2.634(2) and 2.685(2) respectively . The strengths of these interactions are very similar. The bond angles of N2—H4G•••O1and N2—H3G•••O2 are 164(1) and 165(1), respectively. These results indicated that the hydrogen bonding network in this salt complex is in such a way as to match the strongest donor and the strongest acceptor first. The hydrogen bonding details are given in **Table 3.1.4.**

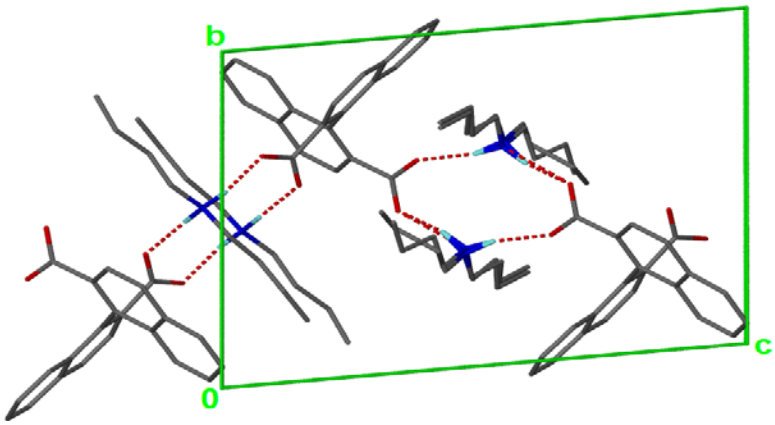

Figure 3.1.22 Hydrogen bonding interactions in **$(BNDA^{2-})(DBA^{+})_2$.**

D-H…A	D(D-H)(Å)	d (H···A)(Å)	<(DHA)(°)	d(D···A)(Å)	Symmetry operator
N2-H4G···O1	0.992(2)	1.665(2)	164(1)	2.634(2)	[-x+2,-y+1,-z+1]
N2-H3G···O2	0.913(2)	1.793(2)	165(1)	2.685(2)	[x, y, z]
N1-H2G···O1’	0.944(3)	1.771(2)	165(2)	2.695(2)	[x,y,z]
N1-H1G···O2’	0.944(2)	1.761(2)	159(1)	2.664(2)	[-x+2, -y+2,- z]

Table 3.1.4: Hydrogen bonding details in **$(BNDA^{2-})(DBA^{+})_2$.**

Thermal analysis

The DSC curve shows 3 endotherms: the first one corresponds to the release of the first guest at a peak of 423.3 K (T_{on} = 411.2 K) and the second DBA guest is released at 501.3 K (T_{on} = 495.5 K). The third endotherm (T_{peak} = 564.9 K) is broad and is due to the host melt.

The TG curve gave 3 mass losses: the first step of 20.8 % is due to the release of one mole of DBA. The release of the second guest occurs simultaneously with the host decomposition. The mass loss expected for the two guests was 42.8 %.

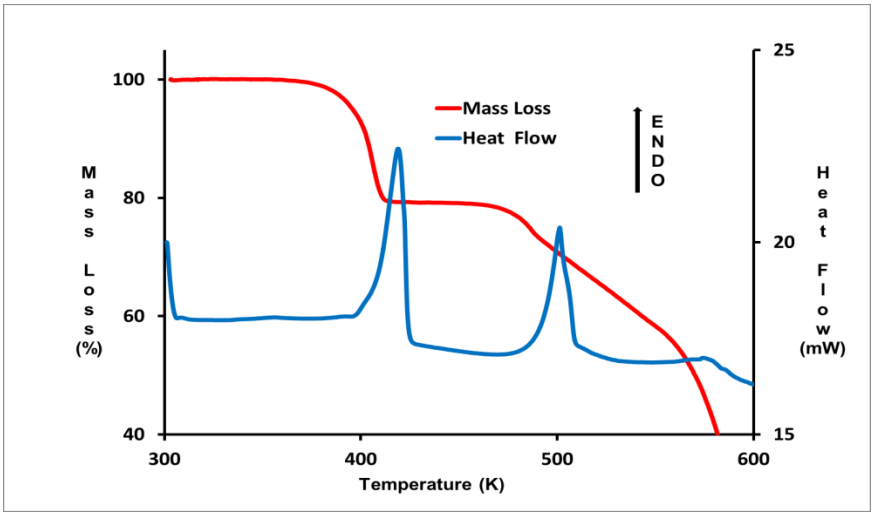

Figure 3.1.23 TG and DSC curves of **$(BNDA^{2-})(DBA^{+})_2$.**

	TG Results		
	Calc. % mass loss	**Exp. % mass loss**	
mass loss 1	21.4 (loss of DBA)	20.8	
mass loss 2	21.4 (loss of DBA)	-	
	DSC Results		
	Endotherm 1	**Endotherm 2**	**Endotherm3 (broad)**
T_{on} (K)	411.2 K	495.5 K	-
T_{peak} (K)	423.3 K	503.1 K	564.9 K

Table 3.1.5 Thermal analysis results of **$(BNDA^{2-})(DBA^{+})_2$.**

Hot stage Microscopy

The decomposition of a crystal of **$(BNDA^{2-})(DBA^{+})_2$** was observed using hot stage microscopy. The crystal was submerged in silicone oil. Photographs were taken at different temperatures **(Figure 3.1.24).** The crystal is still stable at 400 K but at 405.9 K, bubbles indicate the release of DBA. At this stage, the crystal maintains its shape and is still transparent. At 490.07K, the crystal has lost its quality, colour changes are observed and, the second DBA guest is released at the stage (i).

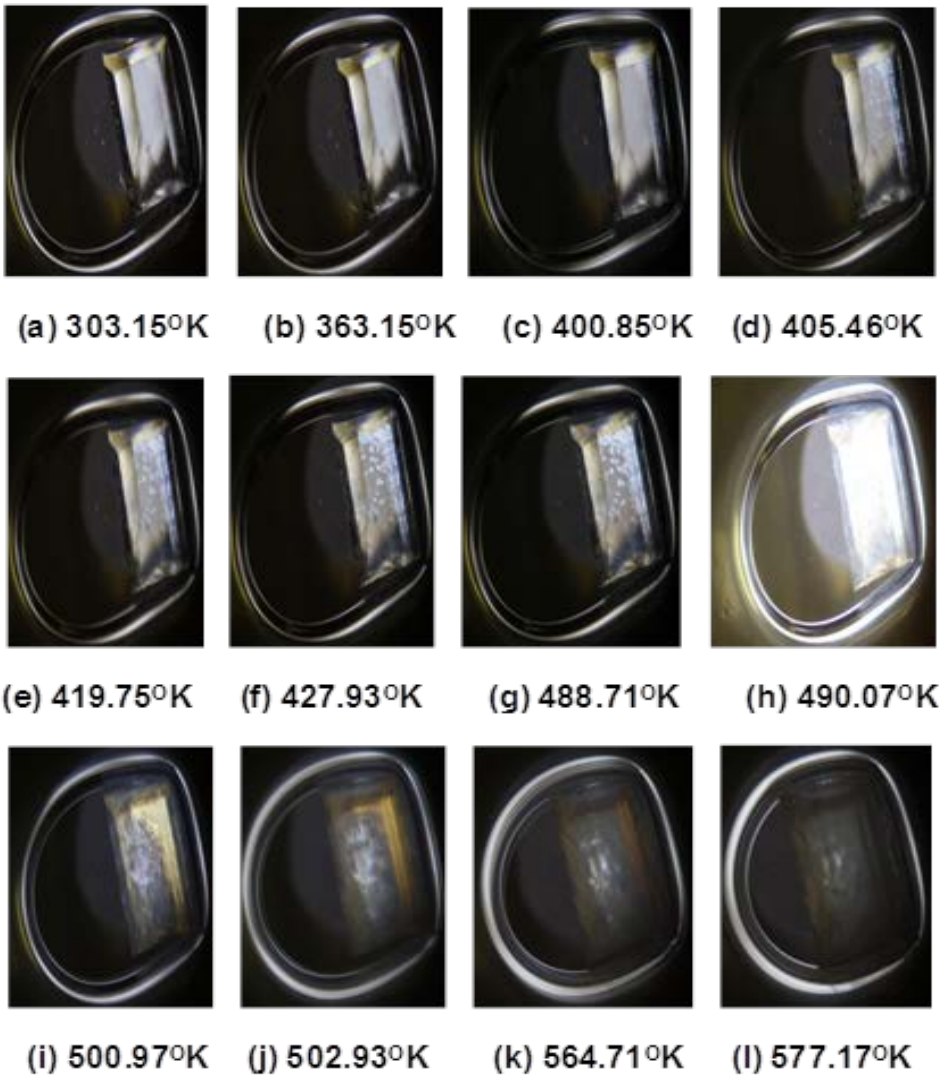

Figure 3.1.24 Thermal decomposition of a crystal of **$(BNDA^{2-})(DBA^{+})_2$.**

PXRD

The pattern of the bulk experimental compound (red) could generally be compared to the Lazy Pulverix calculated PXRD pattern (blue), in **Figure 3.1.25**. The two patterns match correctly.

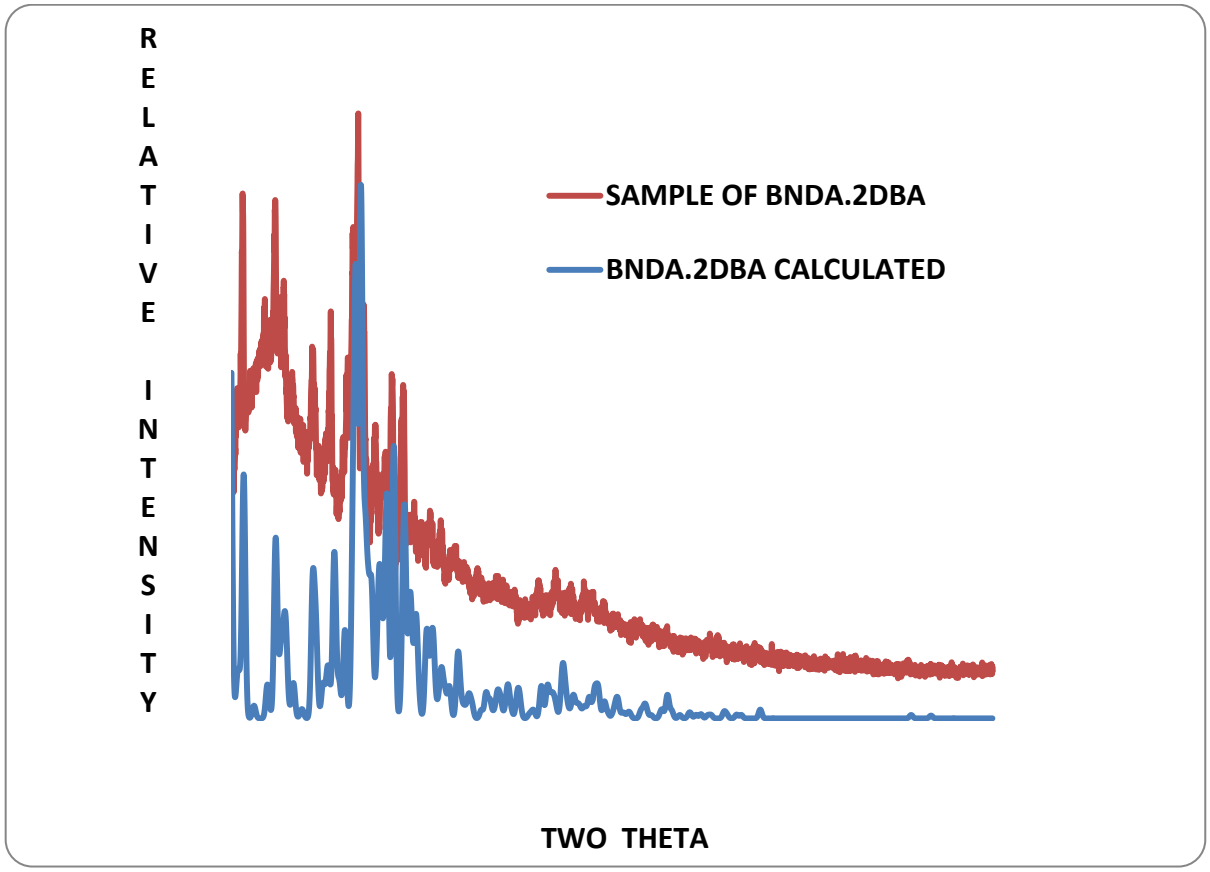

Figure 3.1.25 Comparison between the PXRD pattern of the sample and the calculated PXRD pattern of **$(BNDA^{2-})(DBA^{+})_2$.**

Kinetics of desolvation

A mechanism can be suggested for the desolvation of this salt **$(BNDA^{2-})(DBA^{+})_2$:**

- First step: **$(BNDA^{2-})(DBA^{+})_2$**→ $(BNDA^{-})(DBA^{+})$ + DBA
- Second step: $(BNDA^{-})(DBA^{+})$→ BNDA + DBA
- Sum of the mechanism: **$(BNDA^{2-})(DBA^{+})_2$**→ 2DBA+ BNDA

Non-isothermal kinetics

The first mass loss step was analysed using non-isothermal kinetics. TG curves were run at the heating rates of 2, 4, 8, 16 and 32 K min^{-1}. The curves were analysed over the α range 0 to 0.96 and converted to α-temperature plots represented in **Figure 3.1.26.**

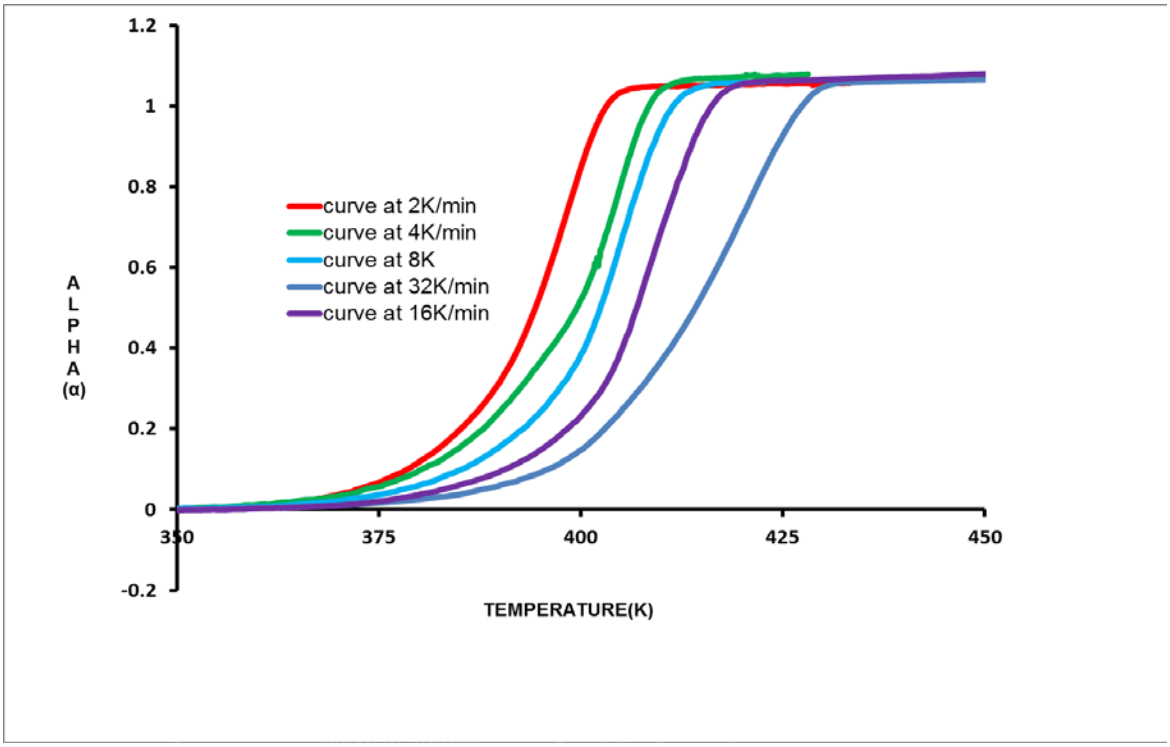

Figure 3.1.26 α versus Temperature plot for the non-isothermal desolvation of **$(BNDA^{2-})(DBA^{+})_2$**.

The corresponding -log beta vs 1/T plots are shown in **Figure 3.1.27**. The activation energies were calculated in the range of 10 to 60 % and reported on the **Figure 3.1.28** as activation energies corresponding to different conversions. From these values, an activation energy range of 159.1-179.14 kJ mol^{-1} has been obtained.

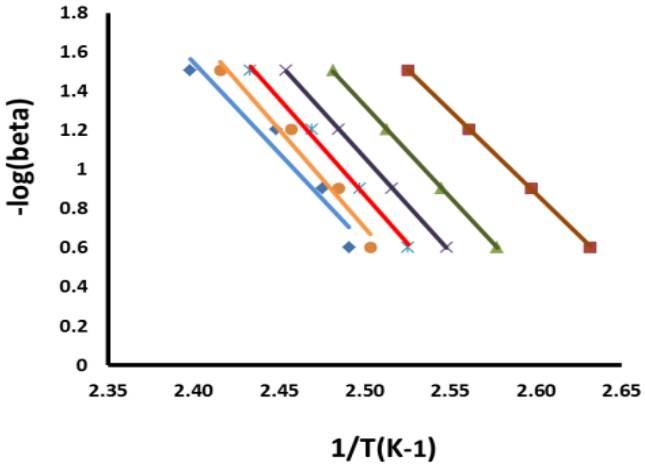

Figure 3.1.27 –log β vs 1/T plots for **$(BNDA^{2-})(DBA^{+})_2$**,first mass loss step.

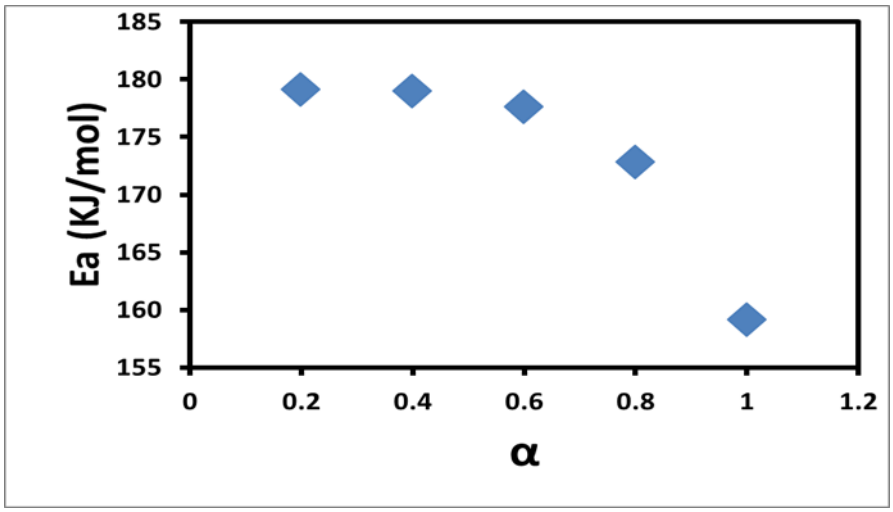

Figure 3.1.28 E_a versus α plot for non-isothermal **$(BNDA^{2-})(DBA^{+})_2$** desolvation evaluated by the Standard method.

b. Isothermal kinetics

It was also possible to determine the kinetics of desolvation for the first TG mass loss using isothermal methods. Hence by using mathematical reaction models, the mechanism and the kinetic parameters of the reactions can be deduced (α, T, t) from the data obtained from those TG curves. This was done using different kinetic models to get the best fit for the experimental results.

- Isoconversional method

Isoconversional methods were applied on data obtained from isothermal TG curves and the activation energy range was from 116.6 to163.04 kJ/mol.

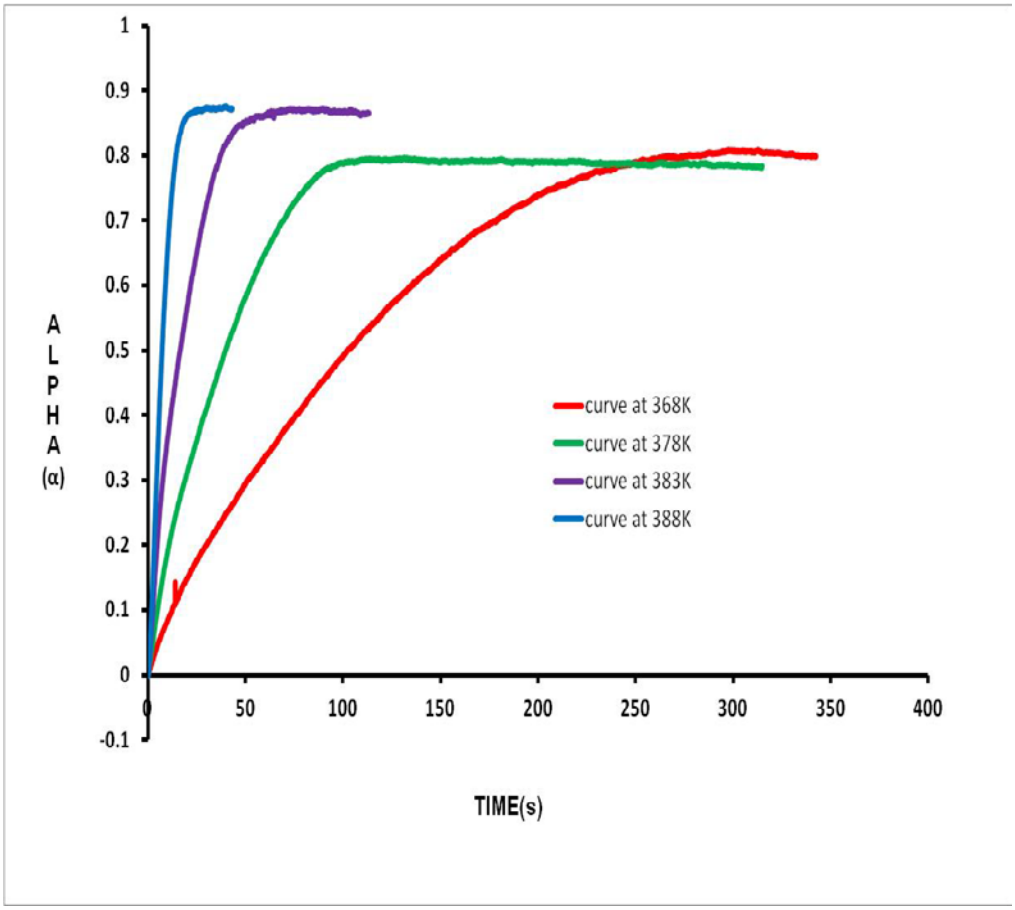

Figure 3.1.29 α versus time plot for the isothermal desolvation of **$(BNDA^{2-})(DBA^{+})_2$** evaluated by the Standard method.

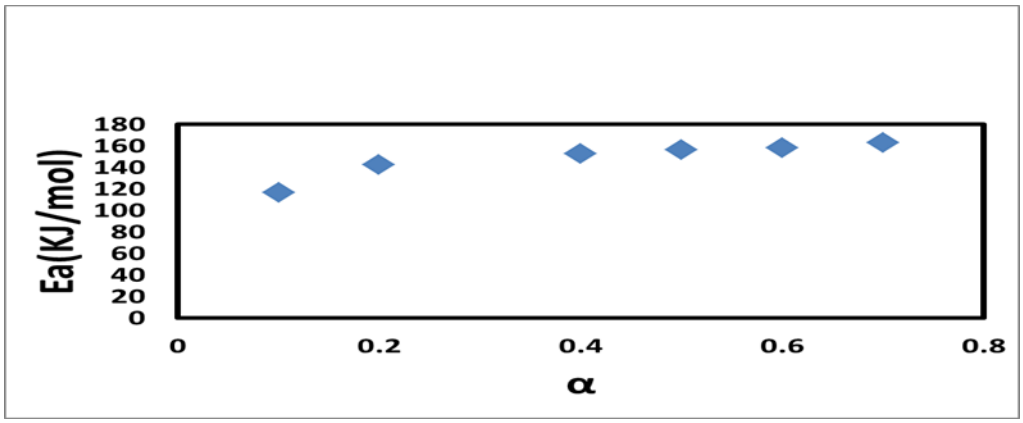

Figure 3.1.30 E_a versus α plot for the isothermal desolvation of **$(BNDA^{2-})(DBA^{+})_2$** evaluated by the Standard method.

- Model-fitting method (mechanism)

Model fitting method uses the isothermal data to test the accuracy of fit to the equations listed in table 3 to identify which expression represents most precisely the system.

Mathematical kinetic models were performed on the isothermal data of **$(BNDA^{2-})(DBA^{+})_2$** using different kinetic models to get the best fit for the experimental results. All the models are represented in **Figure 3.1.31**, showing in percentage the results of the differents methods. This indicated that these reactions are best described by either the contracting volume reaction mecanism (R3) or by first order reaction (F1).The activation energies are for *R*3: 167.3 kJ/mol and for F1:167 kJ/mol The plots are depicted in **Figure 3.1.32.**

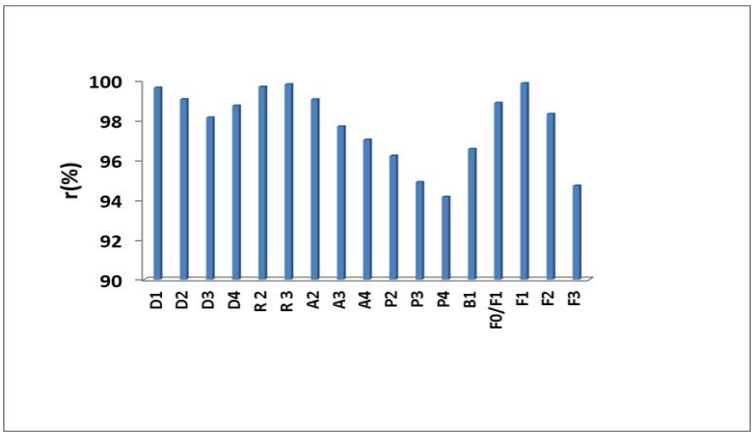

Figure 3.1.31 A histogram showing distribution of model of kinetics vs the standard deviation.

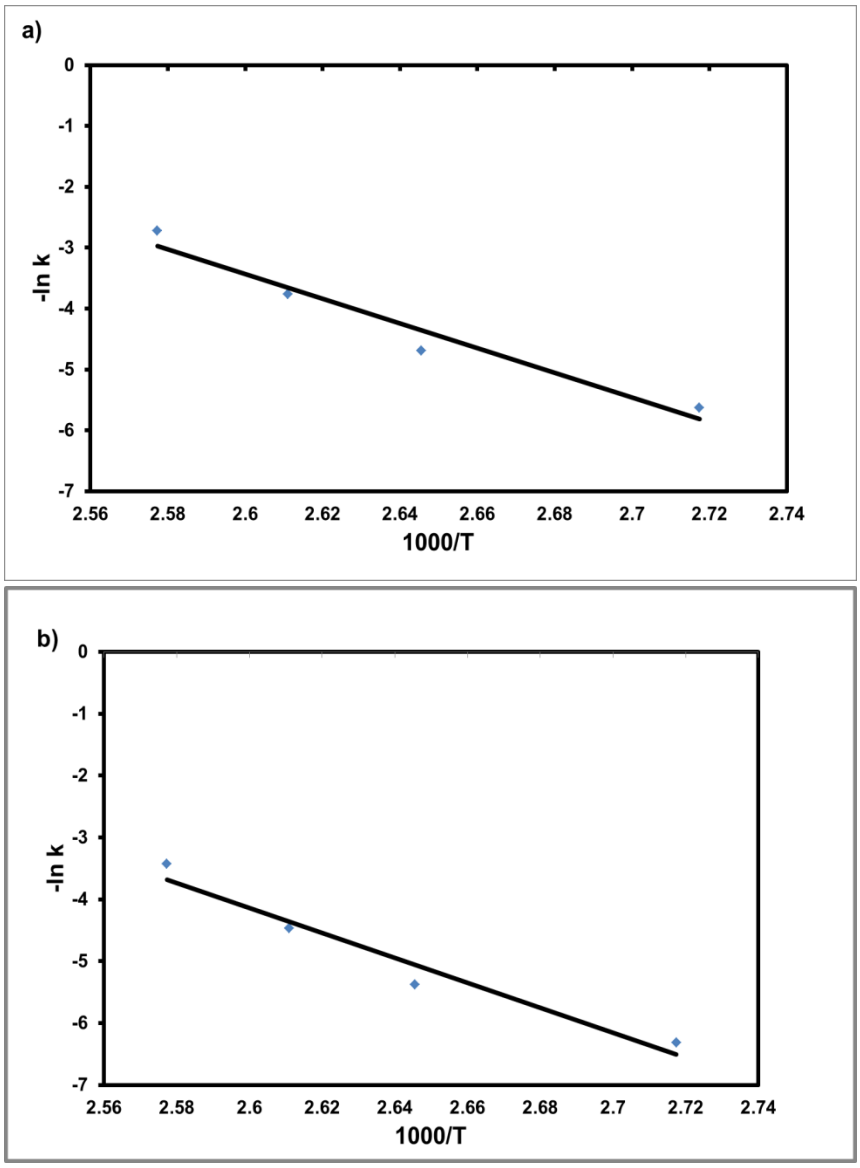

Figure 3.1.32 Plot of ln k vs 1/T for (a) F1 model and (b) R3 model.

3. $(BNDA^{2-})(DBA_2^{+})_2$ POLYMORPH

Compound name: Di-*n*-butyllammonium-1,1'-binaphthyl-2,2'-dicarboxylate

Formula: $(C_{22}H_{12}O_4^{2-})(C_4H_{12}N^{+})_2$

Asymmetric unit:

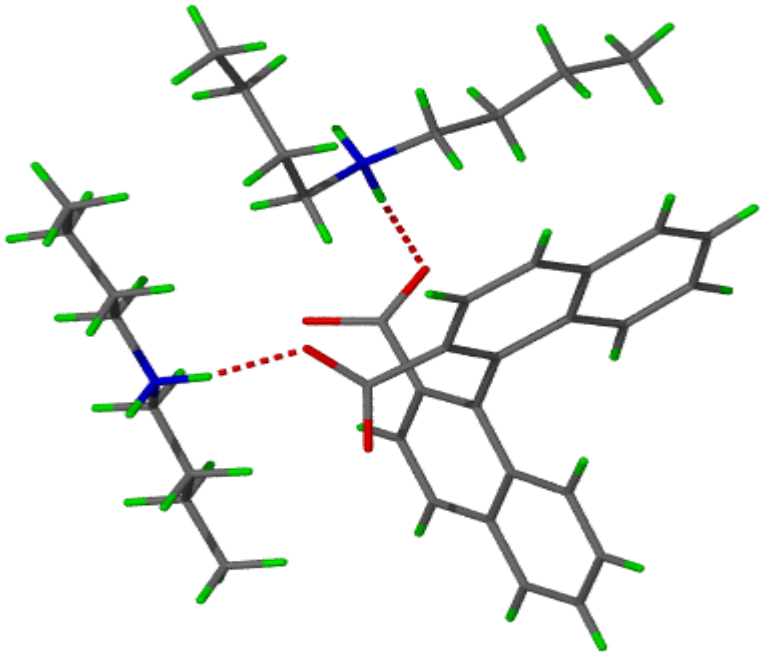

Figure 3.1.33 The asymmetric unit of $(BNDA^{2-})(DBA_2^{+})_2$.

A polymorph of $(BNDA^{2-})(DBA_2^{+})_2$ was formed by dissolution of BNDA in the mixture of 0.40 moles of DBA and 0.60 moles of DEA. We set up a competition experiment between BNDA in a mixture of DBA and DEA at different proportions, and found that DBA was selected. The asymmetric unit of the crystal polymorph $(BNDA^{2-})(DBA_2^{+})_2$ is shown in **Figure 3.1.33.**

Crystal structure and refinement

The crystal unit cell parameters of $(BNDA^{2-})(DBA_2^{+})_2$ were obtained from the Nonius Kappa CCD diffractometer. The salt crystallises in the triclinic crystal system in space group P-1. The calculation of the differences ΔD_{CO} gave 0.009 Å for both carboxylate groups indicating deprotonation of the acid groups, thus confirming that the compound formed is a salt.[1]

The asymmetric unit consists of an anion of $BNDA^{2-}$ and two cations of DBA^{+}, which corresponds to a host: guest ratio of 1: 2.

The crystal structure was solved by direct methods. The non-hydrogen atoms were found in the difference electron density map. All non-hydrogen atoms of the host and the guest were refined anisotropically. All hydrogens not involved in hydrogen bonding were placed with geometric constraints and allowed to refine isotropically. Aromatic hydrogens were fixed at a distance of C-H = 0.95 Å and the $-CH_3$ and $-CH_2$ hydrogens were fixed with C-H = 0.98 Å. The N-H hydrogens of the cations were found in the difference electron density map and allowed to refine isotropically. This is explained by location of four possible different peaks of hydrogens for the two nitrogens of DBA; the N1-H1G distance is 0.898 Å, N1-H2G distance is 0.943 Å, N2-H3G distance is 0.939 Å and N2-H4G distance is equal to 0.975 Å. The naphthyl fragments are nearly perpendicular to each other and the dihedral angle between the naphthyl moieties was calculated with the program Olex2[2] and gives an angle of 81.4°(2). This value does not fall in the narrow range found for BNDA and its inclusion compounds studied previously.[3] The distance between the centroids of the two naphthyls is 4.674 Å. The structure refined successfully to R_1= 0.0459 with wR_2 = 0.1201.

Crystal packing

The unit cell contains two anions of BNDA and four cations of DBA with the host anions and the guest cations located in general positions. Thus, this gives a Z equal to 2.

The packing diagrams of **$(BNDA^{2-})(DBA_2^{+})_2$** are shown in **Figure 3.1.34**. The two guest dibutylammoniums are crystallographically independent and are oriented perpendicular to one another. The two independent cations are represented in red and blue to depict their different orientations **(Figure 3.1.35)**. The structure is stabilised by the ionic- hydrogen bonding. Host- guest interactions are illustrated in **Figure 3.1.37.**

The host and guest ions form hydrogen bonded dimers of the form (host)-COO^{-} ···$^{+}$N(guest). The hydrogen bonding details are given in **Table 3.1.6.**

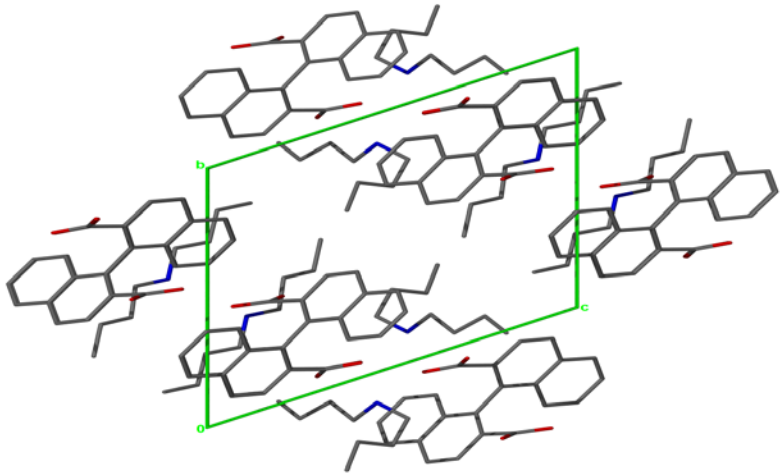

Figure 3.1.34 Packing diagram of **(BNDA)(DBA$^{+}_{2}$)$_2$** down [100].

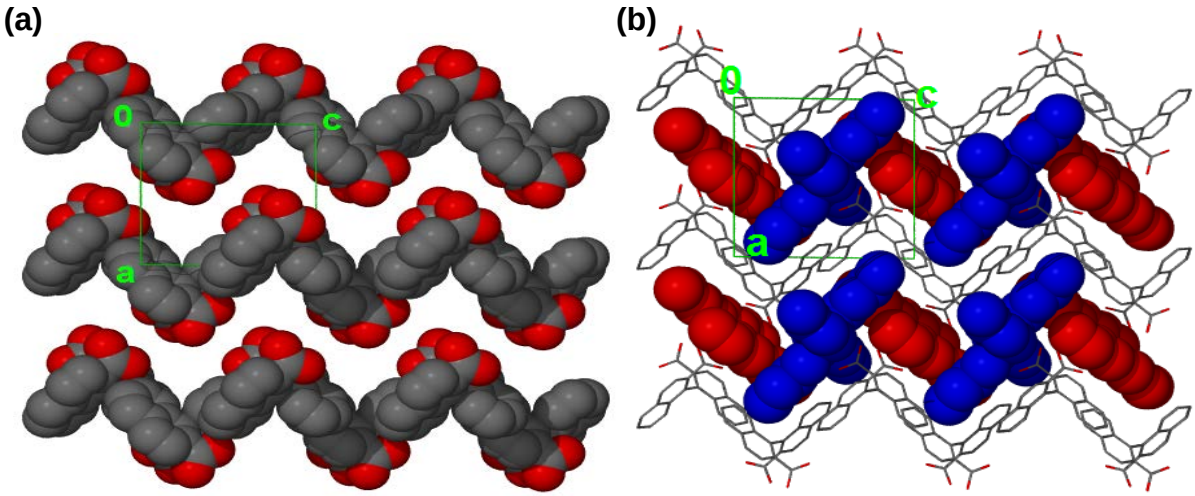

Figure 3.1.35 Space filled packing diagrams for **(BNDA)(DBA$^{+}_{2}$)$_2$** (a) viewing along [010], where the guest are omitted and the channels in which the guest reside can be seen and (b) the guests are shown, with their van der Waals radii highlighted for clarity.

The channels occupied by the guests were also viewed using the program Mercury[4] (**Figure 3.1.36).** This analysis was carried out with a probe radius of 1.5 Å.

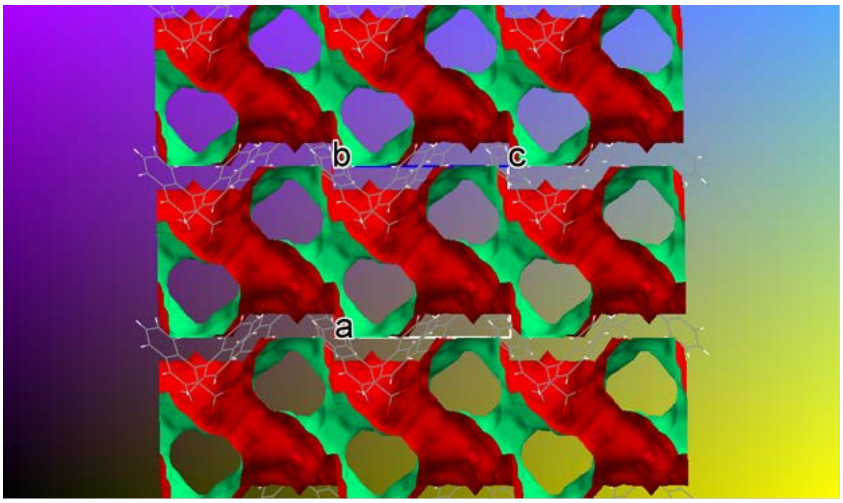

Figure 3.1.36 Channels occupied by the dibutylammonium cations in **$(BNDA^{2-})(DBA_2^{+})_2$.**

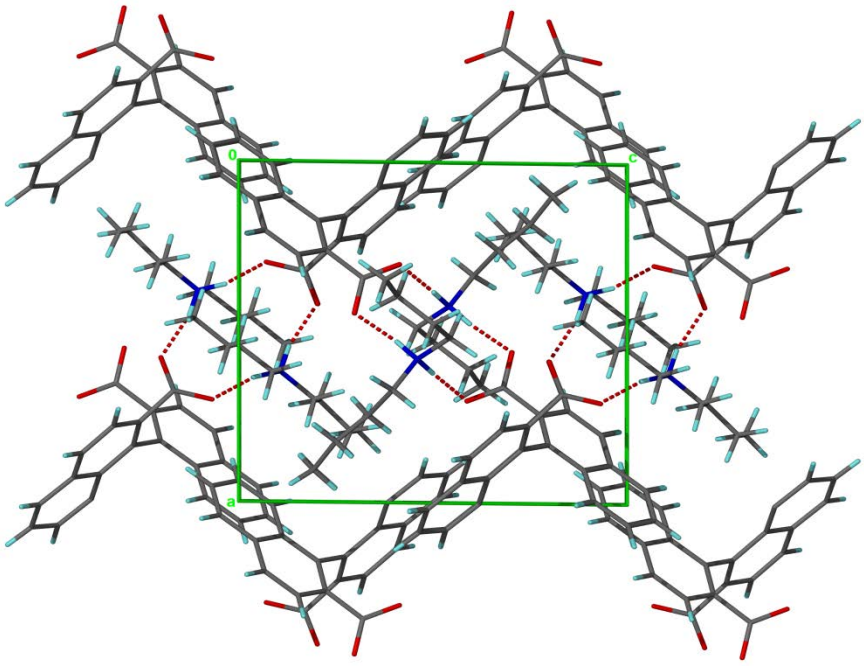

Figure 3.1.37 Hydrogen bonding interactions in **$(BNDA^{2-})(DBA_2^{+})_2$.**

D-H···A	d(D-H)(Å)	d (H···A)(Å)	<(DHA)(^{o})	d(D···A)(Å)	Symmetry operator
N1-H2G···O1'	0.943(2)	1.799(2)	167(2)	2.727(2)	[-x+1, -y+1, -z]
N2-H4G···O1	0.975(2)	1.703(2)	169(2)	2.666(2)	[x, y, z]
N2-H3G···O2	0.939(2)	1.796(2)	172(2)	2.728(2)	[-x+1, -y, -z+1]
N1-H1G···O2'	0.898(2)	1.795(2)	167(2)	2.678(2)	[x, y, z]

Table 3.1.6 Hydrogen bonding interactions in **$(BNDA^{2-})(DBA^{+}{}_{2})_{2}$**

Thermal analysis

TG and DSC analyses were performed on the crushed **$(BNDA^{2-})(DBA^{+}{}_{2})_{2}$.** The experimental mass loss is similar to the expected value corresponding to a host : guest ratio of 1:2. The TG curve (**Figure 3.1.38)** indicated the loss of one dibutylamine followed by the loss of the second dibutylamine together with the host melt. This is similar to the previous polymorph **$(BNDA^{2-})(DBA^{+})_{2}$.** The DSC endotherm showed 3 peaks: the first one corresponds to the release of the first guest at T_{peak} = 411.1 K (T_{on} = 377.3 K) and the second DBA was released at T_{peak} = 502.1K (T_{on} = 489.8 K). The third peak is broad and is due to the host melt.

A mechanism for the desolvation of this salt of **$(BNDA^{2-})(DBA^{+}{}_{2})_{2}$** can be suggested as below, to explain clearly the thermogravimetric analysis.

$(BNDA^{2-})(DBA^{+}{}_{2})_{2}$ $\rightarrow (BNDA^{-})(DBA^{+}) + DBA$ (1)

$(BNDA^{-})(DBA^{+}) \rightarrow BNDA + DBA$ (2)

The TG curve gave 2 mass losses: the first step of 21 % corresponds to the release of one mole of DBA. The second mass loss for the release of the second guest was difficult to determine experimentally because it occurs together with the host melt. The mass loss expected for the two guests was of 42.8 %. The thermal analysis summary is given in **Table 3.1.7.**

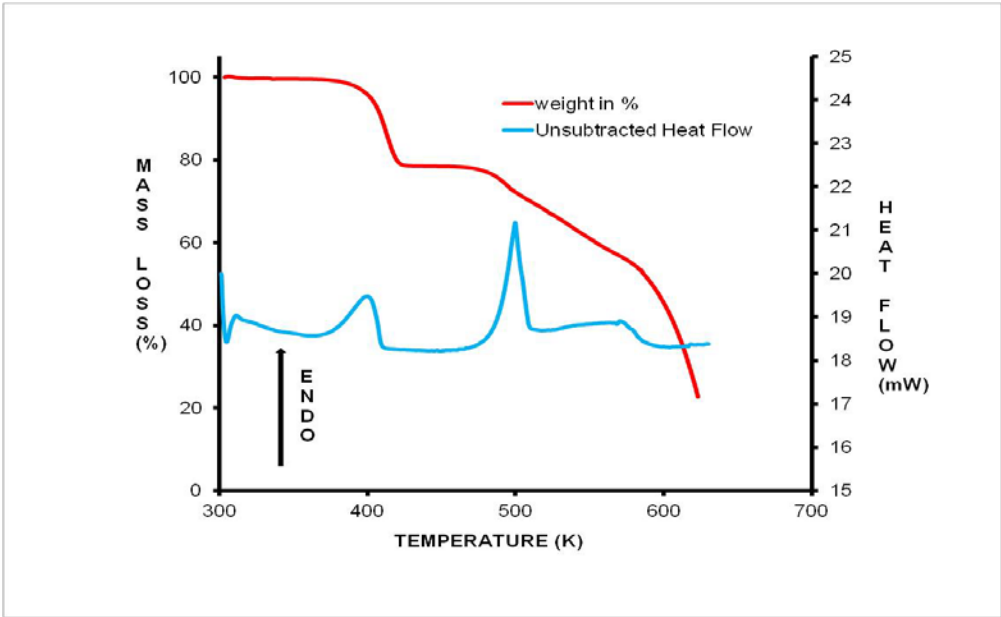

Figure 3.1.38 TG and DSC curves of **$(BNDA^{2-})(DBA_2^{+})_2$.**

	TG Results		
	Calc. % mass loss	**Exp. % mass loss**	
mass loss 1	21.4 (loss of DBA)	20.8	
mass loss 2	21.4 (loss of DBA)	-	
	DSC Results		
	T_{on}(K): Peak1	**T_{on}(K): Peak 2**	**T_{on}(K): Peak 3**
	377.3; 411.1	489.8; 502.1	564.9 K (broad)

Table 3.1.7 Thermal analysis results of **$(BNDA^{2-})(DBA^{+}_2)_2$**

Kinetics of desolvation

A. Non-isothermal

Kinetic experiments were performed at heating rates of 1, 2, 10 and 16 K min^{-1} and the first mass loss was studied. The TG curves were analysed at the percentage mass loss of 10 % to 60 % and converted to α-temperature plots (**Figure 3.1.39**).

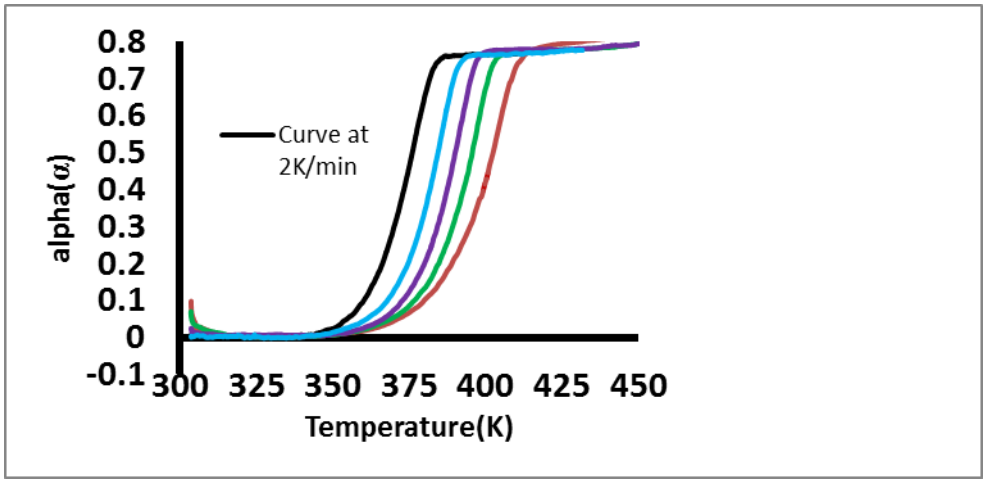

Figure 3.1.39 α vs 1/T plots for **$(BNDA^{2-})(DBA^{+}_{2})_2$.**

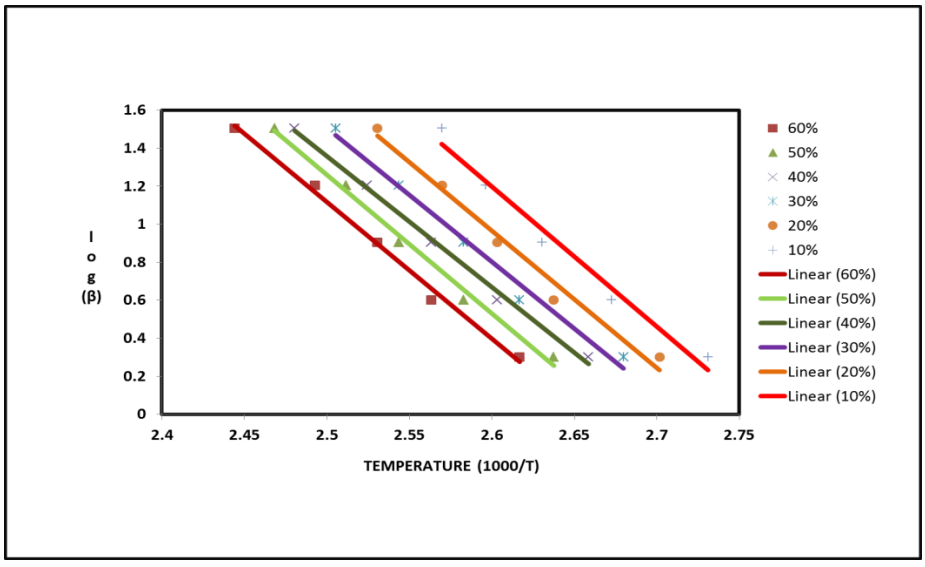

Figure 3.1.40 –log β vs 1/T plots for **$(BNDA^{2-})(DBA^{+}_{2})_2$** for the first mass loss step.

The activation energies for the loss of one mole of DBA were calculated and reported in the **Figure 3.1.41**. The range for the activation energy of

$(BNDA^{2-})(DBA^{+}_{2})_2$ was found to be 125.4 – 146.9 kJ/mol.

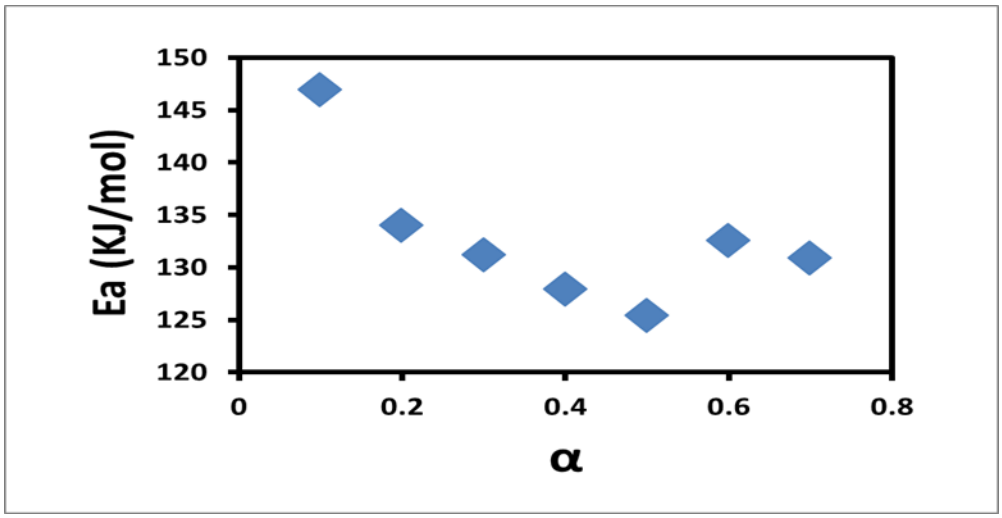

Figure 3.1.41 E_a versus α plot for non-isothermal **$(BNDA^{2-})(DBA^{+}_{2})_2$** desolvation evaluated by the Standard method.

B. Isothermal

By thermal analysis techniques it was possible also to follow isothermally the degree of conversion in the reaction (again for the first mass loss) by means of the TG measurements. Hence by using mathematical reaction models, the mechanism and the kinetic parameters of the reactions can be deduced (α, T, t) from the data obtained from those TG curves. This was been done using different kinetic models to get the best fit for the experimental results

- <u>isoconversional method</u>

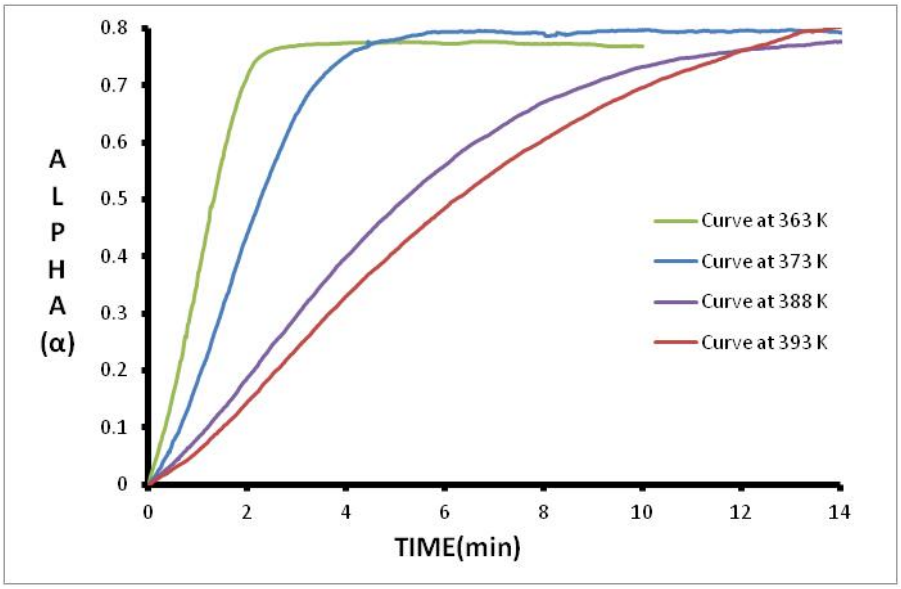

Figure 3.1.42 TG curves for isothermal kinetics **$(BNDA^{2-})(DBA^{+}_{2})_2$**

Isoconversional methods were applied on data obtained from isothermal TG curves and the activation energy range was from 57.1 to70.5 kJ/mol.

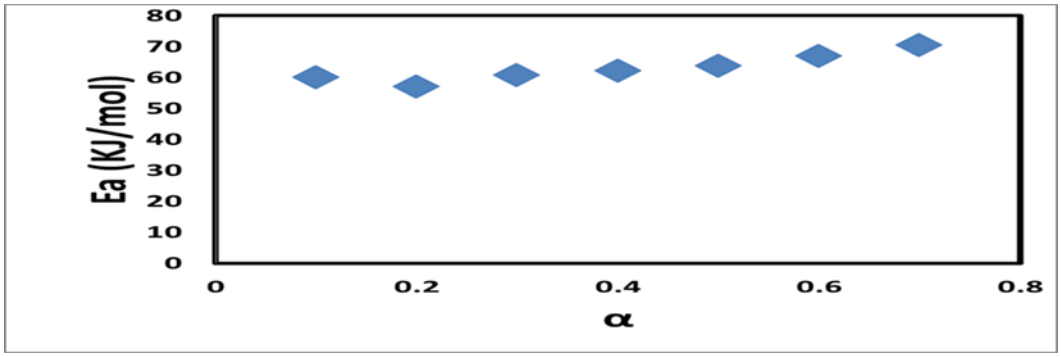

Figure 3.1.43. E_a versus α plot for isothermal **$(BNDA^{2-})(DBA_2^{+})_2$** desolvation evaluated by Standard method.

- Model-fitting kinetics

The kinetics were studied from the isothermal data of **$(BNDA^{2-})(DBA_2^{+})_2$** using the model fitting method. The results showed that the desolvation reaction is best described by either the second order kinetics controlled reaction mecanism R2 or by three-dimensional diffusion function R3. The activation energies for R2 and R3 found were respectively 103.9 and 103.4 kJ mol^{-1}.

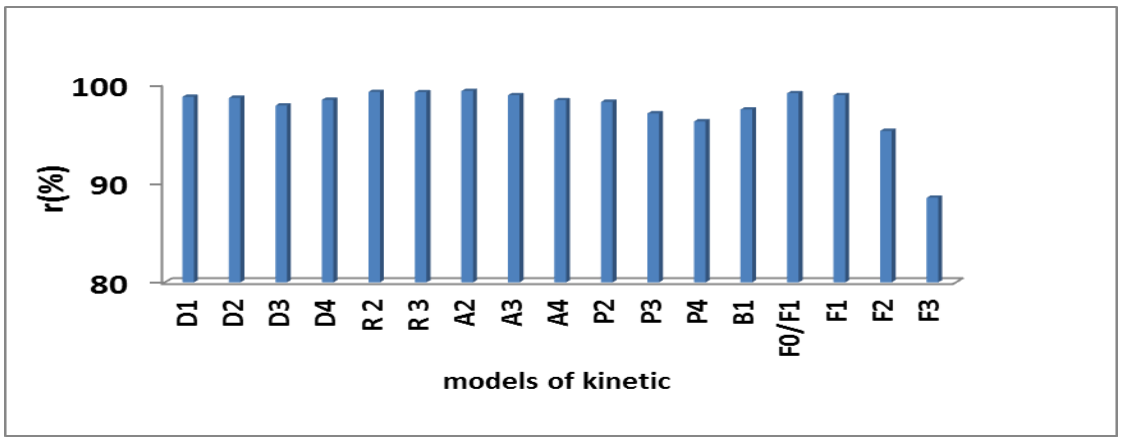

Figure 3.1.44 A histogram showing distribution of model of kinetics vs deviation.

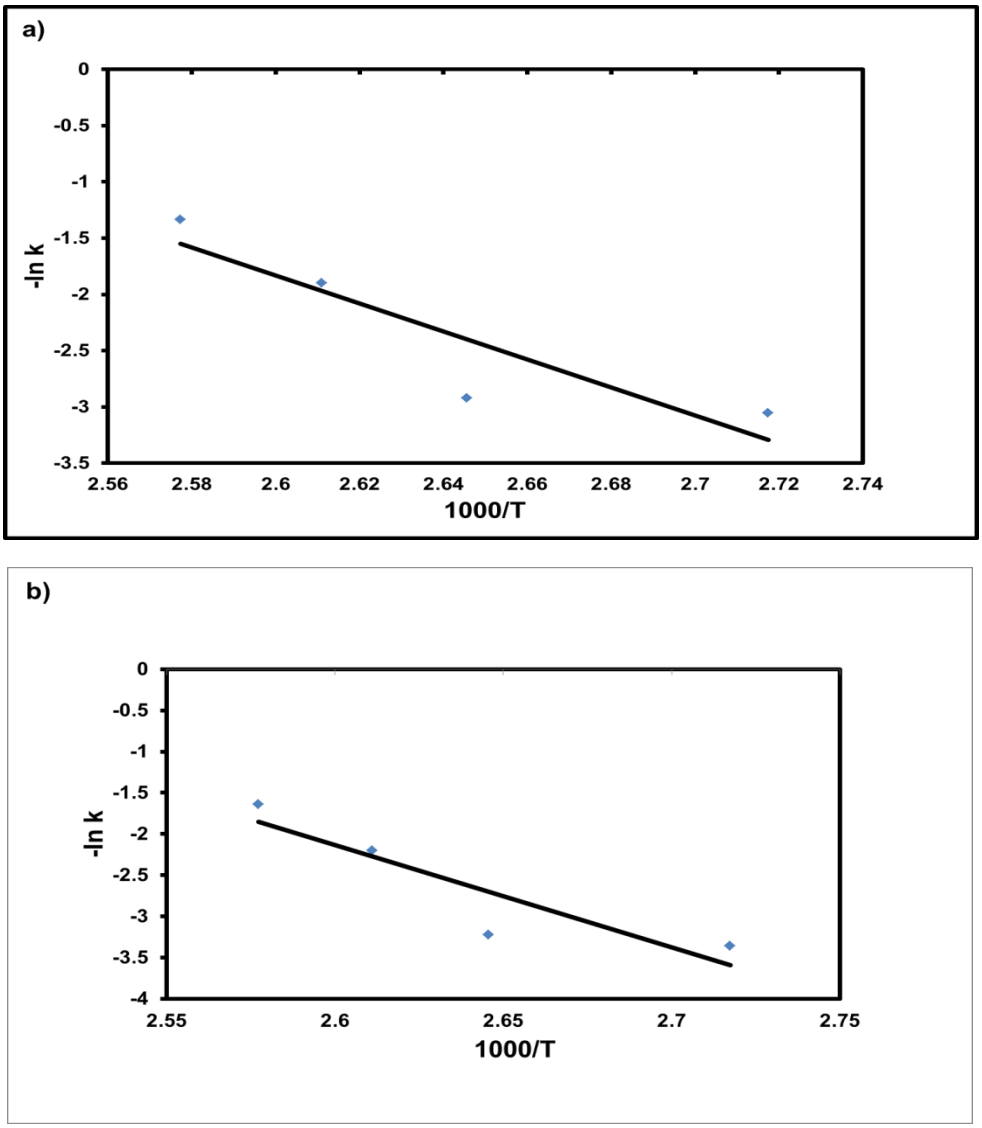

Figure 3.1.45 ln k vs 1/T graph for (a) R2 model fit and (b) R3 model kinetics.

DISCUSSION

Three salts were been elucidated in this chapter with the racemic host BNDA: **$(BNDA^{2-})(DEA^{+})_2$, $(BNDA^{2-})(DBA^{+})_2$** and **$(BNDA^{2-})(DBA_2^{+})_2$.** The latter salt is a polymorph formed from the competition experiment where BNDA was dissolved in a 60% DEA and 40% DBA mixture.

For all the salts the host: guest ratio was 1: 2. Both **$(BNDA^{2-})(DBA^{+})_2$** and **$(BNDA^{2-})(DBA_2^{+})_2$** crystallised in the triclinic space group P-1, yet **$(BNDA^{2-})(DEA^{+})_2$** crystallised in the monoclinic space group C2/c.

The salts are all stabilised by hydrogen bonding between the carboxylate groups of the host anions and the ammonium groups of the guest cations. Each carboxylate group is hydrogen bonded to two guest cations. The hydrogen bonding pattern can be described as $N_2 = R_4^4(12)$

Thermal analysis shows that the three compounds undergo the same mechanism of decomposition. The TG results showed two steps for all three compounds. The first giving the mass loss of the first guest and the second step gave the mass loss of the second guest. The experimental mass loss for the release of the second guest was difficult to determine as it occurred together with the host melt. The ratio of the onset temperature (T_{on}) and their boiling point (T_b) was used to measure the thermal stability. The T_{on}/T_b values for **$(BNDA^{2-})(DEA^{+})_2$**, **$(BNDA^{2-})(DBA^{+})_2$** and

$(BNDA^{2-})(DBA_2^{+})_2$ were respectively 1.24, 1.00 and 0.90. This indicated that the

$(BNDA^{2-})(DEA^{+})_2$ is the most stable salt. For the competition experiments whereby BNDA was dissolved in mixtures containing different proportions of DEA and DBA the BNDA selected the DBA guest exclusively. Comparison of the T_{on}/T_b values and the competition experiments indicate that the formation of the DBA salt is a kinetic result.

Kinetics of desolvation for the first mass loss step was performed for all three salts. Many methods including isothermal and non-isothermal methods were tested. The highest activation energy was seen for **$(BNDA^{2-})(DEA^{+})_2$** which coincides with the higher T_{on}/T_b value indicating greater stability.

III.2. Salts of 1, 1'-binaphthyl-2, 2'-dicarboxylic acid with non-chiral cycloamines

$(BNDA^{2-})(CHA^{+})_3(C_7H_{11}NO_2^{-})\bullet(CHA)\bullet(H_2O)$ and **$(BNDA^{-})(DCHA^{+})\bullet CH_3OH\bullet H_2O$** were formed respectively between 1,1'-binaphthyl-2,2'-dicarboxylic acid (BNDA) with cyclohexylamine (CHA) and dicyclohexylamine (DCHA) in methanol. The thermal analyses results and their crystal structures will be elucidated in this chapter. For these crystal structure discussions, presented in **Table 3.2.1** the crystal data for these two salts **$(BNDA^{2-})(CHA^{+})_3(C_7H_{11}NO_2^{-})\bullet(CHA)\bullet(H_2O)$** and **$(BNDA^{-})(DCHA^{+})\bullet(CH_3OH)\bullet(H_2O)$.**

Compound	**$(BNDA^{-})(CHA^{+})_3(C_7H_{11}NO_2^{-})(CHA)(H_2O)$**	**$(BNDA^{-})(DCHA^{+})_2\bullet CH_3OH\bullet H_2O$**
Molecular Formula	$(C_{22}H_{14}O_4^{-})(C_6H_{13}N^{+})_3(C_7H_{11}NO_2^{-})(CHA)(H_2O)$	$(C_{22}H_{14}O_4^{-})(C_{12}H_{23}N^{+})_2(H_2O)(CH_3OH)$
Molecular Mass ($gmol^{-1}$)	900.2	755.0
Data collection temp.(K)	296 (2)	173 (2)
Crystal system	Triclinic	Monoclinic
Space group	*P*-1	$P2_1/n$
a (Å)	10.1634(1)	13.9704 (3)
b (Å)	11.2464(1)	19.9644 (4)
c (Å)	11.3684 (1)	15.1274 (3)
α (°)	114.509(2)	90.00
β (°)	95.702 (2)	97.878 (3)
γ (°)	103.502(2)	90.00
Volume ($Å^3$)	1121.04 (5)	4179.37 (5)
Z	2	4
D_c, Calculated density ($g\ cm^{-3}$)	1.2368	1.200
Final R indices [I>2sigma(I)]	R_1= 0.0498 wR_2= 0.1594	R_1= 0.0446 wR_2= 0.0897
R indices (all data)	R_1= 0.0887 wR_2= 0.1500	R_1= 0.0446 wR_2= 0.1306
Largest dif peak&hole ($eÅ^{-3}$)	0.70; -0.24	0.27; -0.18

Table 3.2.1: Crystal data table of salts of BNDA with CHA and DCHA.

1. $(BNDA^{2-})(CHA^{+})_3(C_7H_{11}NO_2^{-})\bullet CHA\bullet H_2O$

Compound name: tricyclohexylammonium-1,1'-binaphthyl-2,2'-dicarboxylate cyclohexamine hydrate

Formula: $(C_{22}H_{14}O_4^{2-})(C_6H_{13}N^{+})_3(C_7H_{11}NO_2^{-})\bullet CHA\bullet H_2O$.

Asymmetric unit:

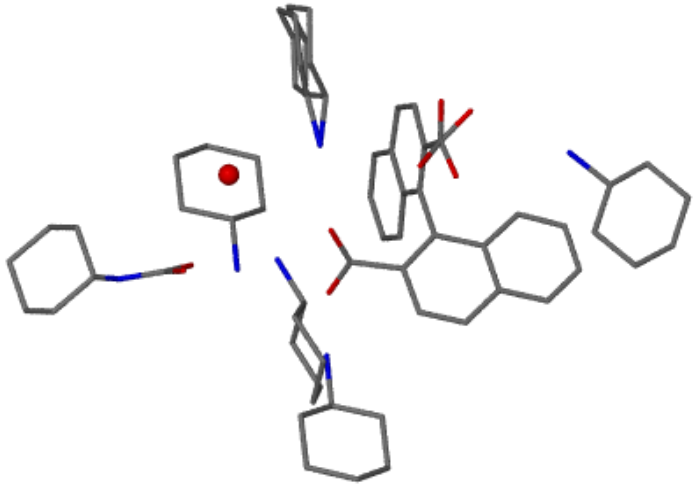

Figure 3.2.1 Asymmetric unit of $(BNDA^{2-})(CHA^{+})_3(C_7H_{11}NO_2^{-})\bullet CHA\bullet H_2O$ with all the hydrogens omitted for clarity.

Crystal structure and refinement

The crystal unit cell parameters were also obtained from the same Nonius Kappa CCD diffractometer. This salt structure crystallises in the triclinic crystal system in the space group P-1.

The non-hydrogen atoms were found in the difference electronic density map and were refined anisotropically. The hydrogens of the water and the N-H hydrogens were found in the difference electronic density and were refined anisotropically. Aromatic hydrogens were fixed at a distance of C-H = 0.95Å. The guest CH_2 hydrogens were fixed with a C-H distance of 0.99 Å. One of the host carboxylate moieties are disordered over two positions **(Figure 3.2.2 a).** Two of the carboxylate oxygens (O1, O2, O3 and O4) of the host are disordered with site occupancy factors

of 0.91 and 0.09. One of the cyclohexylammonium cations is disordered with site occupancy factors of 0.81 and 0.19 **(Figure 3.2.2 b).** A second cyclohexylammonium cation presents with four extra peaks in the electron density map. Several attempts made at modelling the disorder were unsuccessful due to the high thermal parameters obtained in the final refinement. The dihedral angle between the naphthyl rings was calculated and found to be 101.70°.[5] The structure refined successfully to $R_1 = 0.0463$ with $wR_2 = 0.1259$.

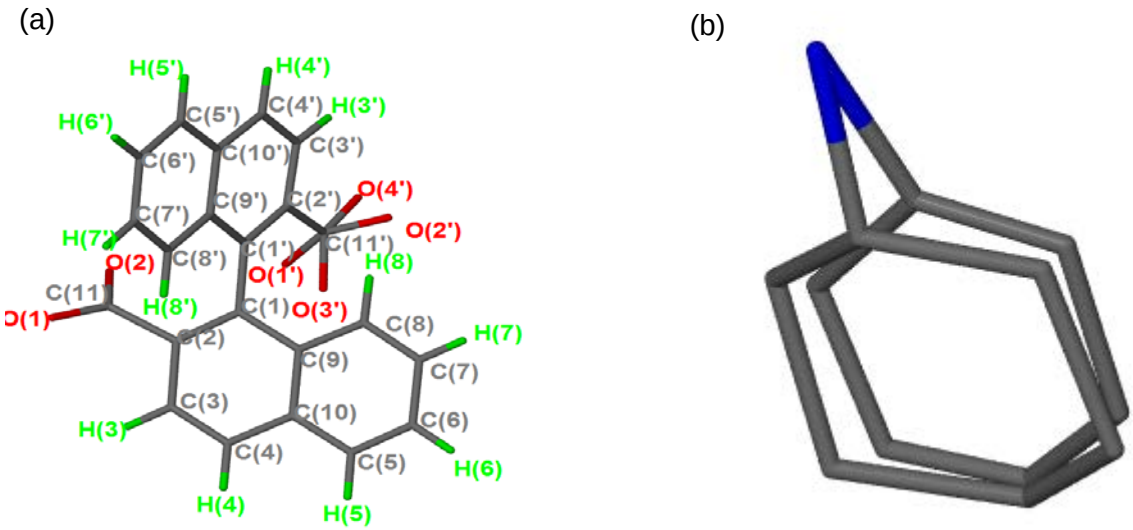

Figure 3.2.2 (a) Host disorder and (b) guest disorder (its hydrogens were omitted for clarity).

Crystal packing

The packing diagram of **$(BNDA^{2-})(CHA^{+})_3(C_7H_{11}NO_2^{-})(CHA)\bullet(H_2O)$** is shown in **Figure 3.2.3.** The asymmetric unit contains one host anion, three cyclohexylammonium cations, one neutral cyclohexylamine, one water molecule and one carbamate anion. Carbon dioxide from the atmosphere reacted with one CHA molecule to give a carbamate anion, $C_7H_{11}NO_2^{-}$. The host and guests are located in general positions.

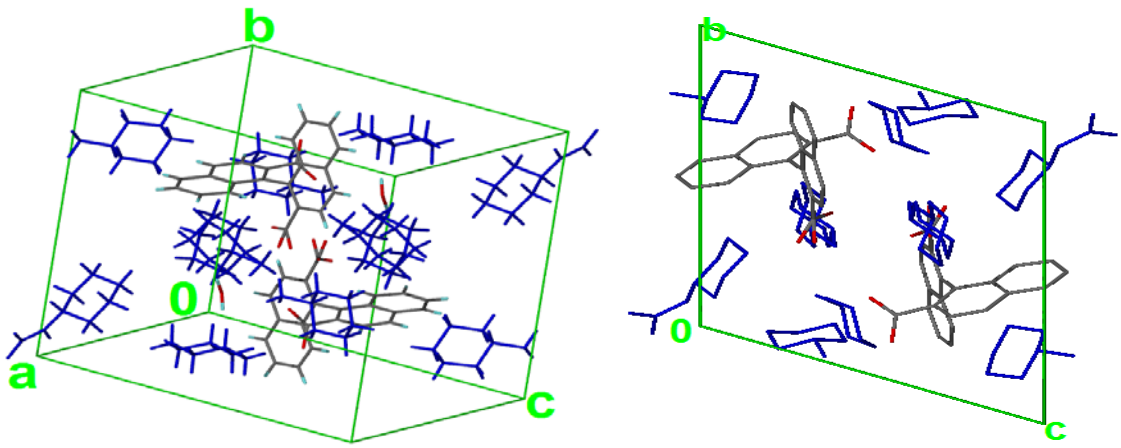

Figure 3.2.3 Packing diagrams of **$(BNDA^{2-})(CHA^{+})_3(C_7H_{11}NO_2^{-})(CHA)\bullet(H_2O)$.**

The guest cations are packed in a constricted channel formed by the framework of the hosts in the direction [100] in **Figure 3.2.4(a).** It shows the guest with their van der Waals radii and **Figure 3.2.4(b)** illustrates the framework of the host with its van der Waals radii, where the guests are removed. Here, the channels formed are clear. The void volume of 1182.9 $Å^3$ was calculated with Mercury, which is approximately 46 %, when the guest is removed. These channels are shown with Mercury in **Figure 3.2.5.**

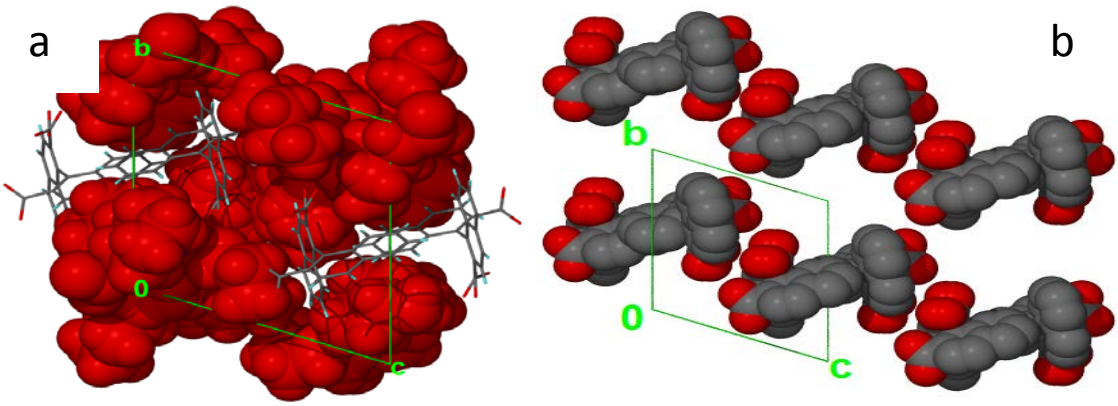

Figure 3.2.4 Space filled packing diagrams of **$(BNDA^{2-})(CHA^{+})_3(C_7H_{11}NO_2^{-})(CHA)\bullet(H_2O)$** (a) viewing along [100], where the guests are shown, with their van der Waals radii highlighted for clarity and (b) where the guests are omitted and the channels in which the guest reside can be seen

The channels occupied by the guests were also viewed using the program Mercury[4] (**Figure 3.2.5.).** This analysis was carried out with a probe radius of 1.5 Å.

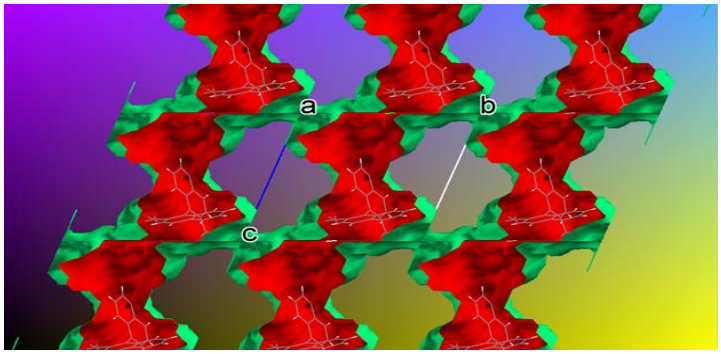

Figure 3.2.5 channel created by the voids in **(BNDA^{2-})(CHA^{+})$_3$(C$_7$H$_{11}$NO$_2^{-}$)(CHA)•(H$_2$O).**

The structure is stabilised by O-H•••N hydrogen bonding. Anion host-cation guest interactions are illustrated in **Figure 3.2.5.**

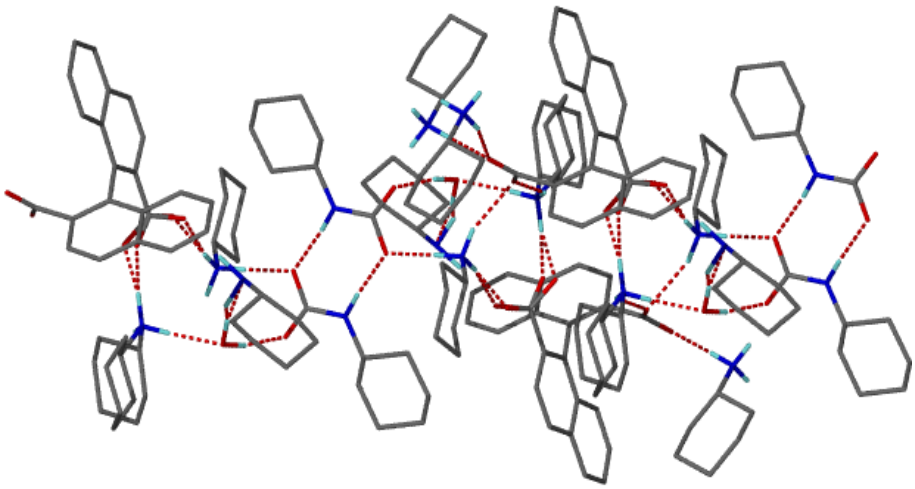

Figure 3.2.6 Hydrogen bonding in **(BNDA^{2-})(CHA^{+})$_3$(C$_7$H$_{11}$NO$_2^{-}$)(CHA)•(H$_2$O)**

D-H…A	D(D-H)(Å)	d (H…A)(Å)	<(DHA)(^{o})	d(D..A)(Å)	Symmetry operator
N3-H7G…O4	0.941(2)	2.010(2)	175.79(2)	2.949(1)	[-x+1, -y, -z]
N2-H5G. O2	0.889(3)	2.201(3)	160.60(2)	3.054	[x, y, z]
N3-H8G… O1	0.919(2)	1.800(2)	174.99	2.717(1)	[x, y, z]
O5-H1…N1	1.129	1.619	170.88	2.739	[-x+1, -y+1, -z]
N5-H12G… O5	0.919(3)	2.546(3)	124.30(2)	3.157	[x, y, z]
N5-H11G… O1’	0.993(3)	1.720(3)	172.77	2.708	[-x+1, -y+1, -z]
N5-H11G…O1A	0.993	1.947(3)	147.77	2.837	[-x+1, -y+1, -z]
N1-H1G… O1A	0.914	2.176	160.19	3.052	[-x+1, -y+1, -z+1]
N1-H1G…O2’	1.011	1.740	169.79	2.740	[x,y,z]
N5-H13G…O1’	0.904(3)	2.333	123.28	2.928	[x, y, z]
N5-H13G…O2	0.904(3)	2.110(3)	135.24(3)	2.824	[x, y, z]
O5-H2…O4	1.151	1.675(5)	170.85	2.818	[x, y, z]
N4G-H10G…O3	0.948(2)	2.004	174.53	2.949	[-x, -y, -z-1]
N2G-H4G...O2A	0.931(2)	1.826	148.85	2.666	[-x+1, -y+1, -z]
N2G-H4G… O2’	0.931 (2)	1.847	169.55	2.768	[-x+1, -y+1, -z]
N2G-H6G…O3	0.933	1.788	173.80	2.717	[x,y,z]
N2G-H6G…O4	0.933	2.541	123.99	3.158	[x,y,z]
N3-H9G…O1	0.917(2)	1.842	172.30	2.754	[x,y,z]

Table 3.2.2 Hydrogen bonding details of **$(BNDA^{2-})(CHA^{+})_3(C_7H_{11}NO_2^{-})(CHA)\bullet(H_2O)$**

Thermal analysis

Thermal analysis of desorption of **$(BNDA^{2-})(CHA^{+})_3(C_7H_{11}NO_2^{-})(CHA)\bullet(H_2O)$** can be clarified by the reaction mechanism below:

$(BNDA^{2-})(CHA^{+})_3(C_7NO_2H_{11}^{-})\bullet CHA\bullet H_2O \rightarrow (BNDA^{2-})(CHA^{+})_3\bullet (3CHA) + CO_2 + H_2O$ (1)

$(BNDA^{2-})(CHA^{+})_2\bullet (3CHA) \rightarrow (BNDA^{2-})(CHA^{+})_2\bullet (2CHA) + CHA$ (2)

$(BNDA^{2-})(CHA^{+})_2\bullet (2CHA) \rightarrow (BNDA^{2-})(2CHA^{+})_2 + 2CHA$ (3)

The DSC endotherm shows 3 peaks: the first one which corresponds to the first reaction comes out at a peak of 354.7K (T_{on} = 338.0 K) and the second peak is shown at 394.7K (T_{on} = 378.8 K). The third peak appears clearly around 444.7 K (T_{on} = 433.0 K). The host melt appears at 597.9 K.

The TG curve gave 3 mass losses which can be interpreted as: experimentally, the first mass loss of 7.5 % (reaction 1) corresponds to the desolvation of the water molecule and the carbon dioxide. The second mass loss of 11.7 % is due to the loss of the first guest of CHA; and the third mass loss of 22.1 % is due to the release of two molecules of CHA. These are followed by the host melt and decomposition. The total mass loss expected was 89.9 %. The details of the thermal analysis are given in the **Table 3.2.3**.

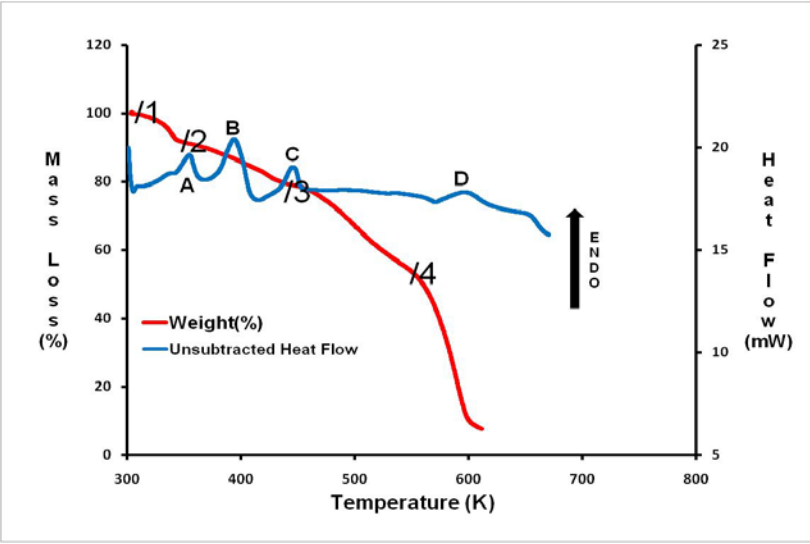

Figure 3.2.7 TG and DSC curves for **$(BNDA^{2-})(CHA^{+})_3(C_7H_{11}NO_2^{-})\bullet CHA\bullet H_2O$**

	TG Results			
	Calc. % mass loss		**Exp. % mass loss**	
mass loss 1	6.9 (loss of H_2O and CO_2)		7.5	
mass loss 2	11.0 (loss of CHA)		11.7	
mass loss 3	22.0 (loss of 2 CHA)		22.1	
	DSC Results			
	T_{on}(K): Peak1	**T_{on}(K): Peak 2**	**T_{on}(K): Peak 3**	**T_{on}(K): Peak 4**
	338.0; 354.7	378.8; 394.7	433.0; 444.7	597.9

Table 3.2.3 Thermal analysis results for **$(BNDA^{2-})(CHA^{+})_3(C_7H_{11}NO_2^{-})\bullet CHA\bullet H_2O$**

2. $(BNDA^{2-})(DCHA^{+})_2 \bullet CH_3OH \bullet H_2O$

Compound name: Dicyclohexylammonium-1,1'-binaphthyl-2,2'-dicarboxylate hydrate methanol

Formula: $(C_{22}H_{12}O_4^{2-})(C_8H_8N^{+})_2 \bullet CH_3OH \bullet H_2O$

Asymmetric unit:

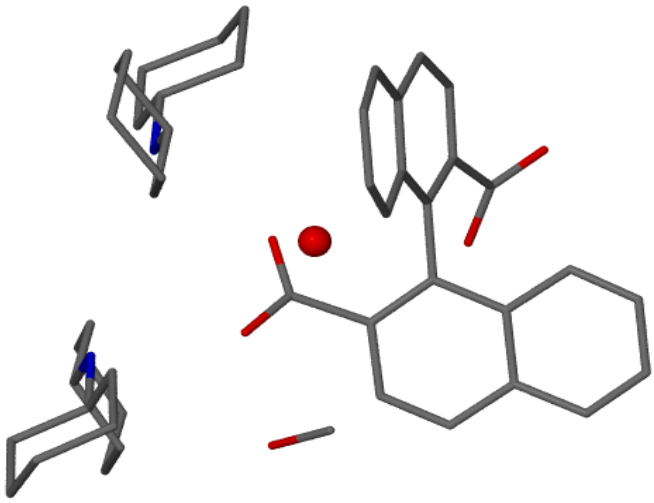

Figure 3.2.8 Asymmetric unit of $(BNDA^{2-})(DCHA^{+})_2 \bullet CH_3OH \bullet H_2O$ with all the hydrogens omitted for clarity.

Crystal structure and refinement

The crystal unit cell parameters of $(BNDA^{2-})(DCHA^{+})_2 \bullet CH_3OH \bullet H_2O$ were also obtained from the Nonius Kappa CCD diffractometer. The salt formed by BNDA in the DCHA crystallises in the monoclinic crystal system, space group $P2_1/n$.

The crystal structure was solved by direct methods. The non-hydrogen atoms were found in the difference map. All non- hydrogen atoms of the host and the guest were refined anisotropically. All hydrogens were found in the electron density maps including the carboxyl hydrogen of the host. Aromatic hydrogen were fixed at a distance of C-H = 0.95Å. The guest CH_2-hydrogens were fixed with a C-H distance of 0.99 Å. the dihedral angle between the naphthyl moieties of BNDA was calculated with Olex 2[2] and found to be 82.91°, a value which is consistent with those found for other inclusion compounds. The structure refined successfully to R_1 = 0.0447 with wR_2 = 0.1307.

Crystal packing

The packing diagram of **$(BNDA^{2-})(DCHA^{+})_2 \bullet CH_3OH \bullet H_2O$** is shown in **Figure 3.2.9.** There are four host and 8 guest molecules in each unit cell. The ratio H: G is 2:1 (Z = 4). The host molecules pack to form layers parallel to the ac plane. The guest cations are packed in a constricted channel formed by the framework of the hosts in the direction [100] in **Figure 3.2.10(a).** it shows the guest with their van der Waals radii and **Figure 3.2.10(b)** describe the framework of the host with its van der Waals radii, where the guests are removed. Here, the channels formed are clear.

The host anions and guest cations form rings of the form (host)-COO^{-}•••N^{+}(guest) via hydrogen bonding. These host-guest rings are located in columns along the [001] direction as shown in **Figure 3.2.12**.

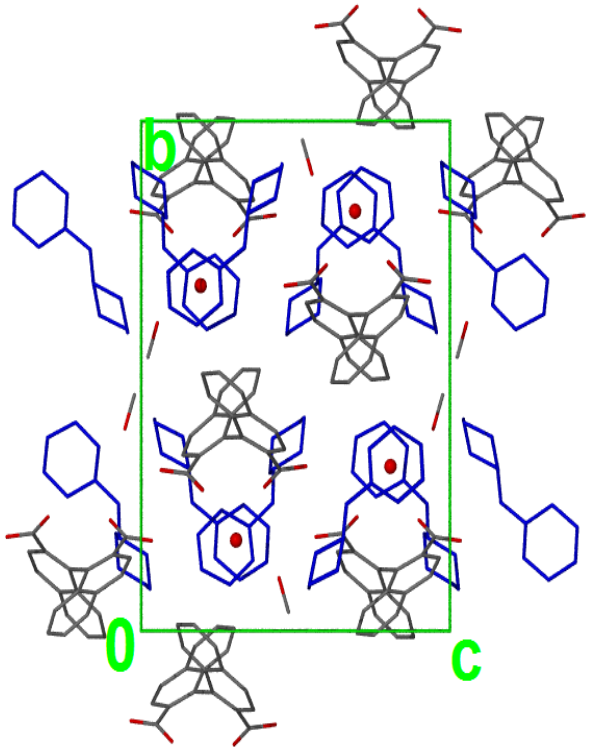

Figure 3.2.9 Packing diagram of **$(BNDA^{2-})(DCHA^{+})_2 \bullet CH_3OH \bullet H_2O$** viewing along [100] showing the guest in blue for clarity

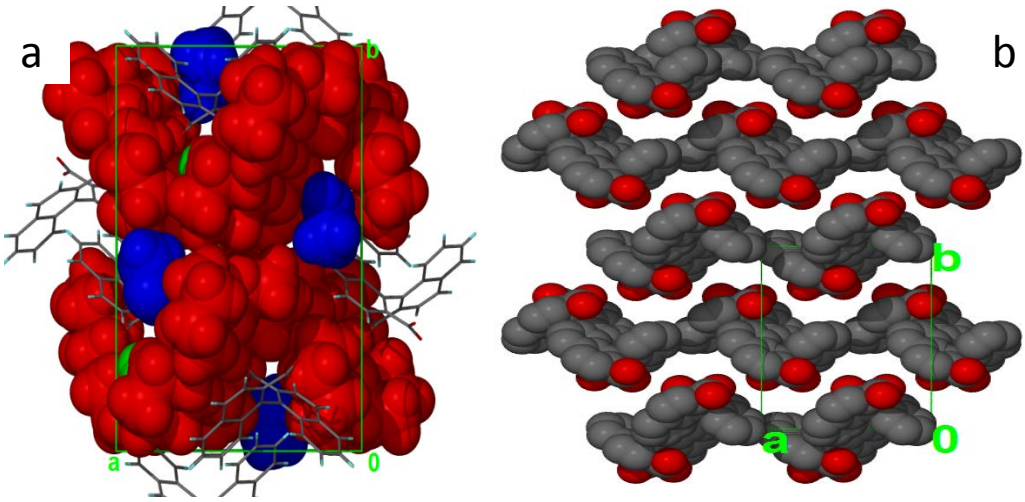

Figure 3.2.10 Space filled packing diagrams for **$(BNDA^{2-})(DCHA^{+})_2 \bullet CH_3OH \bullet H_2O$** (a) viewing along [010], where the guest are shown, with their van der Waals radii highlighted for clarity and (b) where the guest are omitted and the channels in which the guest reside can be seen.

The channels occupied by the guests was also viewed, using the program Mercury[4] (**Figure 3.2.11).** This analysis was carried out with a probe radius of 1.5 Å.

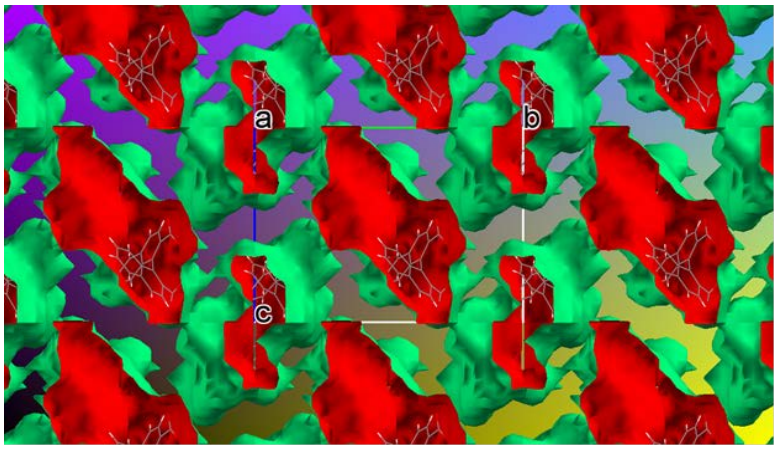

Figure 3.2.11 Channel created by the voids in **$(BNDA^{2-})(DCHA^{+})_2 \bullet CH_3OH \bullet H_2O$**.

The structure is stabilised by a network composed of hydrogen and ionic bonding.

The carboxylates of two host with two ammonium ions from the guest formed a ring. The pattern contains a total of twelve atoms in which two are donors and four acceptors, hence it is designated N_2=$R_2^4(12)$. $R_2^4(12)$. [5] This network is reinforced by secondary hydrogen bonding, two from the oxygen of the water molecules to the host and one from methanol to the carboxylate group.

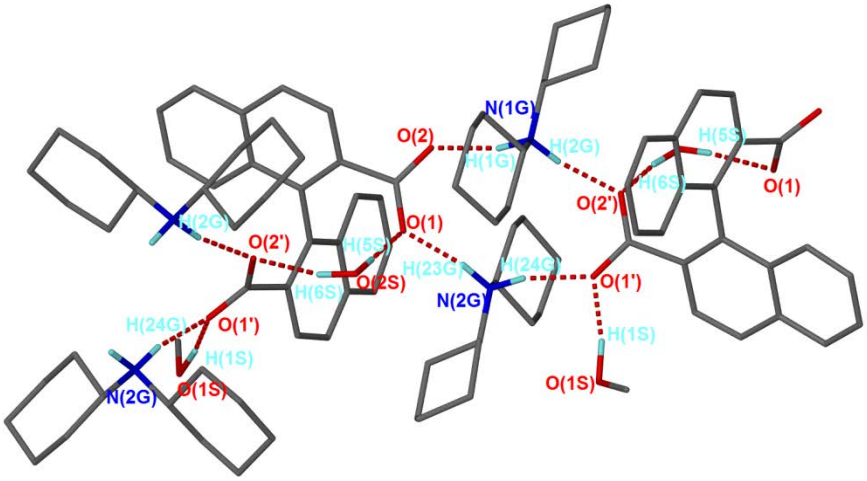

Figure 3.2.12 Hydrogen bonding in **$(BNDA^{2-})(DCHA^{+})_2 \bullet CH_3OH \bullet H_2O$**

D-H…A	D(D-H)(Å)	d (H…A)(Å)	<(DHA)(^{o})	d(D..A)(Å)	Symmetry operator
N2G-H24G…O1’	0.928 (2)	1.873 (2)	164.01 (2)	2.777 (1)	[x,y,z]
O1S-H1S…O1’	1.029 (2)	1.743 (2)	167.10	2.756	[x, y, z]
N1G-H1G… O2	0.912 (2)	1.844	164.38	2.733 (1)	[x-1/2, -y+1/2, z-1/2]
N1G-H2G… O2'	0.925 (2)	1.890 (2)	169.45 (2)	2.804	[x, y, z]
O2S-H6S… O2'	0.954	2.022	158.12	2.928	[x, y, z]
O2S-H5S… O1	0.841	2.000	171.49	2.834	[x, y, z]
N2G-H23G… O1	0.936	1.816	169.70	2.742	[x-1/2, -y+1/2, z-1/2]

Table 3.2.4 Hydrogen bonding details of **$(BNDA^{2-})(DCHA^{+})_2 \bullet CH_3OH \bullet H_2O$**

Thermal analysis

TG and DSC analyses were performed for **$(BNDA^{2-})(DCHA^{+})_2 \bullet CH_3OH \bullet H_2O$.** The experimental mass loss is almost the same with the expected value with the host-guest ratios of 1:1. The endotherm and mass loss on curves were assigned to the loss of one dicyclohexylamine and the other one melt together with the host as the trend with the other inclusions discussed already.

The DSC endotherm shows 3 peaks: the first one which corresponds to the release of the first guest at a peak of 376.3 K (T_{on} = 371.9 K) and the second DCHA came out at 471.0 K (T_{on} = 466.7 K). The third peak which doesn't appear clearly around 530.0K is due to the host melt.

A suggested mechanism for the desolvation of the salt **$(BNDA^{2-})(DCHA^{+})_2 \bullet CH_3OH \bullet H_2O$** is shown below, to explain clearly the thermogravimetric analysis.

$(BNDA^{2-})(DCHA^{+})_2 \bullet (CH_3OH) \bullet (H_2O)$ $\rightarrow (BNDA^{2-})(DCHA^{+})_2 + CH_3OH + H_2O$ (1)

$(BNDA^{2-})(DCHA^{+})_2 \rightarrow (BNDA^{-})(DCHA^{+}) \bullet$ (cyclohexane) + CHA (2)

$(BNDA^{-})(DCHA^{+})$(cyclohexane) $\rightarrow (BNDA^{-})(DCHA^{+})$ + cyclohexane (3)

$(BNDA^{-})(DCHA^{-}) \rightarrow$ BNDA + DCHA (4)

The TG curve gave 3 mass losses: the first step of 6.6 % corresponds to the release of one molecule of methanol and one molecule of water in the first reaction step. This is followed by the loss of one DCHA in two steps (step 2 and 3) of 12.7 % and 11.3 % respectively. The mass loss of the second guest of DCHA was difficult to calculate because the second guest is released together with the host melt. The mass loss expected for the two guests was of 49.9 %. The thermal analysis summary is given in **Table 3.2.5.**

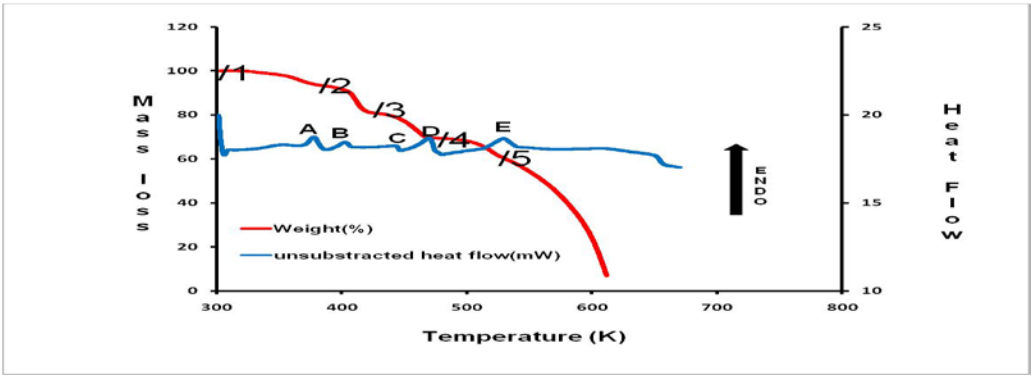

Figure 3.2.13 TG and DSC curves for **$(BNDA^{2-})(DCHA^{+})_2 \bullet CH_3OH \bullet H_2O$**

	TG Results			
	Calc. % mass loss		**Exp. % mass loss**	
mass loss 1	6.6 (loss of H_2O and CH_3OH)		6.6	
mass loss 2	12.9 (loss of CHA)		12.6	
mass loss 3	11.1 (loss of cyclohexane)		11.3	
mass loss 4	24.0 (loss of 1 DCHA)		-	
	DSC Results			
	T_{on}(K): Peak1	**T_{on}(K): Peak 2**	**T_{on}(K): Peak 2**	**T_{on}(K): Peak 4**
	338.0; 354.7	378.8; 394.7	433; 444.7	597.9

Table 3.2.5 Thermal analysis details of **$(BNDA^{2-})(DCHA^{+})_2 \bullet CH_3OH \bullet H_2O$**

DISCUSSION

The racemic host BNDA formed once again salts with a series of two cyclohexylamines; cyclohexylamine (CHA) and dicyclohexylamine (DCHA). The salts formed had totally different host: guest ratios, space groups as well as crystal group systems. **$(BNDA^{2-})(CHA^{+})_3(C_7H_{11}NO_2^{-}) \bullet CHA \bullet H_2O$** had in its asymmetric unit, one divalent host anion, three cyclohexylammonium ions, one molecule of CHA, one molecule of water and the carbamate anion. It crystallised in the triclinic space group P-1. **$(BNDA^{2-})(DCHA^{+})_2 \bullet CH_3OH \bullet H_2O$** had in its asymmetric unit one host anion, two dicyloheaxyammonium cations, a methanol molecule and a water molecule and crystallised in a monoclinic space group $P2_1/n$.

III.3. Salts formed between racemic 1,1'-binaphthyl-2,2'-dicarboxylic acid with racemic amines.

The racemic host BNDA, insoluble in all the other amines, was dissolved in the racemic SecBuam. The solution was allowed to evaporate at room temperature and crystals of the salt **$(BNDA^-)(SecBuam^+)_2 \bullet 3H_2O$** were formed. The salt **$(BNDA^-)(SecBuam^+)_2 \bullet But$** was obtained by dissolution of the racemic 1,1'-binaphthyl-2,2'-dicarboxylic acid with SecBuam using *n*-butanol as a co-solvent. The thermal analyses results and their crystal structures will be elucidated in this chapter. The crystal data for these two salts **$(BNDA^{2-})(SecBuam^+)_2 \bullet 3H_2O$** and **$(BNDA^{2-})(SecBuam^+)_2 \bullet But$** are presented in **Table 3.3.1**.

Compound	**$(BNDA^{2-})(SecBuam^+)_2 \bullet 3H_2O$**	**$(BNDA^{2-})(SecBuam^+)_2 \bullet But$**
Molecular Formula	$(C_{22}H_{12}O_4^{2-})(C_4H_{12}N^+)_2 \bullet 3H_2O$	$(C_{22}H_{12}O_4^{2-})(C_4H_{12}N^+)_2 \bullet C_4H_8O$
Molecular Mass ($gmol^{-1}$)	542.55	562.65
Data collection temp.(K)	296 (2)	173 (2)
Crystal system	Triclinic	Triclinic
Space group	*P*-1	*P*-1
a (Å)	10.1522 (2)	10.8236 (1)
b (Å)	11.4194 (2)	11.4388 (1)
c (Å)	13.6396 (3)	13.7134 (1)
α (°)	70.654 (3)	96.754 (2)
β (°)	79.202 (3)	97.042 (2)
γ (°)	87.297 (3)	109.382 (2)
Volume ($Å^3$)	1465.37 (5)	1566.65 (5)
Z	2	2
D_c, Calculated density ($g\ cm^{-3}$)	1.2297	1.1928
Final R indices [I>2sigma(I)]	R_1= 0.0498 wR_2= 0.1495	R_1= 0.0440 wR_2= 0.0897
R indices (all data)	R_1= 0.051 wR_2= 0.1207	R_1= 0.1138 wR_2= 0.1349
Largest diff. peak&hole ($eÅ^{-3}$)	0.39; -0.32	0.18; -0.19

Table 3.3.1 Crystal data table for salts **$(BNDA^{2-})(SecBuam^+)_2 \bullet 3H_2O$** and **$(BNDA^{2-})(2SecBuam^+)_2 \bullet But$**

1. $(BNDA^{2-})(SecBuam^{+})_2 \bullet 3H_2O$

Compound name: 1-methylpropylammonium-1,1'-binaphthyl-2,2'-dicarboxylate trihydrate
Formula: $(C_{22}H_{12}O_4^{2-})(C_4H_{12}N^{+})_2 \bullet 3H_2O$
Asymmetric unit**:**

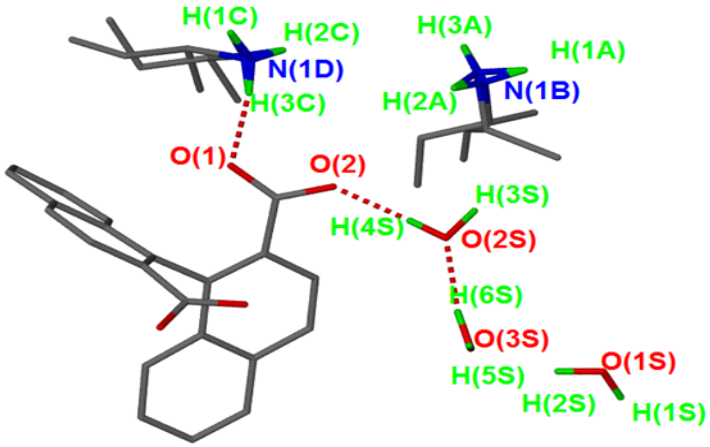

Figure 3.3.1 asymmetric unit of **$(BNDA^{2-})(SecBuam^{+})_2 \bullet 3H_2O$**

Crystal structure and refinement

The crystal unit cell parameters of **$(BNDA^{2-})(SecBuam^{+})_2 \bullet 3H_2O$** were also obtained from the Nonius Kappa CCD diffractometer. The salt formed crystallised in the triclinic crystal system, space group P-1.

The crystal structure was solved by direct methods. The non-hydrogen atoms were found in the difference electron density map. All non- hydrogen atoms of the host and the guest were refined anisotropically. All hydrogens were found in the difference electron density map including the hydrogens attached to the nitrogens of the ammonium cations. Aromatic hydrogens were fixed at a distance of C-H = 0.95 Å. The guest CH_2 were fixed at a C-H distance of 0.99 Å. The two guest cations of secbuam are both disordered over two positions each with site occupancies of 0. 82 and 0.18 for the first and the other showed site occupancies at 0.73 and 0.27. The dihedral angle between the naphthyl moieties of BNDA was been calculated with Olex 2[2] and found to be 89.5 (2) °, which is consistent with the values found

previously. The structure refined successfully to R_1 = 0.051with wR_2 = 0.1495. The disorder in the guest molecules is shown in **Figure 3.3.1.**

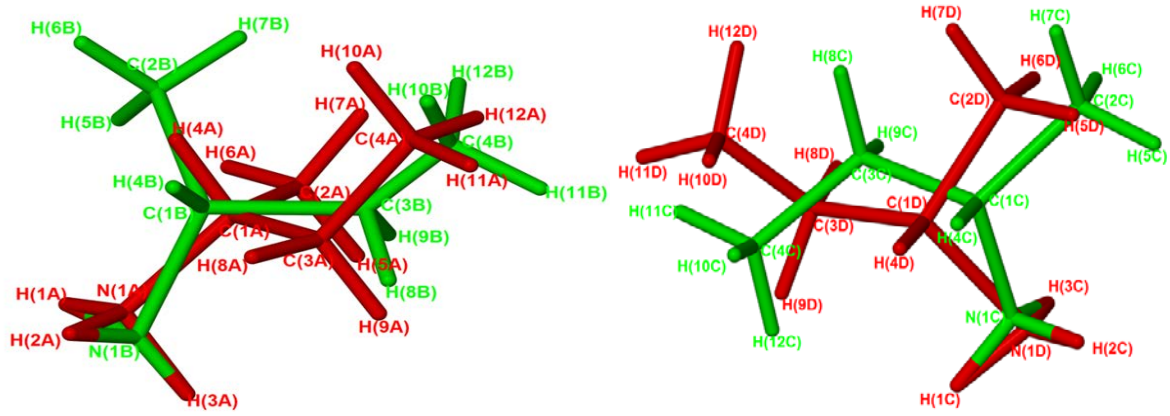

Figure 3.3.1 Disorder in the two guest cations.

Crystal packing

The packing diagrams of **$(BNDA^{2-})(SecBuam^{+})_2 \bullet 3H_2O$** are shown in **Figure 3.3.2.** There are two host anions, four guest cations and six water molecules in each unit cell. Thus the H: G ratio is 1:2 (Z = 2). The host molecules pack to form layers parallel to the ac plane **(Figure 3.3.3.).** The guest cations are packed in a constricted channel formed by the framework of the hosts in the direction [010].

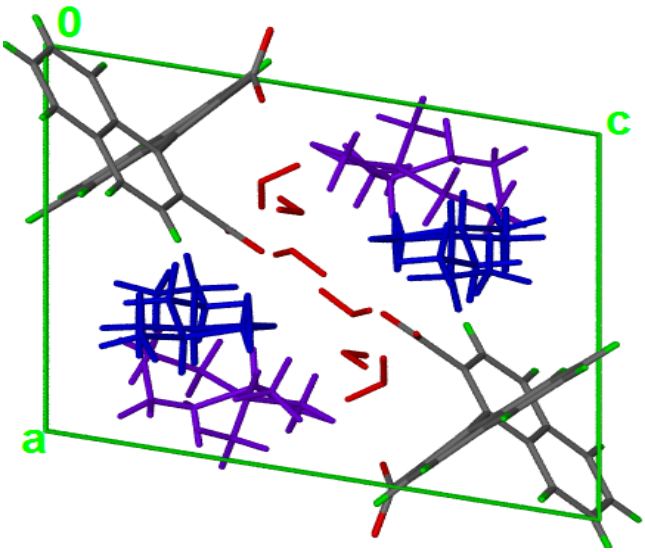

Figure 3.3.2. Packing diagram of **$(BNDA^{2-})(SecBuam^{+})_2 \bullet 3H_2O$** viewing along [001] showing the guest in blue and purple and the water molecules in red for clarity.

The host anions and guest cations form a strong hydrogen bonded network composed of five kinds of rings of the form (host)-COO^{-}•••N^{+}(guest) via hydrogen

bonding. These host-guest rings are configured in a general direction for a better view (**Figure 3.3.5)**. The ring A bonds two donors (2 oxygens O2S) to two acceptors (the two oxygens O2), the ring B which is pentagonal, bonds O1',O2',O2S, O3S and N1G(or N1J). the ring C is composed of O1, O2, O2', O3S, O2S AND N1A(or N1B). the last squared ring D has two O1' and two N1G(or N1J). The graph set notation of the five rings are respectively N_2= $R_4^3(10)$, N_2= $R_5^5(12)$, $N2 = R_3^2(10)$, and N_2= $R_2^4(8)$.

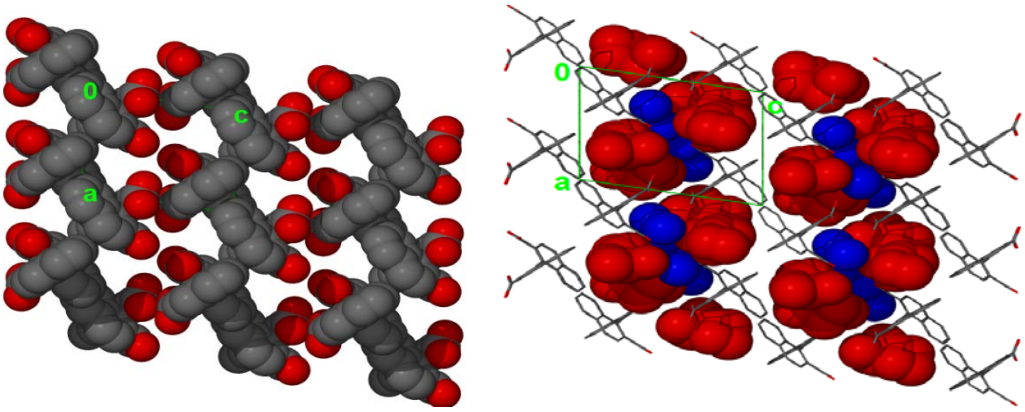

Figure 3.3.3 Space filled packing diagrams for **$(BNDA^{2-})(SecBuam^{+})_2 \bullet 3H_2O$** (a)viewing down [010], where the guests are removed with the host anions shown in van der Waals radii and (b) where the host anions are displayed in stick notation and guest cations and the water molecules shown in the van der Waals radii. The channels occupied by the guests was also seen, using the program Mercury[4] (**Figure 3.3.4).** This analysis was carried out with a probe radius of 1.5 Å .

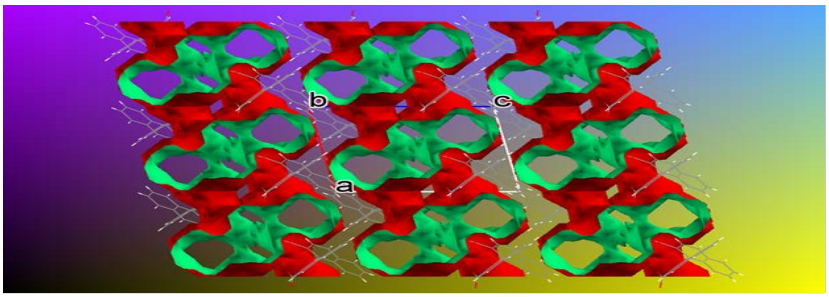

Figure 3.3.4 Channels occupied by the secbutylammonium cations and the water molecules in **$(BNDA^{2-})(SecBuam^{+})_2 \bullet 3H_2O$**

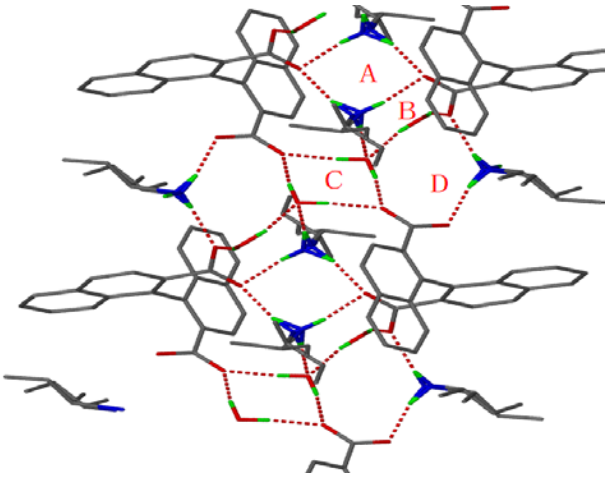

Figure 3.3.5 Hydrogen bonding interactions in **$(BNDA^{2-})(SecBuam^{+})_2 \bullet 3H_2O$.**

D-H···A	D(D-H)(Å)	d (H···A)(Å)	<(DHA)(^{o})	d(D···A)(Å)	Symmetry operator
N1B-H2A···O1	0.878(2)	1.883(3)	168.85(2)	2.750(1)	[x,y,z]
N1A-H1A···O1S	0.946(3)	1.941(2)	151.40(2)	2.808(5)	[-x+1, -y+1, -z+1]
N1B-H3A ··· O2'	0.777(1)	2.014(2)	166.21(2)	2.774(1)	[x+1, y, z]
N1G-H2G··· O1'	0.939(3)	1.838(2)	167.94(2)	2.764(5)	[-x+1, -y+1, -z+1]
O2S-H3S···O2	0.947(1)	1.755(3)	168.24(3)	2.689(2)	[-x+1, -y+1, -z+1]
O2S-H4S···O2	0.906(1)	1.824(3)	163.77(2)	2.706(2)	[x, y, z]
O3S-H6S···O2S	0.970(1)	1.863(3)	158.6(3)	2.789(2)	[x, y, z]
O3S-H5S···O2'	0.938(2)	1.850(3)	165.83(2)	2.769(2)	[-x, -y+1, -z+1]
N1G-H1G···O2S	0.948(4)	2.046(2)	171.43(2)	2.986(1)	[-x+1, -y+1, -z+1]
O1S-H1S···O1	0.874(2)	1.991(2)	158.3(3)	2.82(2)	[x, y-1, z]
O1S-H2S···O3S	0.953(2)	1.919(3)	160.16(2)	2.833(3)	[x, y, z]
N1J-H3G···O1'	0.799(4)	1.833(4)	170.04(2)	2.624(3)	[x+1, y, z]
N1J-H3G···O2'	0.799(4)	2.273(1)	125.66(2)	2.814(3)	[x+1, y, z]

Table 3.2.2 Hydrogen bonding details of **$(BNDA^{2-})(SecBuam^{+})_2 \bullet 3H_2O$**

Thermal analysis

The first broad endotherm in the DSC scan corresponds to the release of the three water molecules, T_{peak} = 342.5 K (T_{on}=318.8 K). For the second endotherm, the first molecule of SecBuam was released at 383.0 K (T_{on}= 372.8 K). The third peak doesn't appear clearly around 534K is due to the melt of the host combined to one molecule of Secbuam.

The TG curve gave 3 mass losses: the first step of 4.8% and the second step of 10.6% which correspond to the release of one mole followed by 2 moles of water. The third mass loss gave 17.6 % which is the release of the first SecBuam and afterwards the melting of the entity $(BNDA^{-})(secBuam^{+})$. A mechanism can be suggested for the desolvation of this salt of **$(BNDA^{2-})(SecBuam^{+})_2 \bullet 3H_2O$**:

$(BNDA^{2-})(secBuam^{+})_2 \bullet 3H_2O$ → $(BNDA^{2-})(secBuam^{+})_2 \bullet 2H_2O + H_2O$

$(BNDA^{2-})(secBuam^{+})_2 \bullet 2H_2O \rightarrow (BNDA^{2-})(secBuam^{+})_2 + 2H_2O$

$(BNDA^{2-})(secBuam^{+})_2 \rightarrow (BNDA^{-})(secBuam^{+}) + secBuam$

$(BNDA^{-})(secBuam^{+}) \rightarrow BNDA + SecBuam$

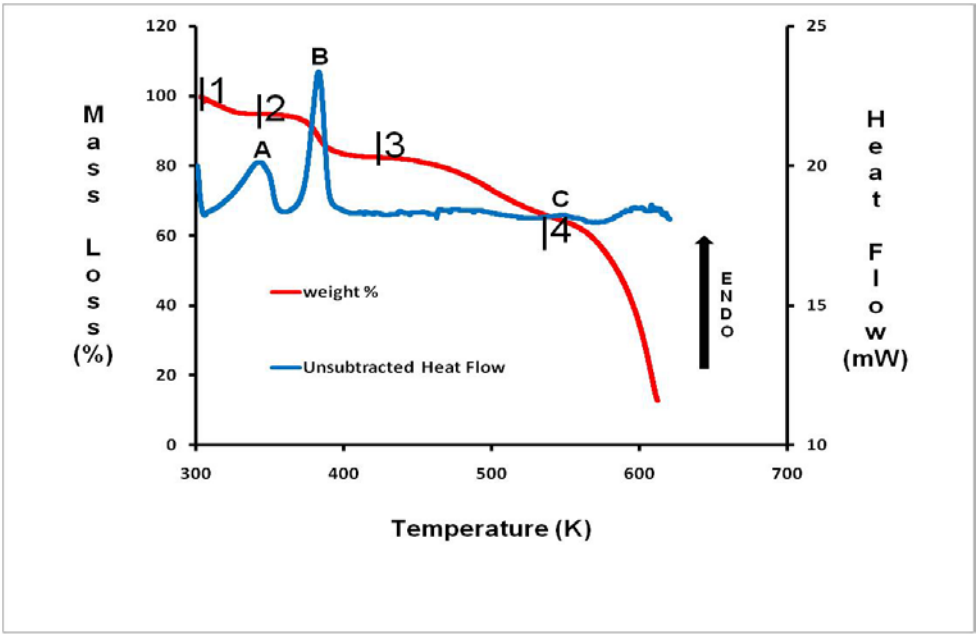

Figure 3.3.6 TG and DSC curves for **$(BNDA^{2-})(SecBuam^{+})_2 \bullet 3H_2O$**

2. $(BNDA^{2-})(SecBuam^{+})_2 \bullet But$

Compound name: 1-methylpropylammonium-1,1'-binaphthyl-2,2'-dicarboxylate butanol

Formula: $(C_{22}H_{12}O_4^{2-})(C_4H_{12}N^{+})_2 \bullet CH_3CH_2CH_2OH$

Asymmetric unit:

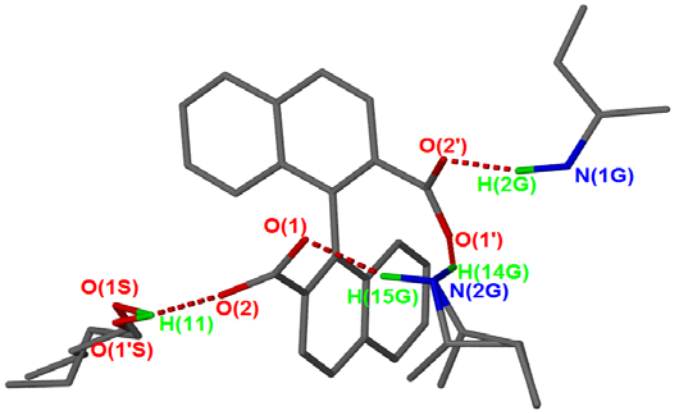

Figure 3.3.7 Asymmetric unit of **$(BNDA^{2-})(SecBuam^{+})_2 \bullet But$**

Crystal structure and refinement

The crystal unit cell parameters of **$(BNDA^{2-})(SecBuam^{+})_2 \bullet But$** were also obtained from the same Nonius Kappa CCD diffractometer. This salt structure crystallises in the triclinic crystal system in space group P-1.

The non-hydrogen atoms were found in the difference electronic density map and were refined anisotropically. The hydrogens of the water and the N-H hydrogens were found in the difference electronic density and were refined anisotropically. Aromatic hydrogen atoms were fixed at a distance of C-H = 0.95 Å. The guest CH_2 hydrogens were fixed with C-H distance of 0.99 Å. The SecBuam and the solvent butanol are disordered over two positions (Figure 3.2.1 a). The site occupancy factors of the SecBuam are 0.81 and 0.19 and those of the butanol are 0.69 and 0.31.

. The dihedral angle between the naphthyl moieties was calculated and found to be 93.6 °(3). The structure refined successfully to R_1= 0.0463 with wR_2 = 0.1259.

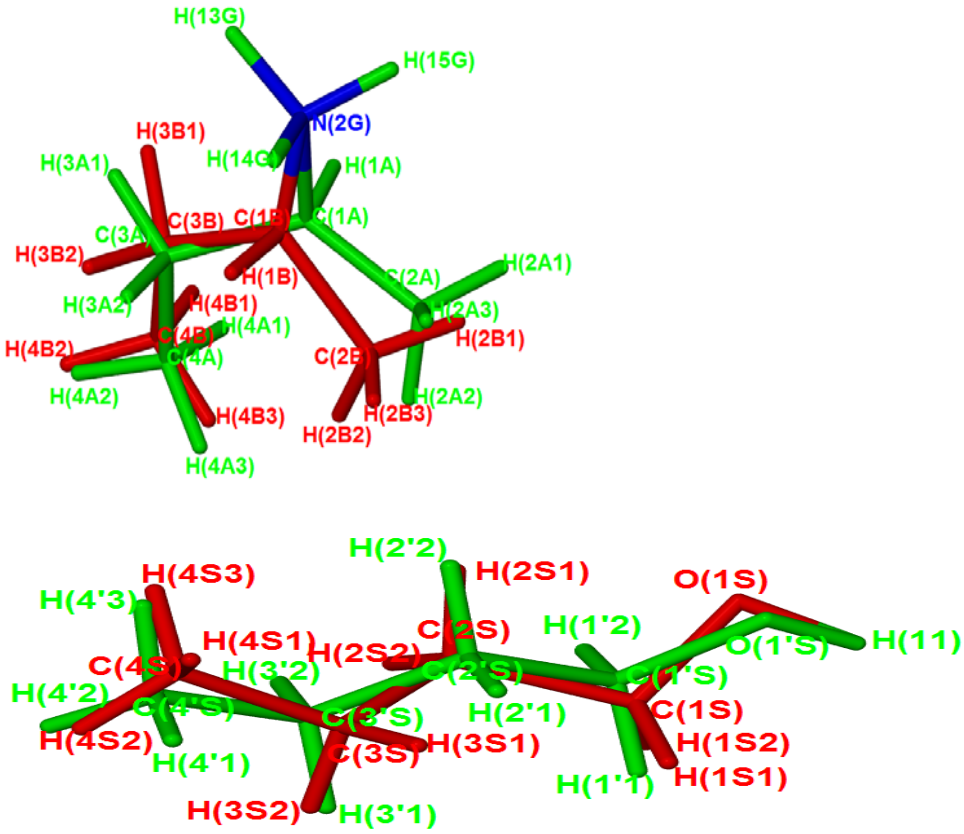

Figure 3.3.8 Disorder in the one Secbuam guest cation and in butanol

Crystal packing

The packing diagram of **(BNDA^{2-})(SecBuam^{+})$_2$●But** down [100] is shown in **Figure 3.3.9**. The unit cell contains two anions of **BNDA^{2-}** and four cations of SecBuam^{+} (Z=2).

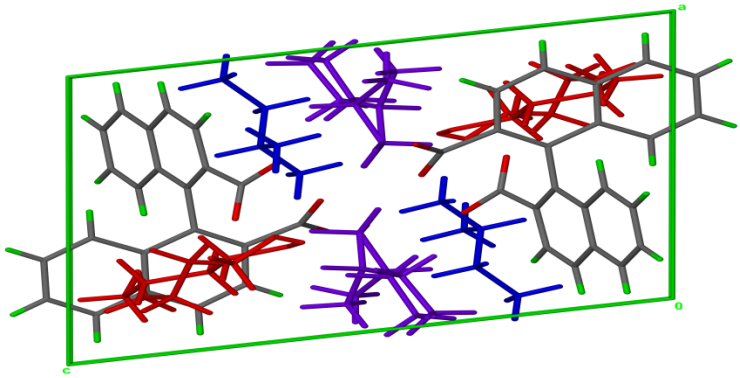

Figure 3.3.9 Packing diagram of **(BNDA^{2-})(SecBuam^{+})$_2$●But** showing the guests in blue and in purple and the butanol in red for clarity

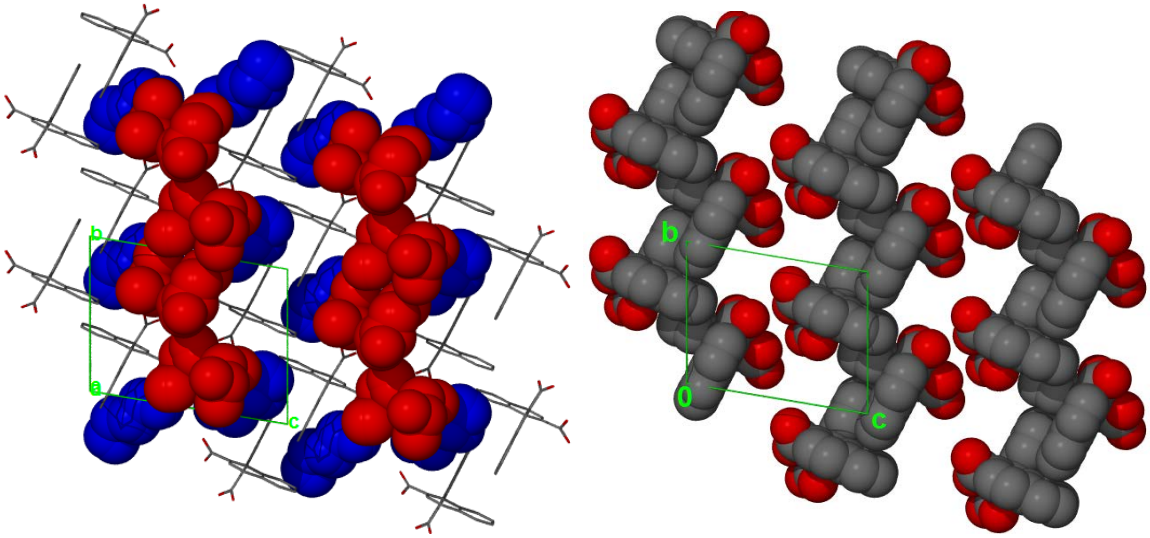

Figure 3.3.10 Space filled packing diagrams for **(BNDA^{2-})(SecBuam^{+})$_2$●But** (a)viewing along [100], where the guest are shown, with their van der Waals radii highlighted for clarity and (b) where the guest are omitted and the channels in which the guest reside can be seen. The channels occupied by the guests was also seen, using the program Mercury[4] (**Figure 3.3.11.).** This analysis was carried out with a probe radius of 1.5 Å.

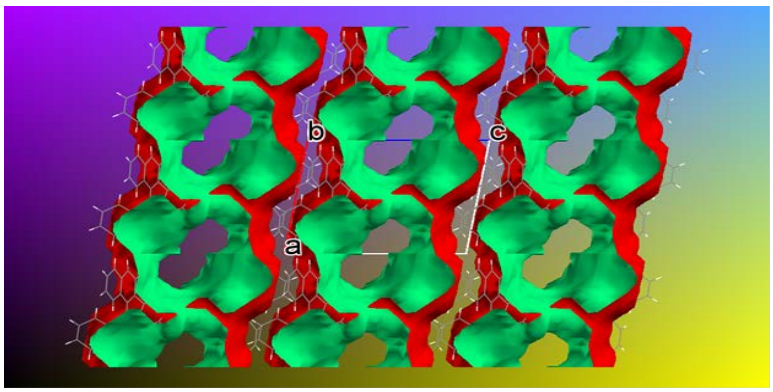

Figure 3.3.11 Channels occupied by the secbutylammonium cations and the butanol in **(BNDA^{2-})(SecBuam^{+})$_2$●But.**

The structure is stabilised by ionic-hydrogen bonding. Hydrogen bonded rings involve the N-H moieties of the secbutylammonium cations acting as donor groups to the carboxylate anions are of three kinds **(Figure 3.1.12).** These rings can be described in graph set notation as ring A [$R_4^2(8)$], ring B [$R_2^4(12)$], ring C [$R_6^4(12)$], ring D [$R_1^1(11)$] and ring E [$R_1^2(11)$]

The interatomic distances of O1'•••N1, O2'•••N1, O1•••N2 and O2•••N2 are 2.695(3), 2.664(3), 2.634 and 2.685 respectively . The hydrogen bonding details are given in **Table 3.1.4.**

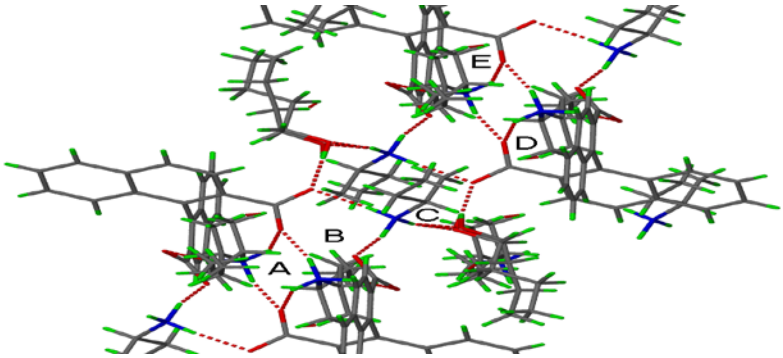

Figure 3.3.12 Hydrogen bonding interactions in **$(BNDA^{2-})(SecBuam^{+})_2$●But**.

D-H…A	D(D-H)(Å)	d (H···A)(Å)	<(DHA)(^{o})	d(D···A)(Å)	Symmetry operator
N1-H1G···O1S	0.907(3)	1.795	160.23	2.666	[x, y+1, z]
N1-H2G···O2'	1.120	1.655	163.43	2.747(3)	[x, y, z]
N1-H1G···O1'S	0.907	2.010	169.77	2.907	[x, y+1, z]
N1-H3G···O2	0.946 (4)	1.830	174.14	2.773(3)	[-x+1, -y+1, -z+1]
N2-H5G···O1'	1.084	1.799	152.97	2.808	[x,y,z]
N2-H4G…O2'	1.024(5)	2.363	120.26	3.011	[-x+1, -y+1, -z+1]
O1S-H1S···O2	0.880	1.791	176.14	2.671	[x,y,z]
N2-H5G···O2'	1.084	2.542	110.38	3.091	[x,y,z]
N2-H6G···O1	1.084	1.712	166.58	2.778	[-x+1, -y+1, -z+1]
N1-H3G···O1	0.946	2.642	119.23	3.212	[-x+1, -y+1, -z+1]
N2-H4G···O1	1.024	2.185	141.85	3.056	[x,y,z]

Table 3.2.2 Hydrogen bonding details of **$(BNDA^{2-})(SecBuam^{+})_2$●But**

Thermal analysis

The DSC shows multiple peaks corresponding to the loss of two secBuam. This is based on the boiling point. The TG curve gave 2 mass losses. The total mass loss is 23.8% which is close to the mass loss expected for the two guests (26.9%). The molecular weight of the *n*-butanol is similar to that of the secBuam guest but the boiling point of *n*-butanol is higher which suggested that the secBuam is released first. The loss of *n*-butanol occurs simultaneously with the host melt.

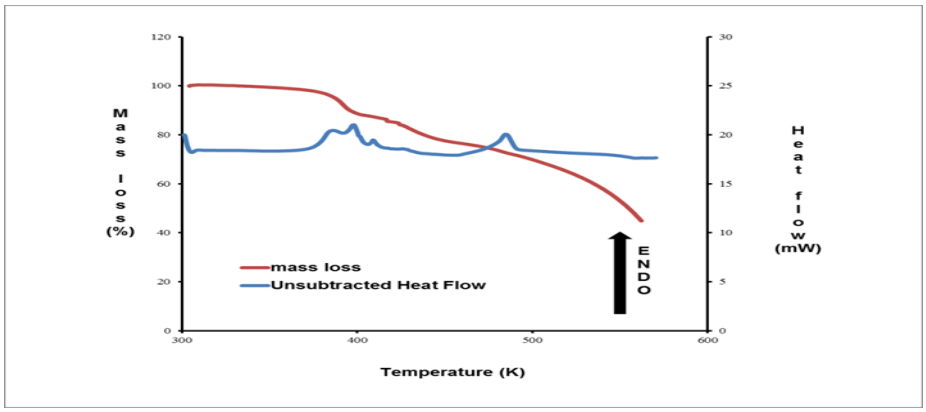

Figure 3.3.13 TG and DSC curves for **(BNDA^{2-})(SecBuam^{+})$_2$●But**

DISCUSSION

The host BNDA forms two salts with the racemic SecBuam. The first one was crystallised in SecBuam without a co-solvent and the second one was crystallised with the SecBuam but by using the *n*-butanol as a co-solvent. Dissolution of BNDA in SecBuam gave a complex with a H:G ratio of 1:2 with three molecules of water. Dissolution of BNDA in SecBuam with n-butanol as co-solvent gave a salt with racemic SecBuam of the same host: guest ratio but with one molecule of butanol included. For both salts, there was a transfer of the two hydrogens from the carboxylic groups of the hosts to the SecBuam and both salts were stabilised by hydrogen bonding between the two carboxylate of the host and the ammonium moieties of the guest bridged by another hydrogen bonding of the solvent.

The guests in both structures were disordered. In **(BNDA^{2-})(secBuam^{+})$_2$●3H2O**, both cations were disordered with site occupancies respectively of 0. 82 and 0.18 for the first cation and of 0,73 and 0.27 for the second cation. For **(BNDA^{2-})(SecBuam^{+})$_2$●But**, disorder was observed for one of the SecBuam cations (0.81 and 0.19) and to the butanol (0.69 and 0.31).

The complexes are all stabilised by hydrogen bonding between the host carboxylate moieties of each host and the ammonium site of the guest cations.

REFERENCES

1. Jacobs, A, Nassimbeni, L R., Ramon, G and Sebogisi, B. K.(2010), *CystEngComm.*, **12**, 3065-3070.

2. Guzei,I.A. (2012). *Notes on Olex2*.

3. Setnicka, V., Urbanova, M., Bour, P., Kral, V. and Volka, K.,(2001) *J. Phys. Chem. A* , **105**, 8931-8938.

4. ConQuest, (2001), *A program for the search of the CSD, Version 1.7*.5. Birkholz, M. (2006) *Thin Film Analysis by X-Ray Scattering*. WILEY-VCH Verlag GmbH & Co. KGaA, Weinheim.

5. Etter, M.C. (1990), *Acc.Chem.Res*. 23,120-126.

6. Ozawa T, (1965), *Bull. Chem. Soc. Jpn.* **38:** 1881-1886.

7. Flynn, J.H. and Wall, L.A., (1966), *J. Polym. Sci., Part B: Polym. Lett.* **4:** 323-328.

8. Simon, P,(2004), *J. Therm. Anal. Cal.* **76:** 123-132

9. Vyazovkin, S.,(2000)., *Thermochim. Acta* **355:** 155-163

10. Khawam A and Flanagan DR, (2005)., *Thermochim. Acta* **429:** 93-102

CHAP IV. INCLUSION COMPOUNDS WITH 1, 1'-BINAPHTHYL-2,2'-DIHYDROXYL

Attempts were made to form inclusion compounds with the same series of amine guests used in the study of 1,1'-binaphthyl-2,2'-dicarboxylic acid, viz, diethylamine, di-n-butylamine, sec-butylamine, cyclohexlamine and dicyclohexylamine. In this chapter the salt cyclohexylammonium-1,1'-binaphthyl-2,2'-dihydroxylate methanol solvate $(BINOL^-)(CHA^+)\bullet CH_3OH$ *and dicyclohexylammonium-1,1'-binaphthyl-2,2'-dihydroxylate* $(BINOL^-)(DCHA^+)$ *will be discussed.*

CHAP IV. INCLUSION COMPOUNDS WITH 1, 1'-BINAPHTHYL-2,2'-DIHYDROXYL

1,1'-binaphthyl-2,2'-dihydroxyl with non-chiral cyclic amine guests.

The structures of **(BINOL$^-$)(*CHA*$^+$)●CH_3OH** and **(BINOL$^-$)(*DCHA*$^+$)** were obtained by crystallizing BINOL with CHA and DCHA respectively using methanol as a co-solvent. The structures obtained have different crystal systems, space groups and Z values. **(BINOL$^-$)(*CHA*$^+$)●CH_3OH** crystallized in the triclinic crystal system, with P-1 as space group, Z = 2. The compound formed with DCHA crystallised in the monoclinic crystal system with $P2_1/n$, Z = 4. The structural results are summarised in **Table 4.1.**

Compound	**(BINOL$^-$)(*CHA*$^+$)●CH_3OH**	**(BINOL$^-$)(*DCHA*$^+$)**
Molecular Formula	$(C_{20}H_{13}O_2^-)(C_6H_{14}N^+)CH_3OH$	$(C_{20}H_{13}O_2^-)(C_{12}H_{24}N^+)$
Molecular mass(gmol^{-1})	401.55	467.65
Data collection temp.(K)	296 (2)	173 (2)
Crystal system	Triclinic	Monoclinic
Space group	*P*-1	$P2_1/n$
a (Å)	10.16(1)	15.02(3)
b (Å)	11.25(1)	10.1(2)
c (Å)	11.37(1)	16.89(3)
α (°)	114.5(2)	90.00
β (°)	95.7 (2)	98.6(3)
γ (°)	103.5(2)	90.00
Volume (Å^3)	1121.04(5)	2531.82 (5)
Z	2	4
D_c, Calculated density (g cm^{-3})	1.2428	1.2267
Final R indices [I>2sigma(I)]	R_1= 0.0465 wR_2= 0.1234	R_1= 0.0440 wR_2= 0.0897
R indices (all data)	R_1= 0.0465 wR_2= 0.1207	R_1= 0.1138 wR_2= 0.1251
Largest diff. peak&hole (eÅ^{-3})	0.22; -0.25	0.18; -0.19

Table 4.1 Crystal data table of the salts of BINOL with CHA and DCHA.

A. $(BINOL^-)(CHA^+)\bullet CH_3OH$

Compound name: 2-Cyclohexylammonium-1,1'-binaphthyl-2,2'-dihydroxylate methanol solvate

Formula: $(C_{20}H_{13}O_2^-)(C_6H_{14}N^+)\bullet CH_3OH$.

Asymmetric unit:

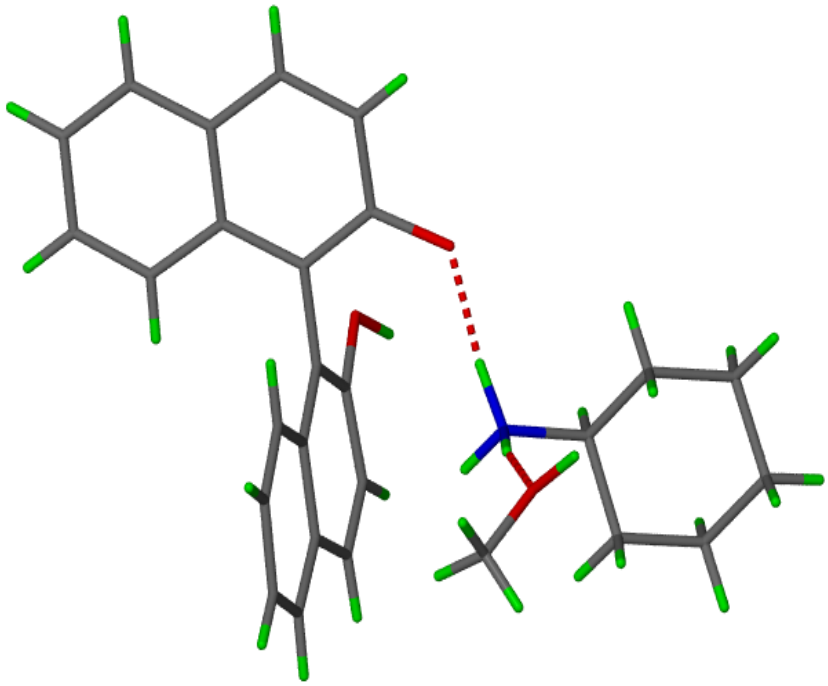

Figure 4.1 Asymmetric unit of $(BINOL^-)(CHA^+)\bullet CH_3OH$.

Crystal structure and refinement

The crystal structure of $(BINOL^-)(CHA^+)\bullet CH_3OH$ was solved in the triclinic crystal system, space group P-1 which was confirmed by the successful refinement of the structure.

The crystal structure was solved by direct methods. The non-hydrogen atoms were found in the difference electron density map. All non-hydrogen atoms of the host and the guest were refined anisotropically. All hydrogens not involved in hydrogen bonding were placed with geometric constraints and allowed to refine isotropically. Aromatic hydrogens were fixed at a distance of C-H =0.95 Å and the $-CH_3$ and $-CH_2$ hydrogens were fixed with C-H = 0.98 Å. The hydrogens attached to the nitrogen of

the cation were found in the difference electron density map and allowed to refine isotropically. The dihedral angle calculated between the two naphthyl planes gave a value of 96 °(7). The structure refined successfully to R_1= 0.0459 with wR_2 = 0.1201.

Crystal packing

The packing diagram of (**$BINOL^-$)(CHA^+)●CH_3OH** is shown in **Figure 4.2.** The unit cell contains two anions of BINOL , two cations of CHA and two methanol molecules with each host anion, the guest cations and the methanol situated in general positions. The ratio $BINOL^-$: CHA^+ : CH_3OH is 1:1:1 (Z = 2).

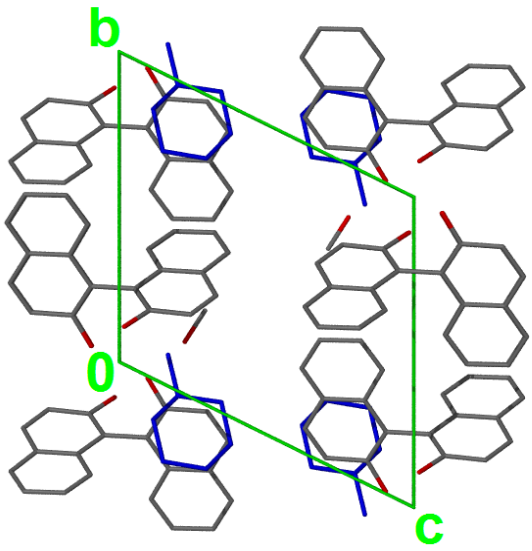

Figure 4.2 Packing diagram of (**$BINOL^-$)(CHA^+)●CH_3OH** viewing along [100] with the guest cyclohexylammonium cations shown in blue for clarity.

The host molecules pack to form channels in the [001] direction, as clearly shown in **Figure 4.3 (a)** the guest shown with its van der Waals radii and in **Figure 4.3.(b)** where the host is shown with its van der Waals radii. The guests occupy these channels forming tubes of guest cations as viewed along [001]. These channels are confirmed by the structure shown using Mercury in **Figure 4.4.**

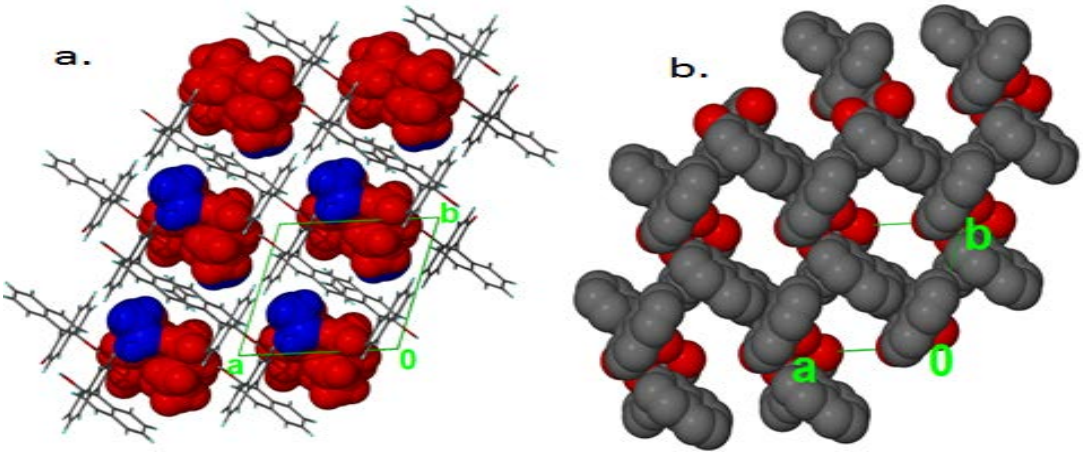

Figure 4.3. Space filled packing diagrams for **(BINOL$^-$)(CHA$^+$)●CH$_3$OH** (a) viewing along [001], where the guest are shown, with their van der Waals radii highlighted for clarity and (b) where the guest are omitted illustrated the channels in which the guest reside.

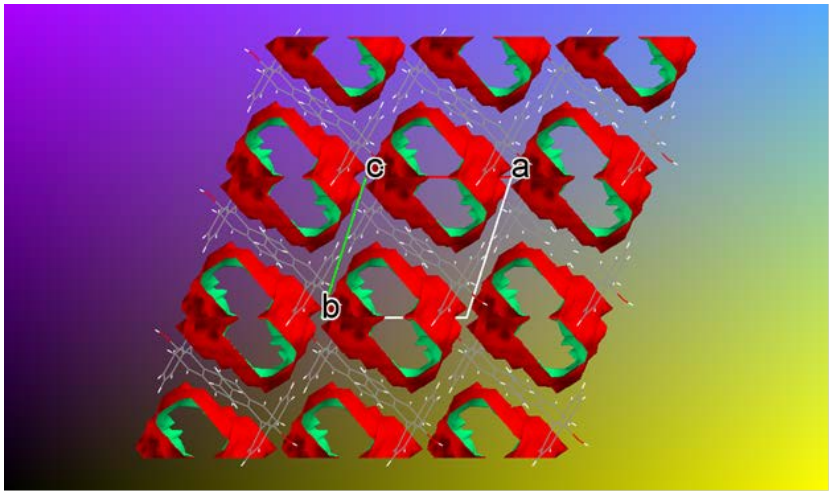

Figure 4.4 Channels occupied by the cyclohexylammonium cations and the methanol molecules in (**BINOL$^-$)(CHA$^+$)●CH$_3$OH.**

The structure is stabilized by hydrogen bonding. These interactions are illustrated in **Figure 4.5** where two host anions formed a hydrogen bonded ring network that can be described as $R_2^2(14)$. In addition to the hydrogen bonded ring network of two anions, two cyclohexylammoniums cations and two molecules of methanol form another ring (B) of the graph notation set of $R_6^4(12)$. The hydrogen bonding details are given in **Table 4.2.**

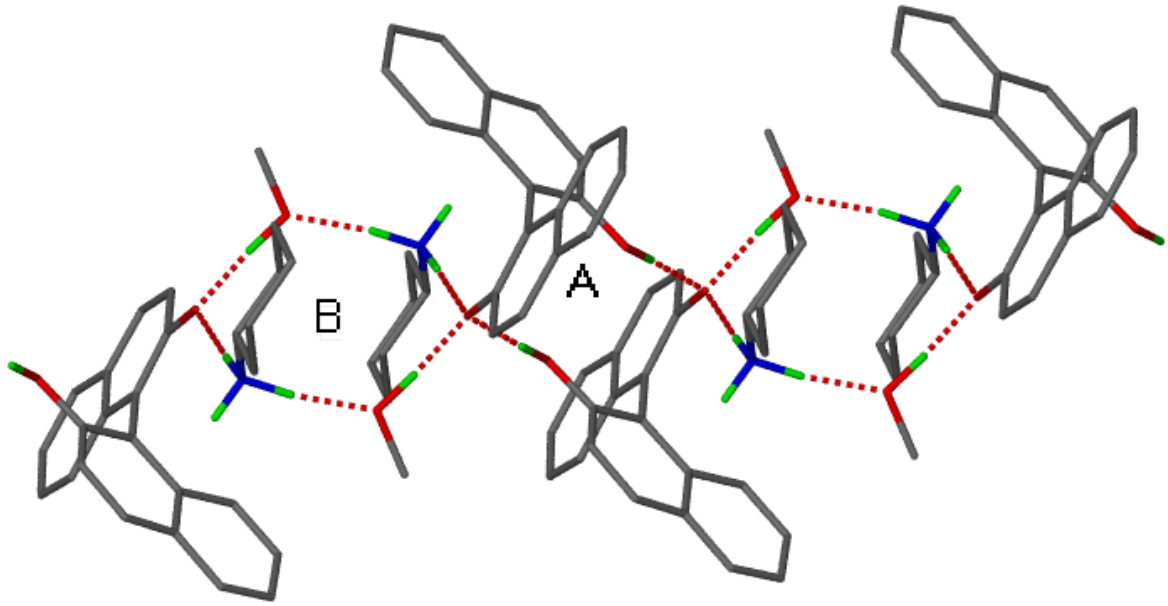

Figure 4.5 Hydrogen bonding interactions in **(BINOL$^-$)(*CHA*$^+$)•(CH_3OH).**

D-H…A	D(D-H)(Å)	d (H…A)(Å)	<(DHA)(°)	d(D..A)(Å)	Symmetry operator
N1-H1G…O1’	1.003 (1)	1.75(2)	172.9(2)	2.74(2)	[x,y,z]
N1-H2G…O1S	1.012 (2)	1.73(2)	168.5(2)	2.73(2)	[x,y,z]
O1-H1…O1’	0.986 (2)	1.65	165.8	2.61	[-x, -y, -z]
O1S-H1S…O1’	1.023	1.6	175.0	2.62(1)	[-x+1, -y, -z]

Table 4.2 Hydrogen bonding interactions for **(BINOL$^-$)(*CHA*$^+$)•(CH_3OH).**

Thermal analysis

The thermal analysis results were inconclusive. The DSC and TG curves for the salt are shown in **Figure 4.6** and the results are summarized in **Table 4.3.**

The DSC results show 3 endotherms: the first peak was initially attributed to the release of the methanol solvent at a peak of 361.5 K (T_{on}= 337.3 K) and the second peak was attributed to the loss of the guest CHA at 411.0K (T_{on} = 406.9 K). The third peak corresponds to the melt of the host at 490.5 K (T_{on}=488.9 K).

However the TG curve gave an experimental mass loss of 24.7% instead of 31.4% expected theoretically, in which 23.7% is expected for the loss of CHA and 7.7% for the methanol. Thus, the sample analysed by thermal analysis does not appear to contain methanol which is clearly different from that of the crystal structure. Attempts at isolating **(BINOL$^-$)(CHA$^+$)** were unsuccessful. The thermal decomposition of **(BINOL$^-$)(CHA$^+$)** is non-stoichiometric with the loss of CHA in two steps.

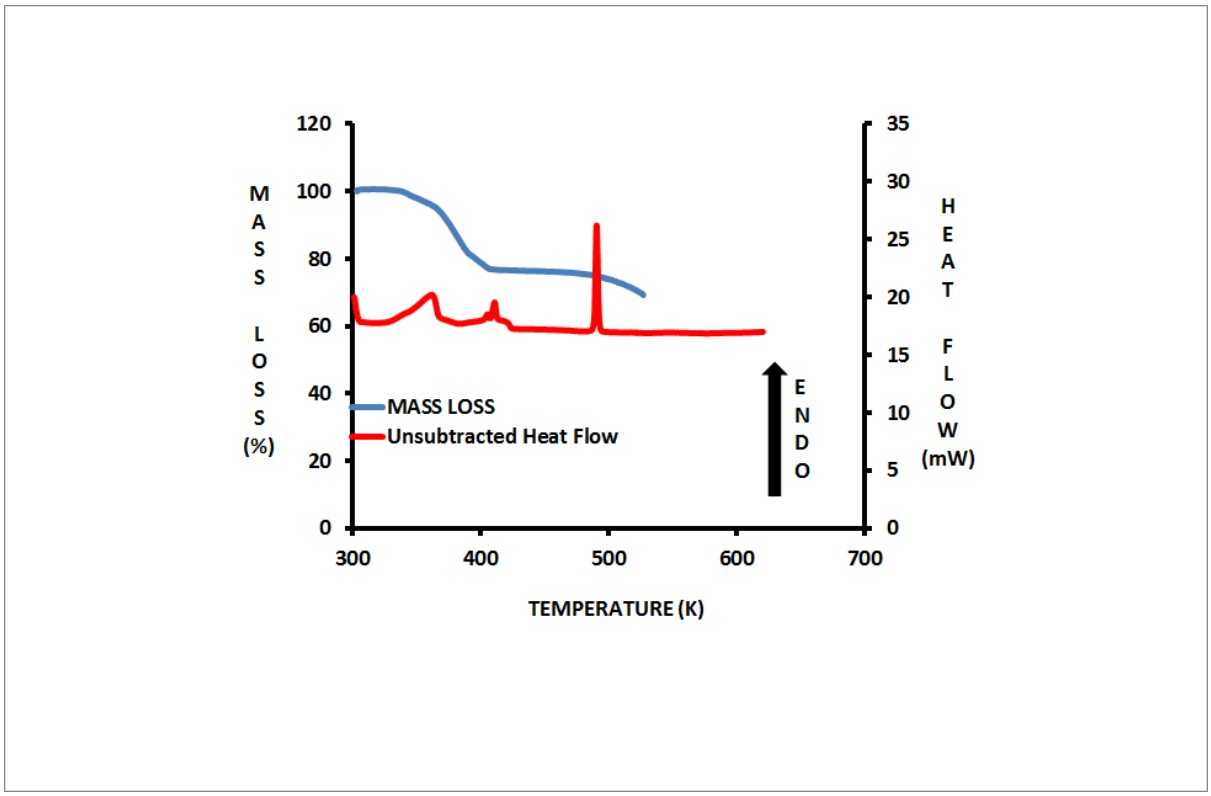

Figure 4.6 DSC and TG curves for (**BINOL$^-$)(CHA$^+$)**

B**. (BINOL$^-$)(DCHA$^+$)**

Compound name: Dicyclohexylammonium-1,1'-binaphthyl-2,2'-dihydroxylate

Formula: **($C_{20}H_{13}O_2^-$)($C_{12}H_{24}N^+$)**

Asymmetric unit:

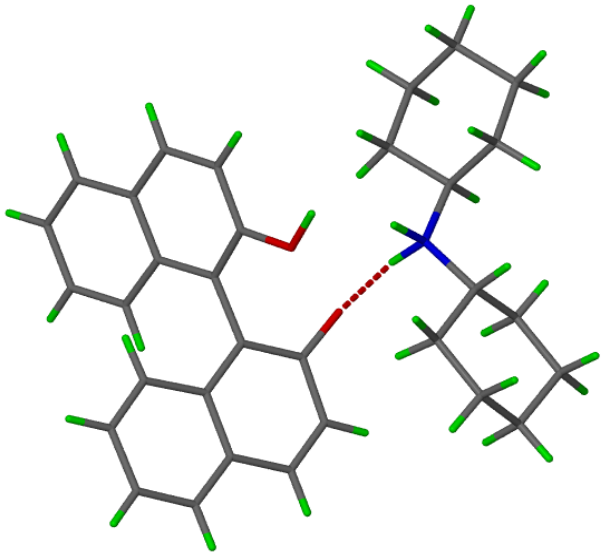

Figure 4.7 Asymmetric unit of **(BINOL$^-$)(DCHA$^+$).**

Crystal structure and refinement

The crystal unit cell parameters of **(BINOL$^-$)(DCHA$^+$)** were also obtained from the same Nonius Kappa CCD diffractometer. The **(BINOL$^-$)(DCHA$^+$)** salt structure crystallises in the monoclinic crystal system in space group $P2_1$ /n.

The crystal structure was solved by direct methods. The non-hydrogen atoms were found in the difference electronic density map. All non-hydrogen atoms of the host and the guest were refined anisotropically. All hydrogens were found in the difference electronic density map including the hydroxyl hydrogen of the host. Aromatic hydrogens were fixed at a distance of C-H = 0.95 Å. The guest CH2-hydrogens were fixed with C-H distance of 0.99 Å. The structure refined successfully with R_1 = 0.0463 with wR_2 = 0.1259.

Crystal packing

The packing diagram of (**BINOL$^-$)(DCHA$^+$)** are shown in **Figure 4.8** There are four host and 8 guest molecules in each unit cell thus the ratio H:G is 1:1 (Z = 4). The host and guest molecules occupy general positions.

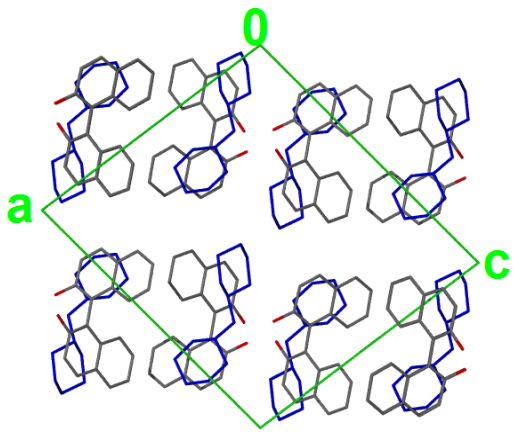

Figure 4.8 Packing diagram of **(BINOL$^-$)(*DCHA*$^+$)** viewed down [010] showing the guest molecules in blue for clarity.

The structure can be considered as a tubulate, as the guest cations pack in channels formed by the host anion framework in the [100] direction (**Figure 4.9.a**). This allows the guest ions to sit in these tubes viewed in the same direction [100] as shown in **Figure 4.9.b.** These channels were confirmed by the structure shown with Mercury in **Figure 4.10,** void space analyzed with the probe size of 1,5 Å.

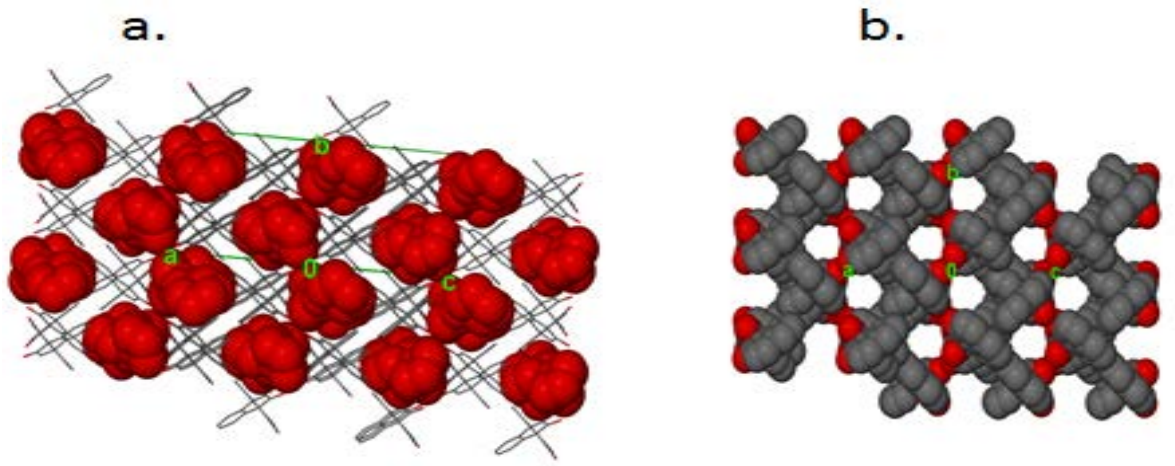

Figure 4.9 Space filled packing diagrams for **(BINOL$^-$)(DCHA$^+$)** (a)viewing along [110], where the guest cations are shown, with their van der Waals radii highlighted for clarity and (b) where the guest are omitted and the channels in which the guest cations reside can be seen.

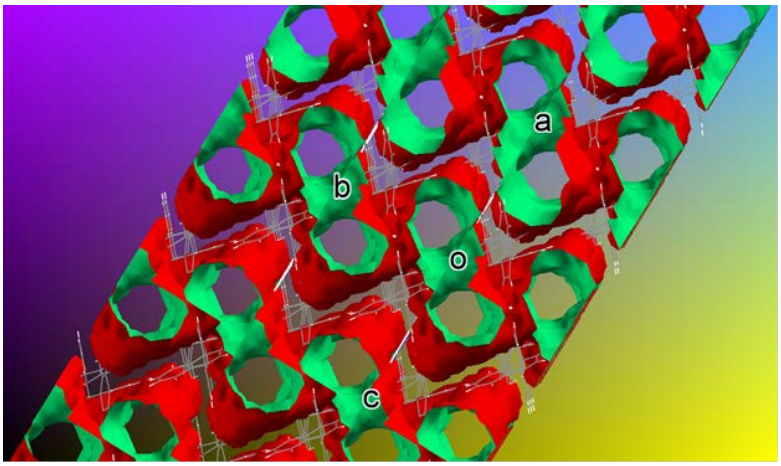

Figure 4.10 Channels occupied by the dicyclohexylammonium cations in **(BINOL$^-$)(DCHA$^+$)**.

Hydrogen bonding is the main form of interaction in the above structure. The hydrogen bonding network is represented in **Figure 4.11.** One host anion and one guest cation form a hydrogen bonded ring that can be described with the graph set $R_2^2(9)$. The rings are linked via (host)OH•••$^-$O(host)-hydrogen bonds. For both, this and the previous structure, the two N-H bonds of ammonium guest are involved in hydrogen bonding. **Table 4.3** shows the hydrogen bond parameters for the **(BINOL$^-$) (DCHA$^+$)** structure.

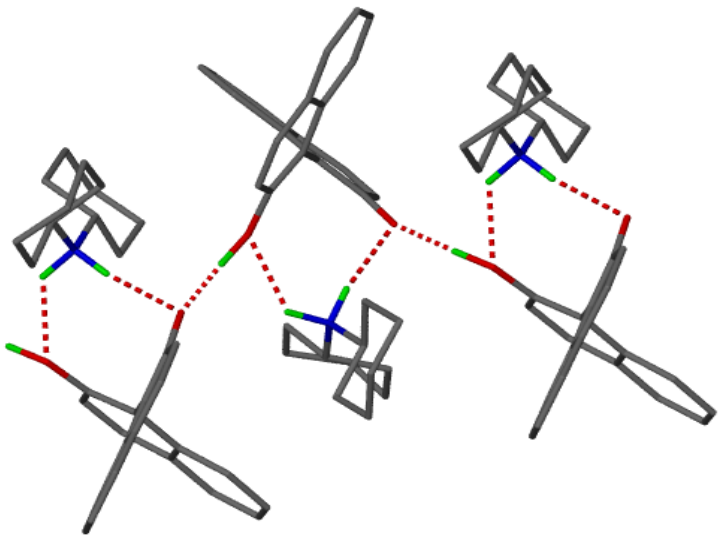

Figure 4.11 Hydrogen bonding interactions in **(BINOL$^-$)(*DCHA*$^+$)**

D-H…A	D(D-H)(Å)	d (H…A)(Å)	<(DHA)(^{o})	d(D..A)(Å)	Symmetry operator
N1G-H1G…O1’	0.94(2)	2.0(2)	169.7(2)	2.93(2)	[-x+1/2, y-1/2,-z+1/2]
N1G-H2G…O1	1.01(3)	2.12(3)	127.4(2)	2.84(2)	[-x+1/2, y-1/2, -z+1/2]
O1-H1…O1’	1.05(2)	1.5	155.6	2.5(1)	[-x+1/2, y-1/2, -z+1/2]
N1G-H2G…O1’	1.01(3)	2.4(2)	162.5(2)	3.38	[x, y-1, z]

Table 4.4 Hydrogen bonding interactions for (**BINOL$^-$)(DCHA$^+$)**

Thermal analysis

TG and DSC analyses were performed for **(BINOL$^-$)(DCHA$^+$)** and are shown in **Figure 4.12.** The experimental mass loss coincides with the expected value confirming the host-guest ratio of 1:1. The TG curve gave an experimental mass loss of 38.9% which correspond to a loss of one molecule of the guest. The DSC curve shows two peaks, the first for the loss of the guest followed by the host melt. The release of guest occurs at 413.5 K (T_{on} = 410.34 K) with the host melt at 490.3 K (T_{on} = 488.7K). The details of the thermal analysis are summarised in **Table 4.5.**

Mechanism of desolvation:

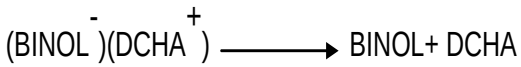

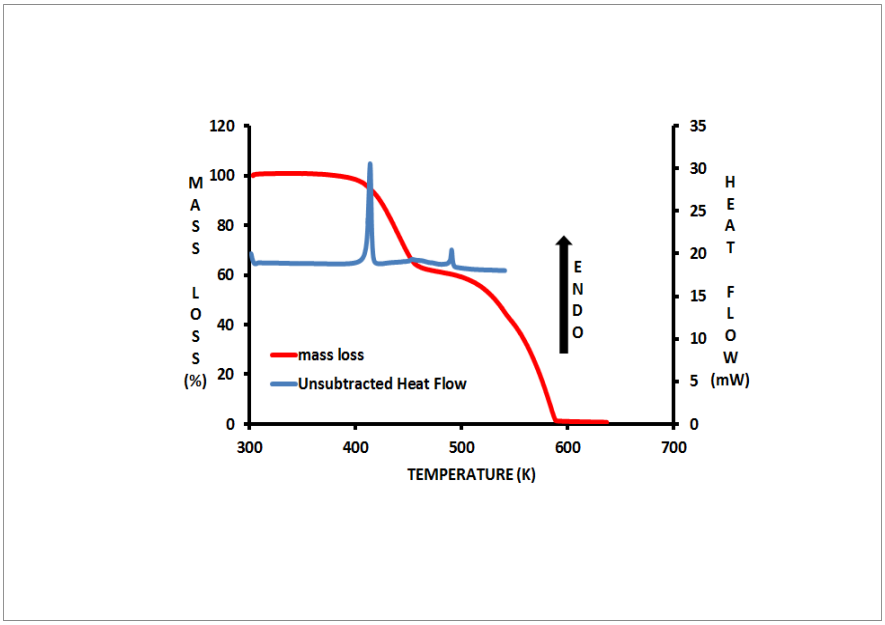

Figure 4.12 DSC and TG curves for (**BINOL$^-$)(DCHA$^+$)**

TG Results	
Calc. % mass loss	**Exp. % mass loss**
39.1	38.9
DSC Results	
Peak$_1$Temperature(K): T$_{on}$, Peak$_1$	**Peak$_2$Temperature(K): T$_{on}$, Peak$_2$**
410.3; 413.5 K	488.9 K ; 490.5 K

Table 4.5: DSC and TG results for (**BINOL$^-$)(DCHA$^+$)**.

DISCUSSION

The host compound **BINOL** forms salts CHA and DCHA respectively. The salts occurred with differing host to guest ratios as well as space groups.

(BINOL$^-$)(CHA$^+$)●CH$_3$OH had an H: G methanol ratio of 1:1:1 and crystallised in the triclinic space group P-1. **(BINOL$^-$)(DCHA$^+$)** had an H: G ratio of 1:1 and crystallised in the monoclinic space group P2$_1$/n.

The salts are all stabilised by hydrogen bonding between the host hydroxyl site and the NH-from the guest forming rings. In **(BINOL$^-$)(CHA$^+$)●CH$_3$OH**, the hydrogen bond forms two type of rings, A and B of graph set notation: D= $R_2^2(14)$ and N$_2$= $R_6^4(12)$ respectively. **(BINOL$^-$)(DCHA$^+$)** has hydrogen bonded rings denoted as N$_2$ = $R_2^2(9)$. These rings are linked via host $^-$O•••OH (Host)-hydrogen bonds.

The TG result of **(BINOL$^-$)(CHA$^+$)●CH$_3$OH** was inconclusive whereas the thermal analysis for **(BINOL$^-$)(DCHA$^+$)** gave the results which matched the ratio of this salt.

CHAP V. INCLUSION COMPOUNDS WITH 1, 1'-BINAPHTHYL-2,2'-DIAMINE

1,1'-binaphthyl-2,2'-diamine(BINDIA) as a basic host, was used to extend our studies on the acid-base properties of binaphthyl derivatives. A series of acidic guests and amides were used for BINDIA. Of all the guests used, BINDIA formed an inclusion compound with the dimethylacetalamide only. The inclusion compound BINDIA•$\frac{3}{2}$–DMA will be discussed in this chapter.

CHAPTER V INCLUSION COMPOUNDS OF 1,1'-BINAPHTHYL-2,2'-DIAMINE

The inclusion compound of **BINDIA•$\frac{3}{2}$*DMA*** was obtained by crystallizing BINDIA in *N,N*-dimethylacetamide (DMA). After one week of slow evaporation at room temperature, the solution gave crystals. The structure of **BINDIA•$\frac{3}{2}$*DMA*** was solved in the monoclinic crystal system, space group *C*2/*c* with Z = 8. The crystal data is shown in **Table 5.1.**

Compound	**BINDIA•$\frac{3}{2}$DMA**
Molecular Formula	$C_{20}H_{16}N_2 \bullet C_4H_9ON$
Molecular Mass ($gmol^{-1}$)	415.04
Data collection temp. (K)	173(2)
Crystal system	Monoclinic
Space group	C2/c
a (Å)	14.1(6)
b (Å)	11.36(2)
c (Å)	28.36(3)
α (°)	90.00
β (°)	96.2(3)
γ (°)	90.00
Volume ($Å^3$)	4514.52(9)
Z	8
D_c, Calculated density ($g\ cm^{-3}$)	1.2211
Final R indices [I>2sigma(I)]	R_1= 0.0512 wR_2=0.0982
R indices (all data)	R_1= 0.0406 wR_2=0.1052
Largest diff. peak and hole ($eÅ^{-3}$)	0.24; -0.19

Table 5.1. Crystal data table of **BINDIA•$\frac{3}{2}$*DMA*.**

BINDIA•$\frac{3}{2}$*DMA*

Compound name: 1,1'-binaphthyl-2,2'-diamine dimethylacetamide solvate.

Formula: **$C_{20}H_{16}N_2$•$\frac{3}{2}$$C_4H_9ON$**

Asymmetric unit:

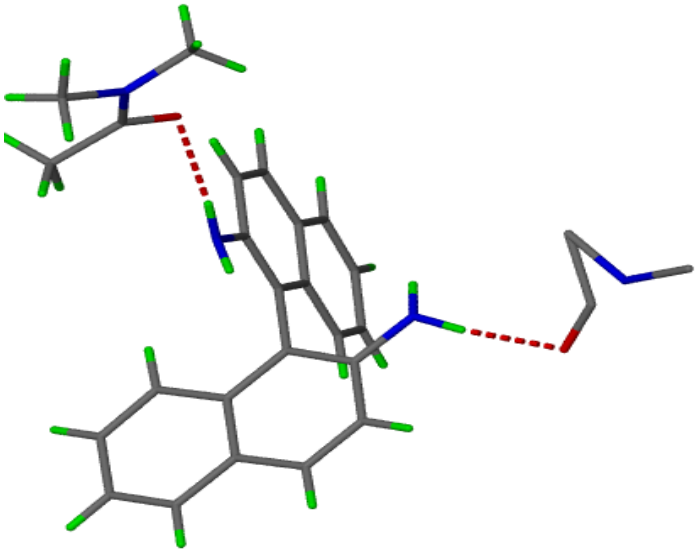

Figure 5.1 Asymmetric unit of **BINDIA•$\frac{3}{2}$*DMA.***

Crystal structure and refinement

The crystal structure of **BINDIA•$\frac{3}{2}$*DMA*** was solved in the monoclinic crystal system, space group C2/c. The asymmetric unit consists of one BINDIA and $\frac{3}{2}$ molecules of DMA, which corresponds to a host:guest ratio of 1:$\frac{3}{2}$.

The crystal structure was solved by direct methods. The non-hydrogen atoms were found in the difference electron density map. All non-hydrogen atoms of the host and the guest were refined anisotropically. All hydrogens not involved in hydrogen bonding

were placed with geometric constraints and allowed to refine anisotropically. Aromatic hydrogens were fixed at a distance of C-H = 0.95 Å and the -CH_3 and -CH_2 hydrogens were fixed with C-H = 0.98 Å. The N-H hydrogens of the ordered guest were found in the difference electron density map and allowed to refine anisotropically. One of the DMA guests lies on a centre of symmetry at Wyckoff position *e* and is disordered (**Figure 5.1)**. All of the atoms of the disordered DMA were assigned site occupancy factors of 0.5 except for C7G which was assigned a site occupancy factor of 1. The hydrogens for this DMA were not included in the final model.

The dihedral angle between the naphthyl moieties was calculated with the program Olex2[2] and gave an angle of 79.7°(2). This value doesn't fall in the range (81.4°−98.1°) found for **BINDIA** and its inclusion compounds studied previously.[3] The structure refined successfully to R_1 = 0.0782 with wR_2 = 0.2593.

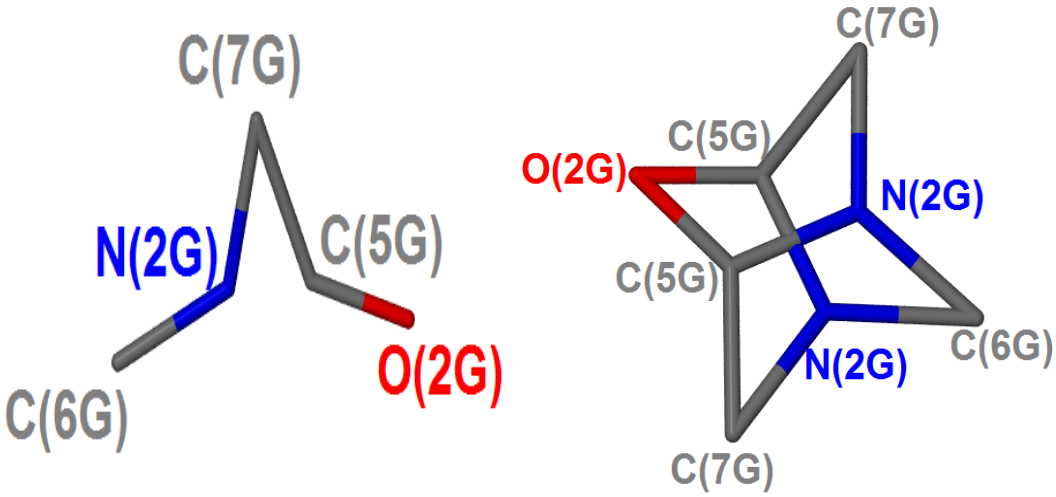

Figure 5.1 Disordered molecule of dimethylacetamide.

Crystal packing

The packing diagram of **BINDIA•$\frac{3}{2}$*DMA*** is shown in **Figure 5.2.** The unit cell contains eight BINDIA and twelve DMA molecules. Thus, this gives Z = 8.

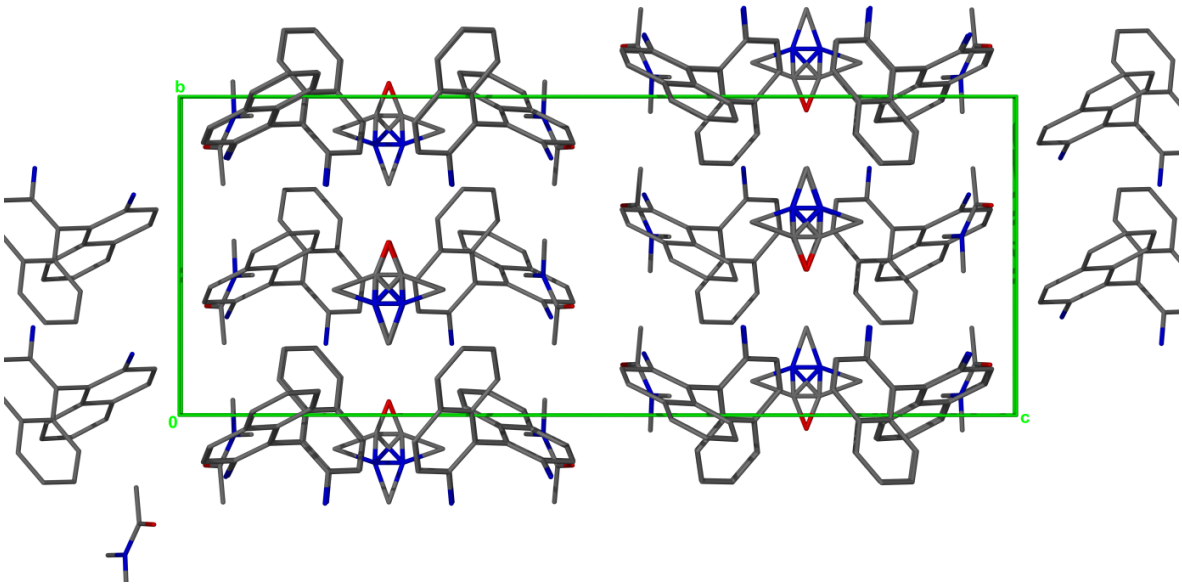

Figure 5.2 Packing diagram of BINDIA•$\frac{3}{2}$*DMA* shown down [100].

This structure can be considered as a tubulate, as the guest pack in channels, shown in **Figure 5.3.**

(a)

(b)

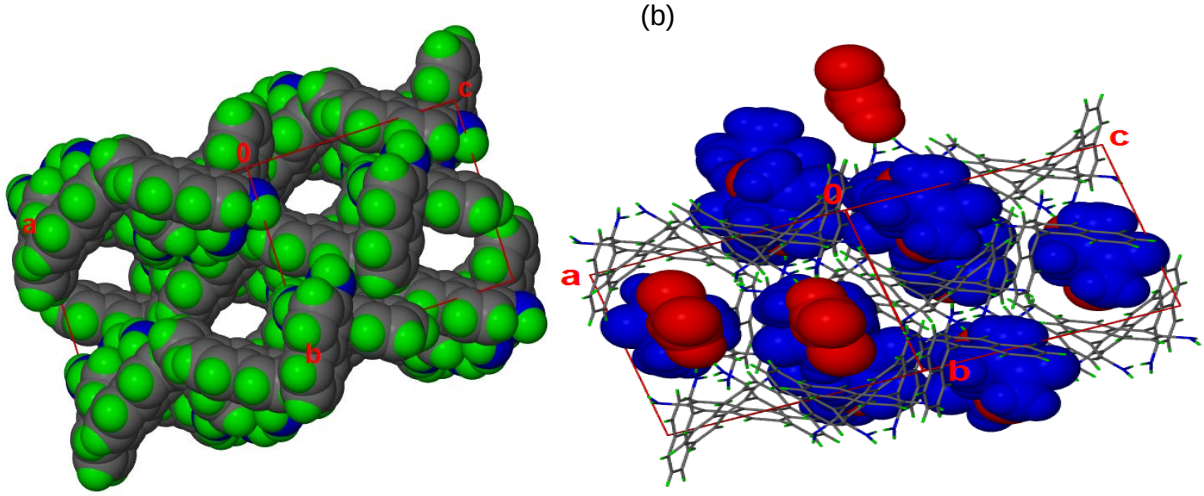

Figure 5.3 Space filling packing diagrams for **BINDIA•$\frac{3}{2}$*DMA*** with (a) the guests omitted and (b) the ordered guests are shown in blue and the disordered guests are shown in red. The host anions are shown in wireframes.

Analysis of these channels was carried out using MERCURY, with a probe radius of 1.5 Å. The voids form infinite channels seen in **Figure 5.4.**

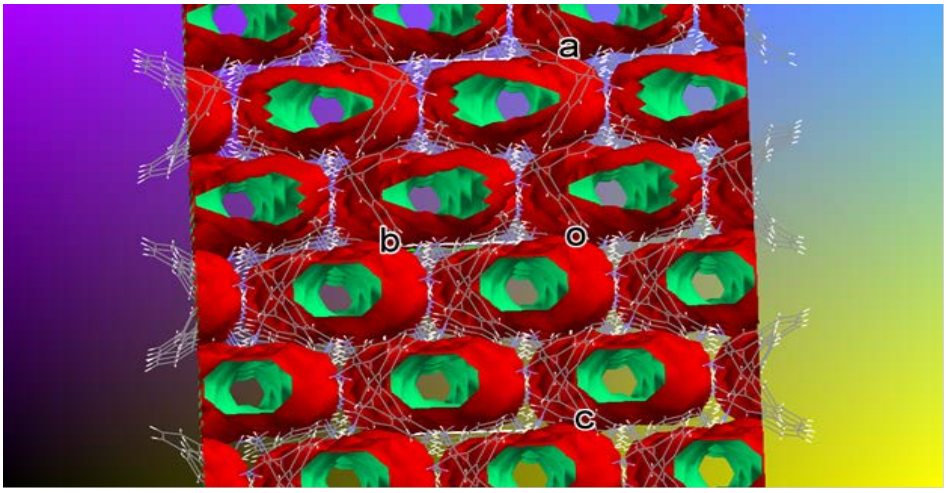

Figure 5.4 Channels occupied by the dimethylacetamide guests in **BINDIA•$\frac{3}{2}$*DMA*.**

The structure is stabilised by hydrogen bonding. Hydrogen bonding involved the N-H moieties of the host acting as donor groups to the oxygen of the DMA **(Figure 5.5).**

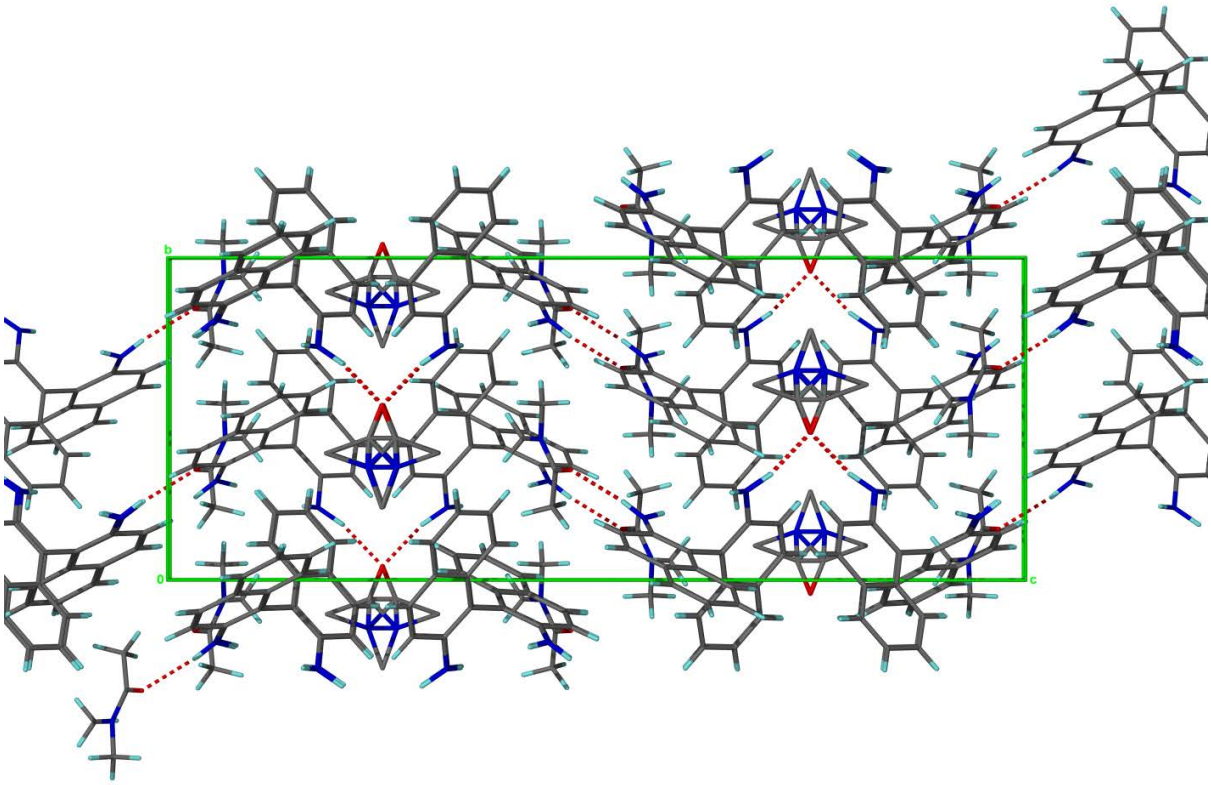

Figure 5.5 Hydrogen bonding interactions in **BINDIA•$\frac{3}{2}$*DMA.***

The hydrogen bonding details are given in **Table 5.2.**

D-H…A	d(D-H)(Å)	d (H…A)(Å)	<(DHA)(°)	d(D..A)(Å)	Symmetry operator
N1-H2G…O2G	0.993	1.972	171.18	2.957	[x, y, z]
N1'-H2'G…O1G	0.955	2.026	167.01	2.964	[x, y, z]

Table 5.2. Hydrogen bonding details in **BINDIA•$\frac{3}{2}$*DMA.***

PXRD

The crystals of **BINDIA•$\frac{3}{2}$*DMA*** were crushed and analysed using powder X-ray diffraction to verify that the crystal selected for single crystal X-ray diffraction was representative of the batch. The diffractogram obtained experimentally with PXRD was in good agreement with the calculated one generated from the program Lazy pulverix[5] as shown in **Figure 5.6.** This result confirmed that the batch was constituted only with the **BINDIA•$\frac{3}{2}$*DMA*** crystals.

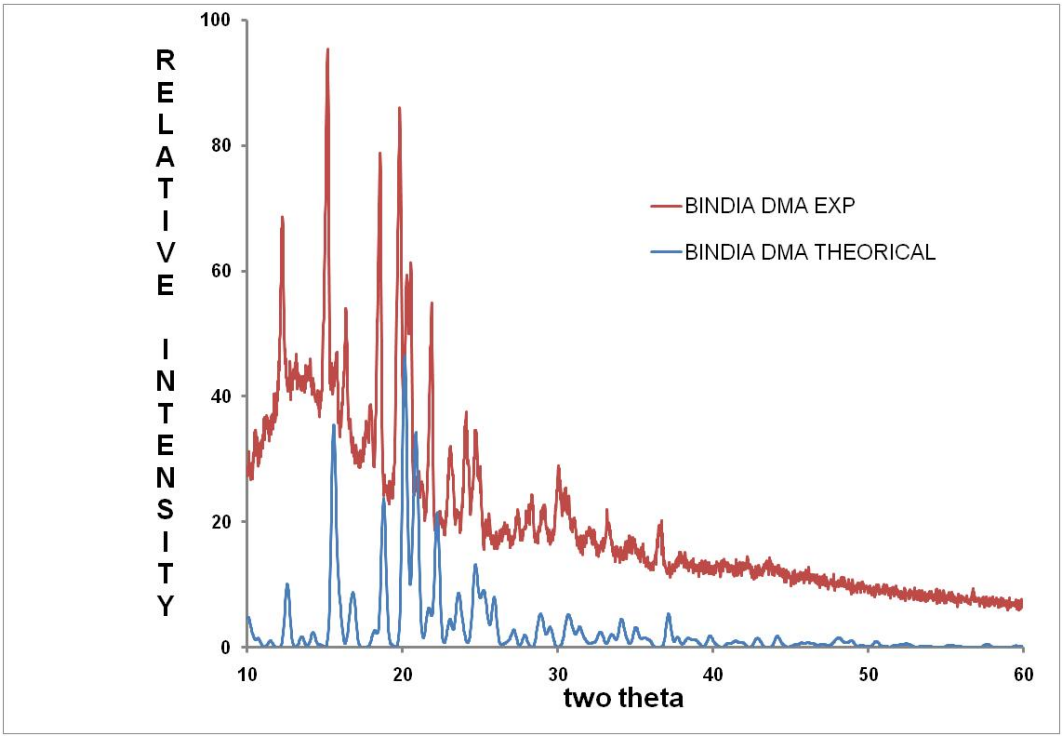

Figure 5.6 Comparison between PXRD pattern of the sample and the calculated PXRD pattern of **BINDIA•$\frac{3}{2}$*DMA*.**

DISCUSSION

The host **BINDIA** forms an inclusion compound with DMA. **BINDIA•$\frac{3}{2}$*DMA*** had a H:G ratio of 1:$\frac{3}{2}$ and crystallised in the monoclinic space group C2/c. The asymmetric unit contained one BINDIA and one DMA molecule in general positions with another DMA guest molecule situated on a centre of symmetry at Wyckoff position *e*.

The inclusion compound was stabilised by hydrogen bonding between the host amine moieties and the oxygen atoms of the guest.

Comparison between the experimental PXRD pattern of the sample and the calculated PXRD pattern of **BINDIA•$\frac{3}{2}$*DMA*** (structure) gave a good match.

CHAPTER VI. CONCLUSION

1,1'-binaphthyl-2,2'-derivatives have found many applications, ranging from chiral ligands in catalysts for asymmetric reactions, to hosts for molecular recognition and enantiomeric separation, and as intermediates for the synthesis of chiral materials. Thus, an understanding of their reactivity is important.

This study dealt with the inclusion behaviour of 1,1'-binaphthyl-2,2'-diol (**BINOL**) , 1,1'-binaphthyl-2,2'-dicarboxylic acid (**BNDA**) and 1,1'-binaphthyl-2,2'-diamine (**BINDIA**) with some small organic molecules, in particular amines for **BNDA** and **BINOL**. For **BINDIA**, organic acids and amides were considered as guests.

Diethylamine, di-n-butylamine, sec-butylamine, cyclohexylamine and dicylohexylamine were used as guest molecules for both 1,1'-binaphthyl-2,2'-diol and 1,1'-binaphthyl-2,2'-dicarboxylic acid respectively. 1,1'-binaphthyl-2,2'-dicarboxylic acid formed salts with all the aforementioned amines in which all the carboxylic groups were deprotonated. The 1,1'-binaphthyl-2,2'-diol, formed two salts with cyclohexylamine and dicyclohexylamine respectively. In each of these structures, only one of the hydroxyl ions of the host was deprotonated. The 1,1'-binaphthyl-2,2'-diamine formed only one inclusion compound with *N,N*-dimethylacetamide.

The crystal structures of all the compounds obtained were elucidated and selected characteristics of these structures are given in Table 5.1.

A majority of the compounds formed, crystallised in the space group P-1. The exceptions include **$(BNDA^{2-})(DEA^{+})_2$** and **$BINDIA\bullet\frac{3}{2}DMA$** which were solved in C2/*c*, and **$(BNDA^{2-})(DCHA^{+})_2\bullet(CH_3OH)\bullet(H_2O)$** and **$(BINOL^{-})(DCHA^{+})$** which were both solved in $P2_1/n$. For the 1,1'-binaphthyl-2,2'-dicarboxylic acid, the dihedral angles vary between 79.7(2) ° and 101.8(3)°.

.

COMPOUND	GUEST + CO - SOLVENT	RATIO	SPACE GROUP	DIHEDRAL ANGLE	HYDROGEN BONDING	INCLUSION MODE
$(BNDA^{2-})(DEA^{+})_2$	DEA in methanol	1 :2	C2/*c*	79.7 (2)°	^{-}O–H•••N^{+}	Salt
$(BNDA^{2-})(DBA^{+})_2$	DBA in methanol	1 :2	P-1	94.5 (2)°	^{-}O–H•••N^{+}	Salt
$(BNDA^{2-})(DBA_2{}^{+})_2$	40% DBA and 60% DEA in methanol	1:2	P-1	81.2 (8)°	^{-}O–H•••N^{+}	Salt
$(BNDA^{-})(CHA^{+})_3(C_7H_{11}NO_2{}^{-})(CHA)(H_2O)$	CHA in methanol	1:3:1:1:1	*P*-1	101.8 (3)°	^{-}O–H•••N^{+}	Salt
$(BNDA^{-})(DCHA^{+})_2 \bullet CH_3OH \bullet H_2O$	DCHA in methanol	1:2:1:1	$P2_1/n$	82.9 (9)°	^{-}O–H•••N^{+}	Salt
$(BNDA^{-})(SECBUAM^{+})_2 \bullet 3H_2O$	SECBUAM	1:2:3	P-1	89.5 (2)°	^{-}O–H•••N^{+}	Salt
$(BNDA^{-})(SECBUAM^{+})_2 \bullet CH_3CH_2OH$	SECBUAM in butanol	1:2:1	P-1	93.6 (3)°	^{-}O–H•••N^{+}	Salt
(BINOL-)(CHA+)	CHA in methanol	1:1	P-1	96 (7)°	^{-}O–H•••N^{+}	Salt
$(BINOL^{-})(DCHA^{+}) \bullet (CH_3OH)$	DCHA in methanol	1:1:1	$P2_1/n$	76.9 (2)°	^{-}O–H•••N^{+}	Salt
$BINDIA \bullet \frac{3}{2}DMA$	DMA in methanol	1:2	C2/*c*	79.7 (2)°	O–H•••N	inclusion

Table 5.1 Selected characteristics of all the structures studied.

Large variations in the host: guest ratios were also found with some of the structures containing solvent molecules. All of the guests included were found to be located in constricted channels and the compounds were stabilised with hydrogen bonds. Thermal analysis showed that all compounds formed with **BNDA** decompose *via* a series of mass loss steps which could be correlated to the stoichiometry. In all the cases, there was always a remaining guest released simultaneously with the host melt and decomposition.

Three compounds were elucidated from BNDA with acyclic amines, **$(BNDA^{2-})(DEA^{+})_2$**, **$(BNDA^{2-})(DBA^{+})_2$** and **$(BNDA^{2-})(DBA_2^{+})_2$.** The latter structure is a polymorph crystallised from the competition experiment of the host 1,1'-binaphthyl-2,2'-dicarboxylic acid in a mixture of 60% of DEA and 40% of DBA. All the three salts have the same ratio of 1:2. These salts were all stabilised by hydrogen bonding between the carboxylate sites and the ammonium site of the guests. The ratios of the onset temperatures for the first endotherm in the DSC and the normal boiling points of the guests, Ton/Tb, were calculated. It was found that **$(BNDA^{2-})(DEA^{+})_2$** was the most stable salt. This corresponded with the kinetics of desolvation for the first mass loss step.

The host **BNDA** formed salts with CHA and DCHA, respectively *viz.*

$(BNDA^{2-})(CHA^{+})_3(C_7H_{11}NO_2^{-})(CHA)\bullet(H_2O)$ and **$(BNDA^{2-})(DCHA^{+})_2\bullet(CH_3OH)\bullet(H_2O)$.** For **$(BNDA^{2-})(CHA^{+})_3(C_7H_{11}NO_2^{-})(CHA)\bullet(H_2O)$,** there was not only a proton transfer from the host to the guest but also a reaction between one of the guests and carbon dioxide in the atmosphere to form a carbamate ion.

$(BNDA^{2-})(DCHA^{+})_2\bullet(CH_3OH)\bullet(H_2O)$ crystallised in the monoclinic space group $P2_1/n$. The salts are all stabilised by hydrogen bonding between the carboxylate sites and the ammonium site of the guests. Each compound has two guests for the two carboxylate site of the host. Because the acid has two carboxylates groups, therefore each host are hydrogen bonded to two guests.

The host **BNDA** also formed two salts with the racemic SecBuam. **$(BNDA^{-})(SECBUAM^{+})_2\bullet 3H_2O$** was crystallised in SecBuam without a co-solvent whereas **$(BNDA^{-})(SECBUAM^{+})_2\bullet CH_3CH_2OH$** was crystallised with SecBuam with *n*-butanol as a co-solvent.

Both salts were stabilised by hydrogen bonding between the two carboxylate groups of the host and the ammonium moieties of the guest bridged by hydrogen bonding of to the solvent.

In **(BNDA^{-})(*SECBUAM*$^{+}$)$_2$●3H$_2$O** both cations of SecBuam were disordered with site occupancy factors respectively of 0.82 and 0.18 for the first one and of 0,73 and 0.27 for the second cation. In **(BNDA^{2-})(SecBuam^{+})$_2$●But,** disorder was observed for the SecBuam cation (0.81 and 0.19) and the butanol (0.69 and 0.31).

The chapter on the **BINOL** shows the formation of compounds with CHA and DCHA. The complexes formed were **(BINOL^{-})(*CHA*$^{+}$)●CH$_3$OH** and **(BINOL^{-})(*DCHA*$^{+}$).** The difference between the compounds of **BINOL** and those from **BNDA** is that with **BINOL**, there is a transfer of only one proton from the host to the guest, which was not the case with **BNDA** (transfer of both protons). This shows that the proton from **BNDA** were more acidic than those ones of **BINOL**.

BINDIA is the only one host which formed an inclusion compound with DMA. The H:G ratio of 1: $\frac{3}{2}$ was obtained.